UNIVERSITY OF CALIFORNIA, SAN DIEGO

Distributed Cooperation for Robust Estimation

A dissertation submitted in partial satisfaction of the
requirements for the degree
Doctor of Philosophy

in

Engineering Sciences (Mechanical Engineering)

by

Michael Ouimet

Committee in charge:

Professor Jorge Cortés, Chair
Professor Raymond de Callafon
Professor John W. Helton
Professor Jules Jaffe
Professor Sonia Martinez

2014

The dissertation of Michael Ouimet is approved, and it is acceptable in quality and form for publication on microfilm and electronically:

_____

_____

_____

_____

_____
Chair

University of California, San Diego

2014

DEDICATION

To my parents, who have always believed in and supported me

EPIGRAPH

Do not go where the path may lead,
go instead where there is no path and leave a trail.
—Ralph Waldo Emerson

TABLE OF CONTENTS

LIST OF FIGURES

LIST OF TABLES

ACKNOWLEDGEMENTS

First, I owe the most to my family. To Mom and Dad, I could never have finished this academic achievement without the last twenty-six years of your help and unwavering support. Your constant encouragement made me believe I could do anything if I really tried. I appreciate all you've given me and the sense of wonder and love of learning you instilled in me. To Katie, you've been a great sister and friend. Now that we've both finished a chapter of our lives, I can't wait to see where each of our futures take us.

To Jorge, I am very grateful for your guidance and support over the last four years. Your deep, intuitive knowledge and wonderful way of explaining abstract concepts helped me immensely, all through my time here. Furthermore, without your endless excitement for the field, sincere motivation, and strong expectations of quality papers, I may have never finished. For all of the knowledge and skills you've helped me gain, I hope that to some extent I've been able to return that favor.

To the rest of my doctoral committee, Professors Raymond de Callafon, Bill Helton, Jules Jaffe, and Sonia Martinez: I appreciate the time and effort you've spent in helping me defend. I'm honored to have each one of you as members of my committee.

To Andrew and (especially) Bahman, I'm exceedingly grateful for the help you've given me along the way, especially back when I first started. You've both been great academic role models as well as caring friends.

To Cameron, I can't believe we're actually finishing. I'm happy that we went on this doctoral adventure together. Having someone else going through the same challenges at the same time made the process a lot less stressful. I appreciate all the homework help we gave each other in the first year as well as all of the fun diversions we distracted each other with.

To the rest of Team Jorge/Sonia, both past and present, I'm happy to have met and enjoyed all of your companies through weekly group meetings, insightful research discussions, and International Cafe lunches. I know you will all go on to do great things.

To my friends, thanks for the endless support and making sure I never worked too hard.

I'd like to acknowledge that this work could never have been accomplished without the generous support of NSF awards of OCE-0941692 and CMMI-0908508.

Chapter 3, in part, is a reprint of the material [65] as it appears in 'Hedonic coalition formation for optimal deployment' by M. Ouimet and J. Cortés in Automatica, to appear in 2013. The dissertation author was the primary investigator and author of this paper.

Chapter 4, in part, is a reprint of the material [66] as it appears in 'Robust, distributed estimation of internal wave parameters via inter-drogue measurements' by M. Ouimet and J. Cortés in IEEE Transactions on Control Systems Technology, to appear in 2013. The dissertation author was the primary investigator and author of this paper.

Chapter 5, in part, is a reprint of the material [64] as it appears in 'Collective estimation of ocean nonlinear internal waves using robotic underwater drifters' by M. Ouimet and J. Cortés in IEEE Access 1 in 2013 as well as the material [67] titled 'Robust estimation and aggregation of ocean internal wave parameters using Lagrangian drifters' by M. Ouimet and J. Cortés which was accepted for publication to the American Controls Conference 2014. The dissertation author was the primary investigator and author of these works.

VITA

2009	Bachelor of Science in Mechanical Engineering, *magna cum laude*, University of Notre Dame
2010	Master of Science in Engineering Science (Mechanical Engineering), University of California, San Diego
2014	Doctor of Philosophy in Engineering Science (Mechanical Engineering), University of California, San Diego

PUBLICATIONS

Journal publications:

M. Ouimet and J. Cortés, "Robust, distributed estimation of internal wave parameters via inter-drogue measurements", *IEEE Transactions on Control Systems Technology*, to appear, 2014.

M. Ouimet and J. Cortés, "Hedonic coalition formation for optimal deployment", *Automatica*, vol. 49, no. 11, 2013, 3234-3245.

M. Ouimet and J. Cortés, "Collective estimation of nonlinear internal waves using underwater drifters", *IEEE Access*, vol. 1, 2013, pp. 418-427.

Conference proceedings:

M. Ouimet and J. Cortés, "Robust estimation and aggregation of ocean internal wave parameters using Lagrangian drifters", *American Controls Conference*, Portland, Oregon, USA, 2014, to appear.

M. Ouimet and J. Cortés, "Distributed estimation of internal wave parameters via inter-drogue distances", *IEEE Conference on Decision and Control*, Maui, Hawaii, USA 2012, pp. 2433-2438.

M. Ouimet and J. Cortés, "Coalition formation and motion coordination for optimal deployment", *IEEE Conference on Decision and Control and European Control Conference*, Orlando, Florida, USA, 2011, pp. 6882-6887.

ABSTRACT OF THE DISSERTATION

Distributed Cooperation for Robust Estimation

by

Michael Ouimet

Doctor of Philosophy in Engineering Sciences (Mechanical Engineering)

University of California, San Diego, 2014

Professor Jorge Cortés, Chair

This dissertation contains work in novel algorithms which ensure robust estimation of physical phenomena. In the context of cooperative control of multi-agent networks, robustness refers to the fact that, despite the possibility of individual agent failures and the presence of noisy measurements, we wish to be able to characterize the network's performance at solving a given task (estimation). The contributions come from two problems of spatial estimation. The first problems motivation comes from spatial estimation tasks executed with unreliable sensors. Previous work has considered how to optimally deploy the unreliable sensors over an environment to robustly estimate the random field which they are measuring. For some problems, it has been shown that the optimal deployments correspond

to agents forming clusters of a certain size and then deploying the clusters optimally assuming that one packet from each cluster reaches the center. Motivated by this result, our major contribution in this problem is a distributed algorithmic solution which exactly achieves those desirable network configurations. We also show the algorithms robustness to agent addition and subtraction as well as upper bound the completion time and required number of messages exchanged. The second problem considers a group of robotic drifters whose objective is to estimate the physical parameters (amplitude, wavenumber, frequency) that determine the dynamics of ocean internal waves. Internal waves are important because, as they travel, they displace small animals, such as plankton, larvae, and fish. While underwater, drifters do not have access to absolute position information and only rely on inter-vehicle measurements. Building on this data and the study of their dynamics under the flow induced by the internal wave, we design strategies that are able to characterize the internal wave. Because many wave models exist, we separately consider the tasks of estimating a single *linear* internal wave and a single *nonlinear* internal wave. We devise algorithms that perfectly determine the wave's parameters under noiseless measurements and also analyze the robustness to measurements corrupted by error. Since many parameter estimates may be obtained at different times, we also analyze a methodology for combining these estimates to decrease the final error.

Chapter 1

Introduction

Here, we begin with an introduction to cooperative control, the body of work that this dissertation falls within. Then, we introduce the problems tackled and relate them to the prior literature. After that, we detail the contributions found in this work. We end with an outline which briefly describes the contains of the remaining chapters.

1.1 Introduction and related literature

In this section we introduce the field of cooperative control, introduce the problems which we consider, and compare them to the relevant literature.

1.1.1 Cooperative control

This dissertation sits in the field of cooperative control of multi-agent networks [12, 86, 46]. This area considers problems where a group of robots, equipped with limited sensing/communication, computation capability, mobility, and control authority seek to cooperate to achieve a common, global task. Common cooperative tasks, to name a few, are deployment over and shared surveillance of a physical environment [17, 96, 40], data collection, estimation, and consensus [62, 75, 59, 89, 25], and vehicle formation control [26, 61, 43]. In all of these cases, each robotic agent senses its immediate environment, communicates with

other agents, processes the information it sensed/received, and takes a local action in response to its situation. A concrete multi-agent control problem is the not-so-distant dream of a city full of self-driving cars. Experts believe that by 2040, up to 75% of cars on the road will be self-driving [41]. In order for the network of cars to work well, each car must be able to control itself safely in real-time. Thus, each will need to have speed and position measurements and communicate its velocity and direction changes to the cars in its vicinity. Together, the individual cars can achieve the task of moving passengers to their destinations quickly and safely.

Whatever the specific problem, multiple robots performing a collaborative task provides a number of inherent benefits. For instance, in problems where more agents yields better solutions, there is an inherent robustness to individual failures. Many agents spatially distributed and interacting locally can readily adapt to a changing environment, making algorithms tolerant to uncertain or dynamic environments. Finally, multiple agents working in unison may be able to achieve tasks beyond any individual agents' capabilities.

One can consider centralized or distributed approaches to cooperative, multi-agent control. A *centralized* approach is one where an omniscient leader effectively receives all the relevant information, solves the task, and communicates this to all other agents. For many situations, this setup is valid. However, in scenarios where the information is distributed over the network and transmitting and collecting the data centrally is costly, insecure, or slow, a *distributed* solution might make more sense. We say that an algorithm to solve a problem is distributed if the robotic agents are able to solve the desired global problem each using only a subset of the total data and communicating with their local neighboring agents [50, 74, 55, 91] Another shortcoming of a centralized approach is that they are not robust to any individual agent's failure. Furthermore, the communication and processor burden falls on one entity, so as the number of agents grow, the leader's capability must also increase. For these reasons, we focus on distributed approaches.

For example, suppose a group of agents are tasked with deploying themselves across an environment so that each agent is far away from all of the others.

This sort of deployment is useful when random events occur in the environment and the network of agents wish to minimize the time it takes for the closest agent to reach the event. This, in turn, is analogous to the urban planning problem of choosing hospital locations in a city so that no matter where someone gets hurt, the closest hospital is not far [22]. In this situation, an agent cares little about what the agents very far from it are doing; a good distributed strategy might be to simply move away from the agent closest to it [16].

There are many other additional challenges to distributed, cooperative problems. A desire for adaptive behavior means that designers must create feedback-based strategies which compute control actions in real-time, rather than pre-computing an open-loop strategy for a known/static setup. The interaction between many robotic agents requires a carefully defined information flow. Questions such as which agents have access to what information, with which other agents can they exchange information, how and when do these exchanges occur need to be answered. Since the agents have motion capabilities, the answers to these questions may also be dynamically changing. Given that these algorithms are used in unknown environments, where the events might be happening dynamically or the task evolving is in time, reliability is of chief concern. Achieving robust, predictable behavior in the presence of uncertainty is a worthwhile, but difficult challenge to achieve. Furthermore, one might wish to know specifics about the algorithm's performance, such as how much communication is required, how long it takes to achieve the objective, or how much processing is required of each agent. In the presented approaches, we address all of these challenges.

Both of the problems considered here focus on robust estimation of spatial phenomena. Here, we will be more specific about what we mean by robust estimation. The first problem is motivated by a problem of deploying a mobile sensor network for the purpose of estimating the environment. Because a certain, unknown fraction of the sensors are assumed to be malfunctioning at any given time, the cost function is designed to account for this. Thus, the optimal deployment, which minimizes that cost function, is robust to these agent failures. Our work provides an algorithmic method to reach these configurations, and so, it provides

deployment for robust estimation. In the second problem, the designed algorithm is also robust to individual agent failures. Furthermore, the algorithm, whose purpose is to estimate model parameters, produces parameter estimates when given data with error. It is in this sense that we say the solution is robust to measurement error. We contrast the above ideas with the notion of robust estimation in signal processing [97]. In that context, robustness deals with the deviation from distributional assumptions. For instance, many problems in engineering assume that data is corrupted by additive, Gaussian errors. This structure makes building optimal estimators more tractable, however, in practice this assumption is often not true. A robust estimator is able to quantify the possible degradation in performance stemming from similar distribution assumption deviations.

1.1.2 Coalition formation and deployment for optimal estimation

This dissertation contains work on two distinct but related problems in distributed control: distributed coalition formation and deployment for optimal spatial estimation and distributed estimation of ocean internal waves. The first problem is motivated by optimal spatial sampling problems under possibly failing communications. Consider a group of mobile robotic sensors that take point measurements of a random field over an environment and relay them back to a data fusion center. Assume that because of the features of the medium and the limited agent communication capabilities, it is known that only a fraction of these packets will arrive at the center, but it is not a priori known which ones will. Given that some sensors are not working and their identity is unknown, a reasonable strategy consists of grouping sensors together into clusters so that the likelihood of obtaining a measurement from the position of each cluster is higher. The aim is to design a distributed algorithm that makes the network autonomously create groups of a desired size such that (i) members of each individual group become coincident, and (ii) the groups deploy optimally with regards to the spatial estimation objective.

There is an increasing body of research that deals with spatial estimation problems with possibly failing communications where packets are either received

without corruption or not received at all, see e.g., [88, 82, 35, 15]. In particular, [15] shows that, for the problem motivating our algorithm design, the clustering strategy outlined above is optimal in some cases: the configurations that maximize the expected information content of the measurements retrieved at the center correspond to agents grouping into clusters, and the resulting clusters being deployed optimally. Achieving such desirable configurations is challenging because of the spatially distributed nature of the problem and the agent mobility. In this regard, the notions of spatial coverage and agent clustering (the latter understood as physical co-location), as well as our proposed algorithmic solution, are different from those in typical hierarchical clustering problems, see e.g. [93, 5], where sensors are static and the objective is to minimize the cost incurred when relaying messages to a data fusion center. Closer to our setup, [40] define clusters as groups of mobile sensors in locations such that their density is above the expected average density. Using a control law based on whether sensors are in a cluster or not, the network minimizes the distance traveled by the sensors to deploy. Our technical approach combines elements of spatial facility location [60], rendezvous and deployment of multi-agent systems [12], and coalition formation games [10, 6]. From a game-theoretic perspective, our analysis of the coalition formation dynamics is novel because of the consideration of evolving and partial interaction topologies. From a motion coordination perspective, the novelty relies on the coupled dynamics between the coalition formation, the clustering, and the network deployment. Other works in cooperative control employ game-theoretic ideas to solve tasks such as formation control, target assignment, self-organization for efficient communication, consensus, and sensor coverage, see e.g. [34, 52, 3, 80, 85, 70]. Given the algorithmic design choice of the agents' utility function, our work has connections to weakly acyclic games [53, 51]. Specifically, under a fixed, complete communication graph where all agents can join any coalition they wish, our game can be cast as a weakly acyclic game. However, in general, the limited information available to agents, the dynamic interaction topology, and the dependence of the individual action sets on this topology makes the framework of weakly acyclic games not directly applicable. To characterize the performance of the algorithm, we upper bound the expected

completion time and required number of messages sent per timestep as a function of the total network size by building on the well-established notions of time and communication complexity in distributed algorithms [69, 50, 12]. Since in the repeated coalition formation game agents take probabilistic actions, we consider the expected time complexity. In principle, our algorithm can be described as a Markov chain, where the coalition formation time can be exactly defined as the first hitting time for the set of goal states [57, 47]. However, defining the probabilistic transition function becomes difficult as the number of total agents grows. Thus, we adopt a drift analysis approach [36] to provide an upper bound on the time complexity.

1.1.3 Estimation of ocean internal waves

The second problem is concerned with estimating oceanic internal waves. Internal waves are waves that propagate within a fluid, rather than on its surface [8, 20, 63]. The type that we consider here corresponds to a moving oscillation in the boundary surface between two layers of a stratified fluid. In the ocean, these two layer fluids can occur at the mouth of large rivers where brackish (low salinity) water sits above sea water, for instance. Also, a continuously stratified fluid can be modeled as a two-layer fluid, where the interface, called pycnocline, is the surface of constant density where the vertical rate of change in density is largest. Internal waves are associated with high concentrations of various types of planktonic organisms and small fishes [94, 87], as well as an agent of larval transport [73]. This makes their study important to oceanographers, see e.g. [27, 48, 90, 14]. The considered class of internal waves can be broadly categorized into linear and nonlinear. Linear waves have amplitudes small relative to the depth of the water column. They are capable of moving around plankton, animal larvae, and other organisms, as well as creating mixing between the upper and lower layers. In particular, striping of low/high densities in plankton can be well explained by small amplitude, linear internal waves [27]. In contrast, nonlinear waves have larger amplitudes, allowing them to provide the advection required for larval transport [73]. Many models exist for nonlinear waves [37, 39] to account for the wide variety of

conditions and bathymetries found in the ocean.

Traditional methods for studying internal waves have been satellite observations [4], radar imaging [76, 2], acoustic tomography [23], conductance-temperature-depth (CTD) casts [63], and current meters on moorings [63]. However, these methods lack the capability of real-time adaptability. Here, we tackle this problem using a group of drogues capable of drifting underwater near the internal wave's interface to determine the physical parameters that define its motion. A drogue is a robotic Lagrangian drifter able to actuate its depth by changing its buoyancy. While underwater, drogues are subject to the flow induced by the motion of the internal wave and do not have access to exact location information. The basic premise is that the evolution of the inter-drogue distance and distance derivative measurements contains enough information for the drogues to be able to fully characterize the internal wave. To our knowledge, there is no algorithmic procedure available in the literature to solve this problem. Scientists widely use drogues drifting passively as monitoring platforms to gather relevant ocean data [71, 28, 38]. The use of autonomous underwater vehicles to detect and characterize internal waves is a relatively new approach. Whereas previous works use ocean measurements such as conductivity, temperature, pressure data [13, 72] or vertical flow velocity [95] to detect and analyze internal waves, our approach is unique in using inter-vehicles measurements. Recent work [44] explores the possibility of actively selecting tidal currents so that drogues can autonomously reach a desired destination. An increasing body of work in the systems and control literature deals with cooperative networks of agents estimating spatial natural phenomena, including ocean [49, 68, 33], river [78], and hurricane sampling [21]. In the problem considered here, drogues are able to actuate their depth through buoyancy changes, but are completely subject to the force of the internal wave in the flow-wise direction. Because of this, the task of determining the wave parameters can be seen as a data fitting problem [84, 83]. Due to the periodic nature of the inter-drogue distance trajectories, our problem has connections with least-squares spectral analysis problems [18, 24]. In general, however, the fact that the wave parameters appear nonlinearly makes the determination of the exact parameters

challenging. Finally, since the presented algorithm can generate many independent estimates of the parameters. These parameter distributions are implicitly defined and non-Gaussian so we adopt a mixture distribution approach to express the distribution as a sum of simpler distributions [29].

Both problems focus on the 'power of many' mobile robotic sensors to cooperatively achieve tasks impossible for one agent alone and are motivated by real-world scientific/engineering problems. In particular, the presented internal wave estimation algorithms were created in conjunction with the design, fabrication, and deployment of Lagrangian drifters at Scripps Institute of Oceanography [42]. Recently, the drifters reached a state where they have begun taking measurements which our algorithms can be tested with. The first experiment had design constraints (too few drifters ready, drifters spaced too far apart, too small ocean stratification) which made our algorithms not applicable. However, by examining the data, we were able to gain insight to extend our algorithms. The data indicated that multiple dominant waves are a physical possibility, so we have worked to extend the algorithms to handle the presence of two ocean internal waves. As of writing this dissertation, a new set of experiments have been run, which are better suited to test the proposed algorithms. However, we have not received or analyzed the data yet. Ongoing work will be made in testing our algorithms against these experiments and if necessary, further adapting the proposed algorithms to estimate the internal waves found in the the experimental data.

1.2 Summary of results

Here, we briefly outline the contributions in this dissertation. The presentation is split between the two problems considered on coalition formation and deployment and robust estimation of ocean internal waves.

1.2.1 Coalition formation and deployment for optimal estimation

The main contribution in the problem is the design and analysis of the **Coalition Formation and Deployment Algorithm**, which is a synchronous and distributed strategy to allow robotic agents to deploy to the optimizer of the spatial estimation problem described above. Under the algorithm, agents autonomously form groups of a given desired size while clustering together and deploying optimally in the environment. The deployment objective is encoded through a locational optimization function whose optimizers correspond to circumcenter Voronoi configurations. The algorithm design combines a repeated game component that governs the dynamics of coalition formation with a spatial motion component that determines how agents' positions evolve. In the coalitional game, agents take probabilistic actions and seek to join a neighboring coalition that most closely resembles one with the desired size. According to the motion coordination law, agents not yet in a well-formed coalition cluster together, while agents in a coalition of the desired size also move towards the circumcenter of their Voronoi cell. Our main result establishes that, for a large class of probabilistic coalition switching laws, the executions of the **Coalition Formation and Deployment Algorithm** converge in finite time to a configuration where agents are coincident with their own coalition and all coalitions are the desired size, and asymptotically converge to an optimal deployment configuration, each with probability 1. For a specific probabilistic coalition switching law, termed **Proportional-to-Number-of-Unmatched-Agents**, where the probability of switching coalitions is proportional to the number of agents not in desired coalitions, we provide upper bounds on the expected coalition formation time under arbitrary and complete communication topologies. For any switching law, we also upper bound the total number of messages sent per timestep during an execution on an arbitrary communication topology. The algorithm does not require the agents to have a common reference frame, and is robust to agent addition and deletion. Finally, we illustrate the correctness, robustness, and time and communication complexity results in simulation.

1.2.2 Estimation of ocean internal waves

Here, we consider the problem of estimating the physical parameters of an internal wave that is propagating horizontally. A group of underwater drogues with no absolute position information are subject to the flow induced by the internal wave and can only measure inter-drogue distances and distance derivatives. Because the drogues only have access to these relative measurements, they must rely on the presence of other drogues to achieve their task. The benefit obtained here by 'the power of many' in the estimation of the ocean flow field is an original feature of this work. We consider separate cases of the presence of a *linear* and *nonlinear* internal wave, beginning with the linear case. We also detail extensions to the proposed algorithms which move towards testing our algorithms' efficacy when applied to real data taken in the ocean off the coast of La Jolla.

Estimating linear waves

For the estimation of linear internal waves, our first contribution is the establishment of an analytic expression for the dynamic evolution of the drogues. This expression shows that the motion of each drogue corresponds to a sum of a linear function (which is common to all) and a periodic function in time. In particular, this result implies that the distance function between any two drogues is periodic (with a different period than the internal wave). This analysis sets the basis for our second contribution, which is the design of the **Vanishing Distance Derivative Detection Strategy**. This algorithm builds on the expression for the drogue dynamics and the fact that inter-drogue distance derivatives become close to zero multiple times across a wavelength to estimate the physical parameters of the internal wave. To our knowledge, the proposed algorithm is the first and only method capable of solving the problem formally defined in Chapter 4. We establish the correctness of the **Vanishing Distance Derivative Detection Strategy** in the case where the inter-drogue measurements are noiseless. Specifically, we make precise the range of times along the period of the internal wave when our method can determine exactly all the parameters. This allows us to give a bound on the minimum required sampling rate. As a third contribution, we characterize the

robustness of our strategy by providing explicit bounds of the errors in the parameter estimation as a function of the errors in the acquisition of the inter-drogue measurements. Finally, we develop a general scheme for aggregating the estimates of the parameters provided by our algorithm at different time instants under noisy measurements. Even though we assume the measurement noise to be Gaussian, the highly nonlinear nature of the drogue motion induced by the internal wave makes the distributions of parameters non-Gaussian and therefore, challenging to aggregate. Our aggregation scheme, termed p**th-Order Parameter Fusion**, is based on determining a pth-order approximation of a parameter's distribution. Individual estimates are then fused together assuming the pth-order approximation is exact. The aggregation scheme results in smaller errors than the individual estimates. Simulations illustrate our correctness and robustness guarantees.

Estimating nonlinear waves

In the nonlinear wave case, we build on the observation that when the crest of the wave is exactly at the midpoint between two drogues, their inter-drogue distance derivative becomes zero to aid in the design of the **Parameter Determination Strategy**. This algorithm is run on the drogues using only relative measurements and is capable of determining all the wave parameters perfectly in the case of noiseless inter-drogue measurements. We discuss the robustness properties of the **Parameter Determination Strategy** to different sources of error such as noise in measurements, presence of multiple waves, and model uncertainty, which arise in realistic implementations. Because many independent, noisy parameter estimates are calculated by the algorithm, we consider a parameter aggregation scheme to minimize the final parameter estimation error. Several simulations illustrate the robustness performance to measurement noise of the **Parameter Determination Strategy**, the effect of initial drogue locations on the algorithm performance, and the ability of parameter estimate aggregation to minimize estimation error. We also adapt the **Parameter Determination Strategy** method to handle the simultaneous estimation of two nonlinear internal waves, as well as include an alternative method to determine the wavenumber parameter

which is based off determining an analytic expression for the change in inter-drogue distance after the wave has completely passed.

1.3 Outline

Here we present the organization of this dissertation, along with a brief summary of each chapter's contents.

Chapter 2: In this chapter we review preliminaries. It begins with notational conventions and then contains notions in reference frames, derivative estimation, optimal facility location, distributed algorithms, probability theory, and game theory.

Chapter 3: This chapter introduces a distributed algorithmic solution to an optimal deployment problem. Its execution causes a network of mobile robotic sensors to form into groups of a desired size while deploying themselves optimally across a spatial environment, leading to the minimization of a cost function that takes into account sensor failures in the construction of optimal estimators. We investigate the proposed algorithm's correctness, time and communication complexity, and robustness to individual failures. Simulations illustrate the proven results.

Chapter 4: This chapter introduces an estimation problem where mobile underwater robots use their inter-vehicle relative measurements to robustly estimate the parameters which define an ocean linear internal wave. The proposed algorithmic solution's correctness and robustness properties are characterized. Because many parameter estimates many be calculated as the robots drift, we also define an estimate aggregation strategy to efficiently fuse estimates. It concludes with simulations that demonstrate the proven results.

Chapter 5: This chapter builds on the work in the previous chapter. It contains a similar problem setup with the difference being the class of internal

wave being estimated. In this chapter, we focus on *nonlinear* internal waves. Their structure requires a different method to produce estimates. Similarly, we investigate our algorithm's correctness, discuss robustness, and provide illustrative simulations. We also show that the method can be extended to situations where two nonlinear waves are present.

Chapter 6: This chapter contains the concluding remarks and ideas for future work.

Chapter 2

Introductory Material

This chapter contains introductory material on notation, reference frames, derivative estimation, computational geometry

2.1 Notational Conventions

Here we present some basic concepts used in this dissertation, starting with some notational conventions. Let $\mathbb{R}$, $\mathbb{R}_{>0}$, $\mathbb{R}_{\geq 0}$, $\mathbb{Z}$, and $\mathbb{Z}_{\geq 1}$, denote the sets of real, positive real, non-negative real, integer, and positive integer numbers, respectively. For $x \in \mathbb{R}$, let $\lfloor x \rfloor \in \mathbb{Z}$ denote the largest integer satisfying $\lfloor x \rfloor \leq x$. For a continuously differentiable function $f : \mathbb{R}^d \to \mathbb{R}$, For notational compactness in some proofs, we let $\partial_k f$ denote the partial derivative with respect to the k-th component. We refer to real-analytic functions simply as 'analytic'. For a vector $\mathbf{v}$, we define the k-th component as $\text{cpnt}_k(\mathbf{v})$. Finally, the Euclidean norm of vector $\mathbf{v}$ is $\|\mathbf{v}\|$.

2.2 Reference Frames

A reference frame Σ_g in $\mathbb{R}^3$ is composed of an origin $\mathbf{p}_g \in \mathbb{R}^3$ and a set of orthonormal vectors $\{\mathbf{e}_{x_g}, \mathbf{e}_{y_g}, \mathbf{e}_{z_g}\} \subset \mathbb{R}^3$. A point $\mathbf{q}$ and a vector $\mathbf{v}$ can be uniquely expressed with respect to the frame Σ_g and are denoted by $\mathbf{q}^g$ and $\mathbf{v}^g$, respectively. Next, let $\Sigma_b = (\mathbf{p}_b, \{\mathbf{e}_{x_b}, \mathbf{e}_{y_b}, \mathbf{e}_{z_b}\})$ be a reference frame fixed to a moving body.

The origin of Σ_b is a point $\mathbf{p}_b$, denoted as $\mathbf{p}_b^g$ when expressed with respect to Σ_g. The orientation of Σ_b is characterized by the rotation matrix Q_b^g whose columns are the vectors $\{\mathbf{e}_{x_b}, \mathbf{e}_{y_b}, \mathbf{e}_{z_b}\}$ expressed with respect to Σ_g. With this notation, a change of reference frame is given by $\mathbf{q}^g = Q_b^g \mathbf{q}^b + \mathbf{p}_b^g$ and $\mathbf{v}^g = Q_b^g \mathbf{v}^b$.

2.3 Derivative estimation from noisy data

Here, we consider estimating an analytic function $f : \mathbb{R} \to \mathbb{R}$ and its first (time) derivative $f' : \mathbb{R} \to \mathbb{R}$ from n evenly sampled measurements in the sampling window T, when the measurements are corrupted by additive Gaussian noise. So that our method is causal, at any given time we only use the n most recent measurements. Additionally, for computational reasons, at every timestep, we relabel the current timestep as $t = 0$ and the times of all other measurements accordingly, i.e., we have measurements for times $\{t_\zeta = \frac{-\zeta}{n-1}T\}_{\zeta \in \{0,\dots,n-1\}}$. The noisy measurement at t_ζ is

$$\tilde{f}(t_\zeta) = f(t_\zeta) + \epsilon(t_\zeta), \quad \epsilon \sim \mathcal{N}(0, \sigma^2).$$

The method we use is a polynomial smoothing filter approach [81] because this allows us to justify that the derivative estimates are unbiased Gaussian random variables. For $p \ll n \in \mathbb{Z}_{\geq 1}$, we construct a pth-order polynomial filter from n evenly spaced noisy measurements over the sampling window T using the data $\{(t_\zeta, \tilde{f}(t_\zeta))\}_{\zeta \in \{0,\dots,n-1\}}$. Consider the Taylor series expansion,

$$\underbrace{\begin{bmatrix} \tilde{f}(t_0) \\ \tilde{f}(t_1) \\ \vdots \\ \tilde{f}(t_{n-1}) \end{bmatrix}}_{\tilde{\mathbf{F}}} = \underbrace{\begin{bmatrix} 1 & 0 & \dots & 0 \\ 1 & t_1 & \dots & t_1^p \\ \vdots & \vdots & \vdots & \vdots \\ 1 & t_{n-1} & \dots & t_{n-1}^p \end{bmatrix}}_{V} \underbrace{\begin{bmatrix} f(t_0) \\ f'(t_0) \\ \vdots \\ \frac{1}{p!} f^{(p)}(t_0) \end{bmatrix}}_{\mathbf{G}} + \underbrace{\begin{bmatrix} 0 \\ \sum_{j=p+1}^{\infty} f^{(j)}(t_0) \frac{t_1^j}{j!} \\ \vdots \\ \sum_{j=p+1}^{\infty} f^{(j)}(t_0) \frac{t_{n-1}^j}{j!} \end{bmatrix}}_{\epsilon_{\text{bias}}} + \underbrace{\begin{bmatrix} \epsilon_0 \\ \epsilon_1 \\ \vdots \\ \epsilon_{n-1} \end{bmatrix}}_{\epsilon_{\text{random}}}.$$

More compactly, this can be written as $\tilde{\mathbf{F}} = V\mathbf{G} + \epsilon_{\text{bias}} + \epsilon_{\text{random}}$. The least-squares estimates for $f(t_0)$ and $f'(t_0)$ are given by

$$\hat{f}(t_0) = \text{cpnt}_1((V^T V)^{-1} V^T \tilde{\mathbf{F}}),$$
$$\hat{f}'(t_0) = \text{cpnt}_2((V^T V)^{-1} V^T \tilde{\mathbf{F}}).$$

We ignore the bias which arises from considering only the pth-order expansion of f because, for a fixed p, it can be made arbitrarily close to zero by choosing the sampling window T small enough. With this observation in mind, the estimate of $f'(t_0)$ is an (unbiased) Gaussian random variable with variance $\sigma^2_{f'} = \mathrm{cpnt}_{2,2}((V^TV)^{-1})\sigma^2$.

2.4 Computational geometry

Here, we introduce some computational geometric definitions and results that play an important role in the dissertation, beginning with some basic geometric notions.

2.4.1 Basic geometric notions

Given a set $S \subset X$, let $\mathbb{F}(S)$ denote the collection of finite subsets of S, $S^c = X \setminus S$ its complement, and $|S|$ its cardinality. Let $\mathrm{vr} : \mathbb{R}^d \to \mathbb{R}^d$ be defined by $\mathrm{vr}(u) = u/\|u\|$ for $u \in \mathbb{R}^d \setminus \{0\}$, and $\mathrm{vr}(0) = 0$. We let $B(x,r) = \{p \in \mathbb{R}^d \mid \|x-p\| \leq r\}$.

Definition 1 (Circumcenter and circumradius)**.** *The circumcenter of a set of points P, denoted* $\mathrm{CC}(P)$*, is the center of the ball of minimum radius, called the circumradius and denoted* $\mathrm{CR}(P)$*, which encloses all points in P.*

2.4.2 Voronoi partitions and spatial optimization

Definition 2 (Voronoi partition)**.** *Given $Q \subset \mathbb{R}^d$ and a finite set of points $P = \{p_1, \ldots, p_N\} \subset Q$, the Voronoi partition $V(P) = \{V_1(P), \ldots, V_N(P)\}$ of Q is defined by*

$$V_i(P) = \{q \in Q \mid \| q - p_i\| \leq \| q - p_j\|, \ \forall\, p_j \in P\}.$$

Note that $V_i(P)$, the Voronoi cell of p_i, is the set of points in Q closer to p_i than to any of the other points in P. The points p_i and p_j are (Voronoi) neighbors if the boundaries of their cells intersect. To compute the Voronoi cell of p_i, all

that is required is the location of its neighbors in P. [17] introduces a procedure, that we term the **Adjust radius** strategy, which does the following: starting from $r = 0$, it repeatedly grows r until all Voronoi neighbors of p_i are guaranteed to be contained in $B(p_i, r)$.

Given a partition $\{W_1, \ldots, W_N\}$ of Q, the disk-covering function $\mathcal{H}_{\mathrm{DC},N}$ is defined by

$$\mathcal{H}_{\mathrm{DC},N}(p_1, \ldots, p_N, W_1, \ldots, W_N) = \max_{i \in \{i,\ldots,N\}} \max_{q \in W_i} \|q - p_i\|_2.$$

The value of $\mathcal{H}_{\mathrm{DC},N}$ solves the following problem: cover the whole environment with balls centered at the points in $P = \{p_1, \ldots, p_N\}$ with minimum common radius such that $W_i \subset B(p_i, r)$, for $i \in \{1, \ldots, N\}$. For convenience, we set $\mathcal{H}_{\mathrm{DC},N}(p_1, \ldots, p_N) = \mathcal{H}_{\mathrm{DC},N}(p_1, \ldots, p_N, V_1, \ldots, V_N)$.

Two properties are worth noting [12]:

Proposition 2.4.1 (Optimal solutions of disk-covering function)**.** *For a fixed configuration, the Voronoi partition is optimal among all partitions,*

$$\mathcal{H}_{\mathrm{DC},N}(p_1, \ldots, p_N, V_1(P), \ldots, V_N(P)) \leq \mathcal{H}_{\mathrm{DC},N}(p_1, \ldots, p_N, W_1, \ldots, W_N).$$

For a fixed partition, the cells' circumcenters are optimal:

$$\mathcal{H}_{\mathrm{DC},N}(\mathrm{CC}(W_1), \ldots, \mathrm{CC}(W_N), W_1, \ldots, W_N) \leq \mathcal{H}_{\mathrm{DC},N}(p_1, \ldots, p_N, W_1, \ldots, W_N).$$

Under certain technical conditions, see [32], optimizing $\mathcal{H}_{\mathrm{DC},N}$ corresponds to minimizing the maximum error variance in the estimation of a random spatial field, whose model is briefly described in Section 2.6.3. Similarly, in the situation of discrete events happening with equal likelihood everywhere in an environment, placing sensors at an optimizer of $\mathcal{H}_{\mathrm{DC},N}$ yields a configuration which minimizes the worst-case distance (error) between an event and the nearest sensor. The deployment objective function that motivates the problem in Chapter 3 is given by

$$\mathcal{H}_{N,g}(p_1, \ldots, p_N) = \frac{1}{\binom{N}{g}} \sum_{\{s_1,\ldots,s_g\} \in C(N,g)} \mathcal{H}_{\mathrm{DC},g}(p_{s_1}, \ldots, p_{s_g}), \tag{2.1}$$

where $C(N, g)$ denotes the set of unique g-sized combinations of elements in $\{1, \ldots, N\}$. This function corresponds to the expected disk-covering performance of a network of N agents where only g of them are working and their identity is unknown. Optimizers of $\mathcal{H}_{N,g}$ correspond to grouping agents into coincident clusters of a specific size, say κ, that themselves are optimally deployed according to $\mathcal{H}_{\mathrm{DC},\lceil\frac{N}{\kappa}\rceil}$, see [15]. The cluster size κ is a function of N, g, and Q. For instance, for the case where Q is an interval, if only 1 agent is expected to be working correctly, all agents should form one coalition of size N. If 2 agents are expected to function, the optimal coalition size is $N/2$. Finally, if $N-1$ are expected to function, the optimal coalition size is 2.

2.5 Distributed algorithms

Here we describe the notion of a distributed algorithm. Suppose a group of spatially distributed sensing/computing robots are dispersed in an environment. A *centralized* algorithm is a strategy implemented on each robot which solves a given task using the data acquired from all of the robots. A *distributed* algorithm is a strategy which solves the same task but uses only a subset of the total data.

We begin with some basic definitions about graphs.

Definition 3 (Directed graph)**.** *A directed graph or a digraph is a pair $G = (V, E)$ where V is the vertex set and E is the edge set such that $E \subset V \times V$. A vertex $v_i \in V$ is connected to $v_j \in V$ if $(v_i, v_j) \in E$.*

Definition 4 (Undirected graph)**.** *An undirected graph is a digraph $G = (V, E)$ such that $(v_i, v_j) \in E$ implies that $(v_j, v_i) \in E$ as well.*

Definition 5 (Neighbor set)**.** *The neighbor set of agent i in the graph $G = (V, E)$ is the set of agents $\mathcal{N}_i = \{v_j \in V \mid (v_i, v_j) \in E\}$.*

A synchronous network is a group of processors that each possess a local state, exchange messages along the edges of a digraph, and compute an update to their local state based on the received messages. The processors alternate between the two tasks of exchanging messages with its neighboring processors and performing a computation step. Next, we formalize the notion of a network.

Definition 6 (Network)**.** *A synchronous network $\mathcal{S}$ represented by the digraph (I, E_{comm}), where:*

- *$I = \{1, \ldots, n\}$ is the set of unique identifiers and*
- *E_{comm} is a set of directed edges over the vertices $\{1, \ldots, n\}$, called the communication links.*

Next, we define the local state and algorithms that each processor possesses and executes, respectively.

Definition 7 (Distributed algorithm)**.** *A distributed algorithm $\mathcal{DA}$ for a network $\mathcal{S}$ consists of the sets:*

- *$\mathfrak{A}$, a set containing the `Null` element, called the communication alphabet - elements of $\mathfrak{A}$ are called messages,*
- *$W^{[i]},\ i \in I$, called the processor state sets, and*
- *$W_0^{[i]} \subseteq W^{[i]},\ i \in I$, sets of allowable initial conditions*

and of the maps

- $\text{msg}^{[i]} : W^{[i]} \times I \to \mathfrak{A},\ i \in I$, *called message-generating functions, and*
- $\text{stf}^{[i]} : W^{[i]} \times A^n \to W^{[i]},\ i \in I$, *called the state-transition functions.*

Each round of a distributed algorithm contains one execution of $\text{msg}^{[i]}$, one transmission of the generated message to its recipients, the collection of messages generated by other agents, and one execution of $\text{stf}^{[i]}$, for each $i \in I$. Let the set of messages received by agent i at each round of the algorithm be defined as $Y^{[i]} \in \mathfrak{A}^N$.

Definition 8 (Distributed algorithm over a graph)**.** *An algorithm is distributed over the graph $\mathcal{G} = (V, E)$ if the messages received at each round has the following form for all $i, j \in \{1, \ldots, N\}, j \notin \mathcal{N}_i$ implies that $Y_j^{[i]} =$ `Null`.*

Remark 2.5.1 (Algorithm completion and correctness)**.** In this work we define the moment that an algorithm completes as the first instance in which the network-wide task is achieved. Also, we define a *correct* algorithm as one that provably completes the desired task. Because this work considers algorithms for estimating constant parameters, we distinguish this definition from that of a correct estimator, which is an unbiased estimator whose estimation variance asymptotically goes to zero. •

Having defined a distributed algorithm and our definition of algorithm completion, we are now ready to quantify measures of an algorithm's performance. The two which we consider are the time to completion (time complexity) and the number of messages sent per timestep (communication complexity). Intuitively, one would like to design algorithms which solve a given task with a minimal complexity.

Definition 9 (Time complexity)**.** *The worst-case time complexity of an algorithm $\mathcal{DA}$ is the maximum number of rounds required by the execution of $\mathcal{DA}$ among all possible initial conditions until the algorithm completes.*

Definition 10 (Communication complexity)**.** *The worst-case communication complexity of an algorithm $\mathcal{DA}$ is the maximum number of messages required by the execution of $\mathcal{DA}$ among all possible initial conditions until the algorithm completes.*

In this work we consider non-deterministic algorithms, so that the network's evolution starting from a given initial condition is random and non-unique. Thus, we are interested in the *expected*, worst-case complexity.

2.6 Probability notions

Here we gather a variety of probability notions which are needed in this dissertation, beginning with two fundamental results: the Borel-Cantelli Lemma and the Law of iterated expectations [77, 9].

Let X be a random variable that has outcomes $\{x_1, x_2, \dots\}$ with probabilities $\{p_1, p_2, \dots\} \subset \mathbb{R}_{\geq 0}$. An event E is a set of outcomes of X. For brevity, we use $\mathrm{P}\left(E\right) = \mathrm{P}\left(X \in E\right)$.

Definition 11 (Events occurring infinitely often and almost always)**.** *Given a sequence of events* $\{E_n\}_{n=1}^{\infty}$*, let*

$$\limsup_n E_n = \{E_n \ i.o.\} = \bigcap_{n=1}^{\infty} \bigcup_{k=n}^{\infty} E_k,$$

$$\liminf_n E_n = \{E_n \ a.a.\} = \bigcup_{n=1}^{\infty} \bigcap_{k=n}^{\infty} E_k.$$

Here 'i.o.' stands for infinitely often, and 'a.a.' stands for almost always. Note that $\{E_n \text{ i.o.}\}^c = \{E_n^c \text{ a.a.}\}$.

Lemma 2.6.1 (Borel-Cantelli Lemma)**.** *Given a sequence of events* $\{E_n\}_{n=1}^{\infty}$ *satisfying* $\sum_{n=1}^{\infty} \mathrm{P}\left(E_n\right) < \infty$*. Then* $\mathrm{P}\left(\limsup_n E_n\right) = 0$*.*

Definition 12 (Integrable random variables)**.** *A random variable* X *is said to be integrable if* $\mathrm{E}[|X|] < \infty$*.*

Proposition 2.6.2 (Law of iterated expectations)**.** *For random variables* X *and* Y*, if* X *is integrable, then*

$$\mathrm{E}[X] = \mathrm{E}_Y[\mathrm{E}_{X|Y}[X|Y]].$$

2.6.1 Aggregation and convergence of random variables

This section contains definitions on aggregation and convergence of random variables.

Definition 13 (Optimal aggregation of random variables)**.** *Given independent random variables* x_1 *and* x_2 *with mean* $\mathrm{E}[x_1] = \mathrm{E}[x_2] = \mu$ *and variances* $\mathrm{Var}[x_1] = \sigma_1^2$*,* $\mathrm{Var}[x_2] = \sigma_2^2$*, define the optimal aggregating function* OptAgg *by*

$$\mathrm{OptAgg}(x_1, \sigma_1^2, x_2, \sigma_2^2) = \left(\frac{\frac{x_1}{\sigma_1^2} + \frac{x_2}{\sigma_2^2}}{\frac{1}{\sigma_1^2} + \frac{1}{\sigma_2^2}}, \frac{1}{\frac{1}{\sigma_1^2} + \frac{1}{\sigma_2^2}} \right).$$

Here, $\mathrm{cpnt}_1(\mathrm{OptAgg})$ is the new random variables and $\mathrm{cpnt}_2(\mathrm{OptAgg})$ is its variance. This is the convex combination of x_1 and x_2 that results in the random variable with the smallest variance.

Here, we define two notions used for the convergence of sequences of random variables, beginning with convergence in probability.

Definition 14 (Convergence in probability)**.** *A sequence of random variables* $\{X_i\}$ *converges* in probability *towards* X *if for all* $\epsilon > 0$*, the following holds:*

$$\lim_{n\to\infty} \mathrm{P}\left(|X_n - X| \geq \epsilon\right) = 0.$$

Next, we define convergence with probability 1.

Definition 15 (Convergence with probability 1)**.** *A sequence of random variable* $\{X_i\}$ *converges* with probability 1 *towards* X *if the following holds:*

$$\lim_{n\to\infty} \mathrm{P}\left(X_n = X\right) = 1.$$

2.6.2 Markov chains

Here, we define a Markov chain and a useful definition [54, 56].

Definition 16 (Markov chain)**.** *A Markov chain is a sequence of random variables* $\{X_i\}$ *with the Markov property, namely that, given the present state, the future and past states are independent. Formally,*

$$\mathrm{P}\left(X_{i+1} = x | X_1 = x_1, X_2 = x_2, \ldots, X_i = x_i\right) = \mathrm{P}\left(X_{i+1} = x | X_n = x_n\right).$$

Definition 17 (Hitting time)**.** *Given a sequence of random variables* $\{X_i(\omega)\}$ *generated from the randomization* $\omega \in \Omega$ *and goal set* A*, we define the hitting time of set* A*,* τ_A *as*

$$\tau_A(\omega) = \inf\{i \in \{1, 2, \ldots\} | X_i(\omega) \in A\}$$

and the expected hitting time of A *as* $\mathrm{E}_\omega[\tau_A(\omega)]$*.*

2.6.3 Spatial random fields

For completeness, we briefly recall the spatial random field model used in [32], which, as explains in Section 2.4.2 is a motivation of our work. A more complete exposition can be found in the literature of estimation of spatial processes, see e.g., [19, 1].

Definition 18 (Second-order stationary, isotropic random process)**.** *A random process Z is second-order stationary and isotropic if it has constant mean,* $\mathrm{E}[Z(s)] = \mu$*, and its covariance is of the form* $\mathrm{Cov}[Z(p_1), Z(p_2)] = g(\|p_1 - p_2\|)$*, for some decreasing function* $g : \mathbb{R}_{\geq 0} \to \mathbb{R}_{\geq 0}$*.*

The assumed model for the spatial random field Z is

$$Z(s) = \mu(s) + \delta(s), \quad s \in \mathcal{D}, \tag{2.2}$$

with mean function μ known. Also, δ is a zero-mean second-order stationary random process with a known decreasing isotropic covariance function, g.

2.7 Game theory

Here, we introduce some basic notions from game theory [58, 30, 7].

Definition 19 (N-player, simultaneous action game)**.** *A game is defined by* $\mathcal{G} = (\mathcal{I}, \mathcal{A}, u)$*, where*

- $\mathcal{I} = \{1, \ldots, N\}$ *is the set of N players,*
- $\mathcal{A}_i$ *is set of actions available to player i, and*
- $u_i : \mathcal{A} \to \mathbb{R}$ *is the payoff function for player i.*

In this game, all players have knowledge of $\mathcal{G}$. They simultaneously choose an action and receiving the payoff corresponding to the result of all players' actions. Each player wishes to choose its action to maximize its own payoff. The celebrated Nash equilibrium provides an answer to this.

Definition 20 (Pure Nash equilibrium)**.** *A pure Nash equilibrium to the game* $\mathcal{G} = (\mathcal{I}, \mathcal{A}, u)$ *is a joint action set* $(a_1^*, \ldots, a_n^*) \in \mathcal{A}$ *such that*

$$u_i(a_i', a_{-i}^*) \leq u_i(a_i^*, a_{-i}^*), \quad \forall a_i' \in \mathcal{A}_i, \quad \forall i \in \mathcal{I},$$

where a_{-i} is the collection of all joint actions except a_i.

Note that all players choose an action corresponding to a Nash equilibrium implies that no player can improve their payoff by playing a different action a_i'.

Remark 2.7.1 (Existence of (mixed) Nash equilibria)**.** *In many games, pure Nash equilibria are not guaranteed to exist. To aid with this, one can extend the notion of players' actions to include* mixed *strategies, where each player i chooses a probability distribution from which its action is chosen. In the case that the number of actions for each player i, $\mathcal{A}_i$ is finite, there is guaranteed to exist at least one* mixed *Nash equilibrium.*

2.7.1 Coalition formation games

Hedonic coalition formation games [10] are N-player noncooperative games [30, 7] where players attempt to join/stay in preferable coalitions. Each player is hedonic (non-cooperative) because the utility it assigns to a given network coalition partitioning is only a function of its own coalition. Each player's action set is finite: it can stay in the current coalition or join another coalition.

Definition 21 (Coalition partition and coalitions)**.** *For a finite set of players $\mathcal{I} = \{1, \ldots, N\}$, a finite coalition partition is a collection $\Pi = \{S_k\}_{k=1}^{K}$, $K \in \mathbb{Z}_{\geq 1}$, that partitions $\mathcal{I}$. The subsets S_k are called coalitions. For player i and partition Π, let $S_\Pi(i)$ be the set $S_k \in \Pi$ such that $i \in S_k$.*

Definition 22 (Coalition formation game)**.** *A coalition formation game is defined by $\mathcal{G} = (\mathcal{I}, \mathcal{A}, \succeq)$,*

- *$\mathcal{I} = \{1, \ldots, N\}$ is a finite set of players,*
- *$\mathcal{A}_i \subset \Pi \cup \{\emptyset\}$ are the coalitions agent i may join, and*
- *$\succeq_i$ is agent i's coalition preference ordering, defined over the set $\mathfrak{S}_i = \{S \in \mathbb{F}(\mathcal{I}) \mid i \in S\}$.*

Definition 23 (Nash stable partition)**.** *A coalition partition Π is called Nash stable if, for each $i \in \mathcal{I}$,*

$$S_\Pi(i) \succeq_i S_k \cup \{i\}, \quad \forall S_k \in \Pi \cup \{\emptyset\}. \tag{2.3}$$

In coalition formation games, a player has full information about which coalitions all other players are in and may join any of them. This is in contrast to the work in this dissertation, where coalition information is only partial due to the limited capabilities of individual agents. Let us introduce definitions which help capture the spatially-limited nature of coalition information.

Definition 24 (Consistent coalition state)**.** $(S_1, \ldots, S_N)$ *is a* consistent *coalition state if* $i \in S_i$ *and* $S_j = S_i$*, for each* $j \in S_i$*, for each* $i \in \mathcal{I}$*.*

Note that for a consistent coalition state, $\{S_1, \ldots, S_N\}$ reduces to a finite coalition partition of $\mathcal{I}$. Let $\tau_i \subseteq \mathcal{I}$ denote the set of agents whose coalition information i has access. Letting $S_0 = \emptyset$, the function best-set defines the players whose coalitions i most prefers to be a member of,

$$\text{best-set}(\succeq_i, \{(k, S_k)\}_{k \in \tau_i}) = \{j \in \tau_i \cup \{0\} \mid S_j \cup \{i\} \succeq_i S_k \cup \{i\}, \forall\, k \in \tau_i \cup \{0\}\}.$$

Chapter 3

Hedonic coalition formation for optimal deployment

This chapter is motivated by optimal spatial sampling problems under possibly failing communications. Consider a group of mobile robotic sensors that take point measurements of a random field over an environment and relay them back to a data fusion center. Assume that because of the features of the medium and the limited agent communication capabilities, it is known that only a fraction of these packets will arrive at the center, but it is not a priori known which ones will. Given that some sensors are not working and their identity is unknown, a reasonable strategy consists of grouping sensors together into clusters so that the likelihood of obtaining a measurement from the position of each cluster is higher. In this chapter, our aim is to design a distributed algorithm that makes the network autonomously create groups of a desired size such that (i) members of each individual group become coincident, and (ii) the groups deploy optimally with regards to the spatial estimation objective.

Literature review: There is an increasing body of research that deals with spatial estimation problems with possibly failing communications where packets are either received without corruption or not received at all, see e.g., [88, 82, 35, 15]. In particular, [15] shows that, for the problem motivating our algorithm design, the clustering strategy outlined above is optimal in some cases: the configurations that maximize the expected information content of the measurements retrieved at

the center correspond to agents grouping into clusters, and the resulting clusters being deployed optimally. Achieving such desirable configurations is challenging because of the spatially distributed nature of the problem and the agent mobility. In this regard, the notions of spatial coverage and agent clustering (the latter understood as physical co-location), as well as our proposed algorithmic solution, are different from those in typical hierarchical clustering problems, see e.g. [93, 5], where sensors are static and the objective is to minimize the cost incurred when relaying messages to a data fusion center. Closer to our setup, [40] define clusters as groups of mobile sensors in locations such that their density is above the expected average density. Using a control law based on whether sensors are in a cluster or not, the network minimizes the distance traveled by the sensors to deploy. Our technical approach combines elements of spatial facility location [60], rendezvous and deployment of multi-agent systems [12], and coalition formation games [10, 6]. From a game-theoretic perspective, our analysis of the coalition formation dynamics is novel because of the consideration of evolving and partial interaction topologies. From a motion coordination perspective, the novelty relies on the coupled dynamics between the coalition formation, the clustering, and the network deployment. Other works in cooperative control employ game-theoretic ideas to solve tasks such as formation control, target assignment, self-organization for efficient communication, consensus, and sensor coverage, see e.g. [34, 52, 3, 80]. Given the algorithmic design choice of the agents' utility function, our work has connections to weakly acyclic games [53, 51]. Specifically, under a fixed, complete communication graph where all agents can join any coalition they wish, our game can be cast as a weakly acyclic game. However, in general, the limited information available to agents, the dynamic interaction topology, and the dependence of the individual action sets on this topology makes the framework of weakly acyclic games not directly applicable. We build on the well-established notions of time and communication complexity in distributed algorithms [69, 50, 12] to characterize the performance of our. Since in the repeated coalition formation game agents take probabilistic actions, we consider the expected time complexity. In principle, our algorithm can be described as a Markov chain, where the coalition formation time

can be exactly defined as the first hitting time for the set of goal states [57, 47]. However, defining the probabilistic transition function becomes difficult as the number of total agents grows. Thus, we adopt a drift analysis approach [36] to provide an upper bound on the time complexity.

Organization: Section 3.1 states the problem setup, and Section 3.2 contains the description of our algorithm. Section 3.3 analyzes its correctness and Section 3.4 characterizes its complexity. Section 3.5 illustrates our results.

3.1 Problem statement

A group of robotic sensors with unique identifiers $\mathcal{I} = \{1, \ldots, N\}$ moves in a convex polygon $Q \subset \mathbb{R}^2$. Let p_i denote the location of agent i and $P = (p_1, \ldots, p_N)$ denote the overall network configuration. We consider arbitrary agent dynamics, assuming each agent can move up to a distance $d_{\max} \in \mathbb{R}_{>0}$ within one timestep,

$$p_i(\ell + 1) \in B(p_i(\ell), d_{\max}), \quad \ell \in \mathbb{Z}.$$

Through either sensing or communication, we assume each agent i can get the relative position and identity of agents within distance $r_i \in \mathbb{R}_{>0}$. During the coalition formation process, agents can interact with other agents within this radius. Agent i can adjust r_i but the cost of acquiring information is an increasing function of it. Inter-agent communication occurs instantaneously.

Given the problem scenario described above, the network's objective is dual. On the one hand, agents want to cluster into groups of a predefined size κ, which we assume is known a priori. Equivalently, the network wants to self-assemble into $\left\lfloor \frac{N}{\kappa} \right\rfloor$ clusters of size κ, with possibly one additional cluster of size z, $0 \leq z < \kappa$, with $N = \left\lfloor \frac{N}{\kappa} \right\rfloor \kappa + z$. On the other hand, the resulting clusters should be positioned in the environment so as to minimize $\mathcal{H}_{\mathrm{DC},\lceil \frac{N}{\kappa} \rceil}$. As discussed in Section 2.4, such deployments correspond to optimizers of (2.1) for a class of spatial estimation problems with unreliable sensors. For convenience, we define a partition to be a *goal coalition partition* if the cardinality of m of its coalitions is κ, with the cardinality of the remaining one equal to z, if it exists.

A trivial solution to this problem would be to first elect $\lceil \frac{N}{\kappa} \rceil$ leaders and have each leader recruit $\kappa - 1$ followers. Then each group could rendezvous, and afterwards, the overall network would deploy. However, this method is neither distributed nor robust to agent failures. Our aim is to create a distributed algorithm that accomplishes the dual network objective in a robust and efficient way.

3.2 Coalition formation and deployment

Here, we solve the problem posed in Section 3.1 with the **Coalition Formation and Deployment Algorithm**. This distributed, synchronous strategy specifies for each agent the dynamics of coalition formation and spatial motion. Section 3.2.1 outlines the logic used by agents to determine which coalition to join as well as the supporting inter-agent communication and Section 3.2.2 discusses how agents decide to move depending on their coalition size and the deployment objective.

Before specifying the dynamics, we describe the required memory of each agent and appropriate initializations. The memory $\mathcal{M}_i$ of agent i is composed of

- the *coalition set* C_i. Elements of this set are of the form (j, p_j), i.e., identity and position of the member. For convenience, we set $(i, p_i) \in C_i$ and $C_0 = \emptyset$;
- the *communication radius* r_i at which the agent interacts with other agents not necessarily in its coalition;
- the *neighboring set* $\mathcal{N}_i$ corresponding to agents within distance r_i, i.e., $(j, p_j) \in \mathcal{N}_i$ iff $p_j \in B(p_i, r_i)$;
- the *farthest-away radius* $\mathfrak{r}_i$, corresponding to the maximum distance to members of its coalition set.
- the *flag* **last**, which indicates if an agent belongs to the single final coalition not of size κ when $\lceil \frac{N}{\kappa} \rceil \neq \frac{N}{\kappa}$.

The operators $\mathrm{id}(\cdot)$ and $\mathrm{pos}(\cdot)$ extract identities and positions, respectively, from sets with elements of the form (i, p_i). Initialization requires a consistent coalition state $(\mathrm{id}(C_1), \ldots, \mathrm{id}(C_N))$, $r_i \in \mathbb{R}_{\geq 0}$, and **last** = False.

The vocabulary all agents can recognize are

- an agent sends the word *query* to ask for the identities of another agent's current coalition;
- an agent sends a packet with the word *leave*/*join* along with an agent identity to indicate that the agent is leaving/joining the recipient's coalition.

Remark 3.2.1. *(Communication protocol)* The communication radius r_i should be thought of as the distance at which agent i must interact with other agents not necessarily in its coalition. We do not enter into the specifics of how this interaction is actually implemented. This might be through direct, one-hop communication or, if the radius is large, through indirect, multi-hop routing involving other network agents. Lemma 3.2.3 below ensures the radius is kept, at each timestep, at the smallest value that guarantees successful coalition formation. •

3.2.1 Coalition formation game

The formation of coalitions evolves according to a simultaneous-action hedonic coalition game with partial information. Let us start with an informal description.

> *[Informal description]:* The agents' objective is to be in a κ-sized coalition. There are two rounds of communication per timestep. In the first one, each agent acquires information to determine if any neighboring coalition is more attractive than its current one. In the second one, the agents involved in a coalition change (either because they have decided to switch or because someone else decided to join their coalition) exchange information to update the coalition membership.

Next, we formally describe the hedonic coalition formation game. The agent i's preference ordering $\succeq_i$ over $\mathfrak{S}_i$ is

$$\begin{aligned}\{S \in \mathfrak{S}_i \mid |S| = \kappa\} \succ \{S \in \mathfrak{S}_i \mid |S| = \kappa - 1\} \succ \dots \\ \succ \{S \in \mathfrak{S}_i \mid |S| = 1\} \succ \{S \in \mathfrak{S}_i \mid |S| = \kappa + 1\} \succ \dots \\ \succ \{S \in \mathfrak{S}_i \mid |S| = N\}. \quad (3.1)\end{aligned}$$

According to (3.1), agents most prefer to be in κ-sized coalitions. They also prefer to be in a coalition of size 1 over any coalition of size larger than κ.

Next, we specify the two rounds of communication that take place per timestep. Agents who already are in a coalition of size κ do not actively take part in this process; they only respond to other agents' messages. First, agents execute the **Best Neighbor Coalition Detection** strategy described as Algorithm 3.1.

Table 3.1: **Best Neighbor Coalition Detection Algorithm**

Executed by: agents i if $|C_i| \neq \kappa$

1: Acquire $\mathcal{N}_i$ (**get location of neighbors**)
2: Send $(\texttt{query}, r_i)$ at r_i to $\mathrm{id}(\mathcal{N}_i \setminus C_i)$
3: Receive $\mathrm{id}(C_j)$ from all $j \in \mathrm{id}(\mathcal{N}_i \setminus C_i)$ (**request/receive coalition sizes**)
4: **if** $i \notin$ best-set$(\succeq_i, \{k, \mathrm{id}(C_k)\}_{k \in \mathrm{id}(\mathcal{N}_i)})$ **then**
5: **with probability** p **do**
6: Set j^* from best-set$(\succeq_i, \{k, \mathrm{id}(C_k)\}_{k \in \mathrm{id}(\mathcal{N}_i)})$ (**identify best coalition to join**)
7: **if** $j^* \neq 0$ **then** $r_i := \|p_{j^*} - p_i\|$
8: **end if**
9: **end**
10: **end if**

According to this strategy (cf. step 5), an agent that finds a neighboring coalition better than its own will decide to join it with some probability of the form

$$p = \begin{cases} f(|C_1|, \ldots, |C_N|, N, \kappa), & \text{if } |C_i| \neq \kappa, \\ 0, & \text{if } |C_i| = \kappa, \end{cases} \tag{3.2}$$

where the function f takes values in the interval $(0, 1)$ for all finite N. The form of f affects the convergence rate of the algorithm, which we will investigate later.

Remark 3.2.2. *(Justification and tradeoffs for probabilistic actions)* The probabilistic model for actions described in (3.2) helps avoid deadlock situations that may result from the decentralized nature of the game. As an example, in a situation with two groups of size $\kappa - 1$, all agents will desire to join the other group. In such case, a group of size κ would never form. Instead, under (3.2), there is a positive probability that agents in only one of the groups act, breaking the deadlock. In contrast with a one-agent-acting-per-timestep policy, (3.2) allows multiple

agents to switch coalitions at the same timestep. One tradeoff of probabilistic actions is that the identities of the agents in each coalition cannot be known a priori. Another tradeoff is that, at times, agents do not make the most beneficial action to achieve the ultimate objective given a specific configuration. However, as stated above, it is precisely this occasional sub-optimality that helps eliminate deadlock situations. •

Next, all agents run the **Coalition Switching** strategy found in Algorithm 3.2. This strategy builds on the input j^* provided to i by the **Best Neighbor Coalition Detection** strategy. Agents with $j^* \neq i$ switch coalitions. If $j^* = 0$, i forms its own coalition. Otherwise, i interacts with agent j^* to join its coalition. After switching, agents update coalition memberships and the communication radii required to determine the position of other members so that the coalition state remains consistent.

3.2.2 Motion control law

Here, we describe how agents move at each timestep, beginning with an informal description:

> *[Informal description]:* At each timestep, agents adjust their communication radius and move. Both actions depend on the size of their coalition. Agents not yet in a coalition of size κ increase their radius to improve the chances of finding a better coalition and move towards their coalition members. Agents in a coalition of size κ adjust their radius to ensure they can calculate their Voronoi cell and move towards both their coalition members and the cell circumcenter.

Before formally defining the radius adjustment and motion algorithm, we introduce the **get-together-toward-goal** function $\text{gttg} : S \times \mathbb{F}(S) \times S \to S$ that will help define the agents' motion. It's purpose is to get a set of points P closer to each other while moving towards a goal q. Define $\text{gttg}(p, P, q) = p + w_1 + w_2$, where we use the shorthand notation $P_0 = P \cup \{p\}$,

$$w_1 = \min\{\| \operatorname{CC}(P_0) - p\|, d_1(r)\} \ \operatorname{vr}(\operatorname{CC}(P_0) - p),$$
$$w_2 = \min\{\|q - (p + w_1)\|, d_2(r)\} \ \operatorname{vr}(q - (p + w_1)),$$

Table 3.2: **Coalition Switching Algorithm**

Executed by: all agents i

if $j^* \neq i$ **then**
  Send $(\texttt{leave}, i)$ at $\mathfrak{r}_i$ to $\mathrm{id}(C_i)$ (**alert old coalition**)
  if $j^* \neq 0$ **then**
    Send $(\texttt{join}, i, r_i)$ at r_i to j^* (**alert new coalition**)
  end if
end if
$M := \{k \in \mathcal{I} \mid i \text{ gets } \texttt{join} \text{ from } k\}$ (**agents relying on i to aid switch**)
foreach $m \in M$, **send** $(\texttt{join}, m, r_m)$ to $\mathrm{id}(C_i)$
(**alert coalition members of m via $\mathfrak{r}_i$**)
$L := \{k \in \mathcal{I} \mid i \text{ received } \texttt{leave} \text{ from } k\}$ (**agents leaving coalition**)
$J := \{k \in \mathcal{I} \mid \text{an } m \in \mathrm{id}(C_i) \text{ got } \texttt{join} \text{ from } k\}$
$\mathrm{id}(C_i) := (\mathrm{id}(C_i) \cup J) \setminus L$ and $r_i := \mathfrak{r}_i + \max\{r_j\}_{j \in J}$
(**update current coalition and radius**)
foreach $m \in M$, **send** $(r_i, \mathrm{id}(C_i))$ at r_m to m
(**update agents joining i's coalition**)
if $j^* \neq i$ **then**
  if $j^* = 0$ **then**
    $C_i = \{(i, p_i)\}$ (**form a new coalition**)
  else
    $\mathrm{id}(C_i) := \mathrm{id}(C_{j^*})$ and $r_i := \|p_{j^*} - p_i\| + r_{j^*}$
  end if
end if
if $J \neq \emptyset \vee j^* \neq i$ **then**
  Acquire $\mathcal{N}_i$, $\mathrm{pos}(C_i)$
  $j^* := i$ (**reset switching variable**)
end if

and $r = \mathrm{CR}(P_0)/\|q - \mathrm{CC}(P_0)\|$. Here, $d_1 : \mathbb{R}_{\geq 0} \to \mathbb{R}_{\geq 0}$ is an increasing function, continuous on $\mathbb{R}_{>0}$, satisfying

$$d_1(0) = 0, \ \lim_{s\to\infty} d_1(s) = d_{\max}, \ \lim_{s\to 0^+} d_1(s) = d_{\min},$$

for $d_{\max} > d_{\min} > 0$, and $d_2 : \mathbb{R}_{\geq 0} \to \mathbb{R}_{\geq 0}$ is defined by $d_2(s) = d_{\max} - d_1(s)$. Figure 3.1 illustrates the definition of gttg.

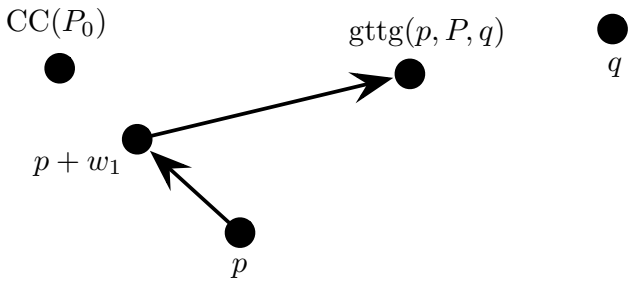

Figure 3.1: Illustration of the action of the function gttg.

The **Radius Adjustment and Motion** strategy is formally described in Algorithm 3.3. Its interaction with the coalition formation dynamics is described in steps 10-16, which governs the set of agents that a robot not yet in a κ-sized coalition interacts with. The next result ensures that agents' communication radius are kept at the smallest values that guarantee successful coalition formation.

Lemma 3.2.3. *(Optimality property for communication radius law) For each $i \in \mathcal{I}$ such that $|C_i| \neq \kappa$, let k_i be the closest agent which is in a coalition different from i's with size different from κ. Let $r_i(P, (C_1, \ldots, C_N)) = \|p_i - p_{k_i}\|$. For consistent coalition states not corresponding to a goal coalition partition, such radii guarantee that at least one agent has an incentive to switch coalitions. Moreover, if the radii of these agents were set according to any other function r_i' with $r_i'(P, (C_1, \ldots, C_N)) < r_i(P, (C_1, \ldots, C_N))$ for some i and P, then this property is no longer guaranteed.*

Proof. If there is at least one coalition of size greater than κ, all agents in this coalition have an incentive to start their own coalition. Consider instead, the case where all coalitions are of size at most κ. An agent i in the smallest coalition has an incentive to join its neighbor k_i and the claimed property follows. Next,

Table 3.3: **Radius Adjustment and Motion Algorithm**

Executed by: all agents i

if $|C_i| = \kappa \vee$ **last** $=$ True **then**
  Update r_i with **Adjust radius** strategy
  Acquire $\mathcal{N}_i$
  $A_i := (\{\mathrm{CC}(\mathrm{pos}(C_i))\} \cup \mathrm{pos}(\mathcal{N}_i)) \setminus \mathrm{pos}(C_i)$
  $V_i := V_1(A_i)$ (**compute Voronoi cell**)
  $\mathrm{goal} = \mathrm{CC}(V_i)$
else
  $\mathrm{goal} = \mathrm{CC}(\mathrm{pos}(C_i))$
  $\mathfrak{C}_i := \{j \in \mathrm{id}(\mathcal{N}_i) \mid |\mathrm{id}(C_i)| = \kappa\}$
  if $\mathrm{id}(\mathcal{N}_i \backslash C_i) \backslash \mathfrak{C}_i \neq \emptyset$ **then**
    $r_i := \min_{k \in \mathrm{id}(\mathcal{N}_i \backslash C_i) \backslash \mathfrak{C}_i} \|p_k - p_i\| + 2d_{\max}$
    (**guarantees a neighbor after motion**)
  else if $\mathrm{id}(\mathcal{N}_i) = \mathcal{I}$ **then**
    last := True (**one non-κ coalition**)
  else
    $r_i := r_i + \delta$ (**increase radius**)
  end if
end if
foreach $j \in \mathrm{id}(C_i)$, **set** $p_j := \mathrm{gttg}(p_j, \mathrm{pos}(C_i), \mathrm{goal})$
  (**compute next position**)
$\mathrm{pos}(C_i) := \{p_j\}_{j \in \mathrm{id}(C_i)}$ (**update positions**)
$\mathfrak{r}_i := \max_{p_j \in \mathrm{pos}(C_i)} \|p_j - p_i\|$ (**recompute radius**)

we show the minimality property. It is enough to show that there is one non-goal consistent coalition state for which a smaller radius assignment would not work. Consider a consistent coalition state at configuration P where all coalitions but one have been formed, and the remaining agents are in two coalitions, one with the single agent, i, and the other one, C, with the rest. Since

$$r_i'(P, (C_1, \ldots, C_N)) < r_i(P, (C_1, \ldots, C_N)) = \|p_i - p_{k_i}\|,$$

agent i has no agents in $\mathcal{N}_i$ that it has incentive to join. Furthermore, given the coalition state, agent i is the only one who could have an incentive to switch coalitions, concluding the proof. □

Steps 10-16 in Algorithm 3.3 implement the result of Lemma 3.2.3. If agent i is not within r_i of a non-coalition agent that is not in a κ-sized coalition, increase r_i. If agent i is within r_i of such an agent, change r_i to the distance between the two agents plus a constant ensuring they remain within communication range after moving.

Remark 3.2.4. *(Voronoi cell computation)* In the Voronoi cell computation of step 5 in Algorithm 3.3, the coalition's circumcenter replaces all the locations of the individual agents which ensures that all coalition members compute the same cell. However, this also implies that the collection of cells computed by the coalition is not a partition of the environment. This issue gets resolved when the members within each coalition are coincident and is treated in the proof of Theorem 3.3.1. •

Remark 3.2.5. *(Choice of parameter δ)* In step 15 of Algorithm 3.3, δ describes the amount that r_i increases if i does not have any neighboring candidate agents to join. Several choices are possible. For instance, when agents are roughly uniformly distributed, $\delta \propto \frac{\text{diam}\,(Q)}{\sqrt{N}}$ makes it likely that the agent discovers at least one new agent. •

The **Coalition Formation and Deployment Algorithm** is composed of Algorithms 3.1-3.3. This strategy does not require agents to share a common reference frame.

Remark 3.2.6. *(Robustness to addition and subtraction)* The **Coalition Formation and Deployment Algorithm** is robust to agents joining or leaving the network under the following assumptions: (i) new agents alert the network of their presence by sending a `query` message, (ii) when an agent fails, the other members of its coalition detect this fact, and (iii) when agents receive a `query` message they set **last** := False. •

3.3 Correctness analysis

This section analyzes the convergence properties of the strategy designed in Section 3.2. Our main objective is to establish the following result.

Theorem 3.3.1 (Algorithm correctness)**.** *Consider a network of N agents executing the* ***Coalition Formation and Deployment Algorithm****. Then,*

1. *there exists a finite time after which the agents are in a goal coalition partition and each is coincident with its coalition members, with probability* 1*;*

2. *the agents' positions and the induced Voronoi partition asymptotically converges toward the set of minimizers of $\mathcal{H}_{\mathrm{DC},\lceil \frac{N}{\kappa} \rceil}$, with probability* 1*.*

The proof of this result requires us to establish several intermediate results. Theorem 3.3.1 states that, with probability 1, the network will not converge to a coalition partition other than the desired one. Agents may stay for some time in a different partition but in finite time they will reach the desired partition with probability 1. This can be traced back to the fact that, in the simplified coalition formation game where agents have both full information and action sets, only the goal coalition partition is Nash stable (see Lemma 3.3.2 below). Theorem 3.3.1 implies that, even in the absence of global information, the Nash stable partitions are the desired ones.

Lemma 3.3.2. *(Nash stable partitions of preference ordering) In the N-agent simultaneous-action game where agents have preference orderings satisfying* (3.1)*, complete knowledge of all other coalition memberships, and their action set is to stay or join any other coalition, only the goal coalition partition is Nash stable.*

Proof. First, let us show that the goal coalition partition is Nash stable. All the agents in coalitions of size κ receive maximal utility, so they satisfy (2.3). Nash stability follows by noting that the agents in the coalition of size z do not prefer to join either a coalition with size κ or start a new coalition. To show the uniqueness result, we reason with a different arbitrary partition and show it is not Nash stable. This arbitrary partition must have either at least one coalition with more than κ agents or at least two coalitions with less than κ agents. In the first case, the agents in a coalition with more than κ agents would benefit by joining any coalition with size less than κ (if any exists), and if not, by forming a new coalition. In the second case, the agents in the smallest coalition with less than κ agents would benefit from joining the other. The same argument holds if coalitions are tied for smallest. These two cases show the goal coalition partition is the only Nash stable partition. □

3.3.1 Analysis of coalition formation dynamics

We define the collection of actions of all agents at a given timestep as a *timestep-event*. Our first result finds a strictly positive lower bound on the probability of any possible timestep-event happening. The result follows by noting that all agents' probabilistic actions are independent and the switching probabilities are given by (3.2).

Lemma 3.3.3. *(Bound on switching probability) Let E be a timestep-event with $\mathrm{P}\left(E\right) > 0$. Then,*

$$\mathrm{P}\left(E\right) \geq \min\{f(|C_1|,\ldots,|C_N|,N,\kappa),(1-f(|C_1|,\ldots,|C_N|,N,\kappa))\}^N.$$

For $\epsilon > 0$, define

$$\Xi_\epsilon(C_1,\ldots,C_N) = \sum_{i\in\mathcal{I}_{\leq\kappa}} \frac{(1+\epsilon)^{|C_i|}}{|C_i|} = \sum_{j=1}^{\kappa} a_j(1+\epsilon)^j, \tag{3.3}$$

where a_j are the number of coalitions of size j. Note that coalitions with size strictly larger than κ do not contribute to Ξ_ϵ. Additionally, Ξ_ϵ is upper bounded by$\lceil N/\kappa\rceil(1+\epsilon)^\kappa$. The next result establishes that one agent joining a coalition of

at least its own current coalition's size has positive effect on the overall network reaching a goal coalition partition.

Lemma 3.3.4 (Ξ_ϵ increase for one switcher)**.** *For any $\epsilon > 0$, when exactly one agent joins a new coalition of at least its current coalition's size, this action strictly increases the function Ξ_ϵ by at least* $\min\{1+\epsilon, \epsilon^2\}$.

Proof. Let i be the size of the coalition being left and j the size of the coalition being joined. We must consider the cases of $i < \kappa$ and $i > \kappa$ separately, starting with the former. Now, by the coalition preference ordering in (3.1), $i \leq j < \kappa$. After switching, Ξ_ϵ has changed by

$$\begin{aligned}
&(1+\epsilon)^{i-1} - (1+\epsilon)^i + (1+\epsilon)^{j+1} - (1+\epsilon)^j \\
&= \epsilon((1+\epsilon)^j - (1+\epsilon)^{i-1}) \\
&\geq \epsilon((1+\epsilon)^i - (1+\epsilon)^{i-1}) \geq \epsilon^2.
\end{aligned}$$

Now, considering the case where $i > \kappa$, one can see that in the worst case, the agent forms its own coalition of size 1, increasing Ξ_ϵ by $1+\epsilon$, which completes the result. □

The next result shows that from any consistent coalition state, there is a finite sequence of timestep-events, each with positive probability of occurring, that leads to a goal coalition partition. Also, there exists an upper bound, independent of the coalition state, on this sequence's length.

Proposition 3.3.5. *(A sequence of switching events leading to the goal coalition partition) From any consistent coalition state, there exists a finite sequence of timestep-events, each having a positive probability of occurring under the* ***Coalition Formation and Deployment Algorithm****, leading to a goal coalition partition. Furthermore, for any $\epsilon > 0$, the length of this sequence is bounded by*

$$L = \frac{\lceil N/\kappa + 1 \rceil (1+\epsilon)^\kappa}{\epsilon^2} \left(\frac{\operatorname{diam}(Q)}{\delta} + 1\right) + \left\lfloor \frac{N}{\kappa} \right\rfloor. \tag{3.4}$$

Proof. Initially, if any coalitions are larger than size κ, let the first timestep-event E_1 be one where the correct number of agents leave one of these large coalitions and

all other agents do not switch, creating a coalition of size κ. From Lemma 3.3.3, $\mathrm{P}\left(E_1\right)$ is bounded away from zero. There can be at most $\left\lfloor \frac{N}{\kappa} \right\rfloor - 1$ more coalitions larger than size κ, and so $E_2, \ldots, E_{\left\lfloor \frac{N}{\kappa} \right\rfloor}$ are defined similarly. From step 15 in Algorithm 3.3, within at most $\frac{\mathrm{diam}(Q)}{\delta}$ timesteps, each agent i will have a radius r_i satisfying Lemma 3.2.3, so at least one agent has an incentive to change coalitions. In the timesteps in which no agents wish to change coalitions, the corresponding timestep-events, $E_{\left\lfloor \frac{N}{\kappa} \right\rfloor+1}, \ldots, E_{\left\lfloor \frac{N}{\kappa} \right\rfloor+\alpha}$, $\alpha \leq \frac{\mathrm{diam}(Q)}{\delta}$, occur with probability 1. Define $E_{\left\lfloor \frac{N}{\kappa} \right\rfloor+\alpha+1}$ to be a timestep-event where exactly one agent joins a coalition it has an incentive to and all others do not switch. By Lemma 3.3.3, the probability of this event is bounded away from zero. Additionally, because all coalitions are at most size κ, the function Ξ_ϵ increases by at least ϵ^2 (c.f. Lemma 3.3.4). If the configuration is not in a goal coalition partition, within at most $\frac{\mathrm{diam}(Q)}{\delta}$ timesteps, at least one agent will have an incentive to switch coalitions. Because the upper-bounded function Ξ_ϵ monotonically increases each time this sequence of timestep-events occurs, the number of times this can occur is at most $\frac{\lceil N/\kappa+1 \rceil (1+\epsilon)^\kappa}{\epsilon^2}$. Therefore, within L timesteps (cf. (3.4)), the agents will be in a goal coalition partition. □

The next result uses the sequence constructed in Proposition 3.3.5 to show that in finite time all agents are in a goal coalition partition, with probability 1.

Theorem 3.3.6. *(Finite-time convergence to goal coalition partition) There exists a finite time after which N agents using the* ***Coalition Formation and Deployment Algorithm*** *are in a goal coalition partition with probability* 1.

Proof. Lemma 3.3.3 asserts that the probability of a timestep-event occurring is lower bounded by $\rho = \min\{f(|C_1|, \ldots, |C_N|, N, \kappa), (1 - f(|C_1|, \ldots, |C_N|, N, \kappa))\}^N$. Given an initial consistent coalition state,

Proposition 3.3.5 guarantees that there exists a finite sequence of timestep-events, whose length is upper bounded by L (cf. (3.4)), leading to the goal coalition partition. If the length of this sequence is smaller than L, this sequence can be extended to one of exactly length L by considering additional timestep-events where no agents wish to change coalitions. The latter occur with probability 1.

Therefore, the sequence of timestep-events leading to a goal coalition partition has a probability of occurring of at least ρ^L, independent of the initial coalition state.

Define a sequence of events $\{A_1, A_2, \dots\}$, where A_n is the event that the coalitions do not exist after nL timesteps. The probability of A_n occurring is at most $(1-\rho^L)^n$. Now,

$$\sum_{n=1}^{\infty} A_n \leq \sum_{n=1}^{\infty} (1-\rho^L)^n < \infty,$$

since it corresponds to a convergent geometric series. Thus, by the Borel-Cantelli Lemma, cf. Lemma 2.6.1, $\mathrm{P}\left(\{A_n \text{ i.o.}\}\right) = 0$. This means $\mathrm{P}\left(\{A_n \text{ i.o.}\}^c\right) = 1$ or, equivalently, $\mathrm{P}\left(\{A_n^c \text{ a.a.}\}\right) = 1$. The result follows by noting that A_n^c is the event that the coalitions occur at some point in nL timesteps and $\{A_n^c \text{ a.a.}\}$ is the event that all but a finite number of events A_n^c occur. □

Finally, we present two results concerning the agents' motion according to gttg. The next result states that if two agents move towards a common point, their distance is non-increasing.

Lemma 3.3.7. *For $d > 0$ and $p_1, p_2, q \in \mathbb{R}^n$, let $p_i^+ = \min\{\|q - p_i\|, d\}\ \mathrm{vr}(q - p_i) + p_i$, $i \in \{1, 2\}$. Then $\|p_1^+ - p_2^+\| \leq \|p_1 - p_2\|$.*

Lemma 3.3.8 determines how much the circumradius of a coalition decreases and how much they get closer to the goal point q after moving according to gttg.

Proposition 3.3.8. *(Application of* gttg *decreases circumradius) Given $P = (p_1, \dots, p_k)$ and $q \in Q$, let $P^+ = (p_1^+, \dots, p_k^+)$ be given by $p_i^+ = \mathrm{gttg}(p_i, P, q)$, $i \in \{1, \dots, n\}$. Then $\mathrm{CR}(P^+) \leq \mathrm{CR}(P) - \delta_1$ and*

$$P^+ \subset B(q, \|\mathrm{CC}(P) - q\| + \mathrm{CR}(P) - \delta_1 - \delta_2),$$

with $\delta_1 = \max_{i \in \{1,\dots,k\}} \min\{\|\mathrm{CC}(P) - p_i\|, d_1(r)\}$ and $\delta_2 = \min\{\|q - \mathrm{CC}(P)\|, d_2(r)\}$.

Proof. Our strategy is to look independently at the effect of the two halves of the motion defined in gttg. Define the intermediate positions P^* by $p_i^* = p_i + w_{1,i}$, $i \in \{1, \dots, n\}$, where $w_{1,i} = \min\{\|\mathrm{CC}(P) - p_i\|, d_1(r)\}\ \mathrm{vr}(\mathrm{CC}(P) - p_i)$. We show that

the circumradius decreases a finite amount while moving from P to P^* and does not increase while moving from P^* to P^+. First, according to the motion prescribed by gttg, we have $P^* \subset B(\mathrm{CC}(P), \mathrm{CR}(P) - \delta_1)$, which by definition of circumcenter, implies that $\mathrm{CR}(P^*) \leq \mathrm{CR}(P) - \delta_1$. Second, to show $\mathrm{CR}(P^+) \leq \mathrm{CR}(P^*)$, let us rewrite p_i^+ as $p_i^+ = p_i^* + w_{2,i}$, where $w_{2,i} = \min\{\|q - p_i^*\|, d_2(r)\}\,\mathrm{vr}(q - p_i^*)$. Let

$$NC^+ = \mathrm{CC}(P) + \delta_2\ \mathrm{vr}(q - \mathrm{CC}(P)). \tag{3.5}$$

By Lemma 3.3.7, for all $i \in \{1, \ldots, n\}$,

$$\|p_i^+ - NC^+\| \leq \|p_i^* - \mathrm{CC}(P)\| \leq \mathrm{CR}(P^*),$$

where we have used the fact that $\mathrm{CC}(P^*) = \mathrm{CC}(P)$. Finally,

$$\mathrm{CR}(P^+) \leq \max_{i \in \{1,\ldots,k\}} \|p_i^+ - NC^+\|,$$

which implies that $\mathrm{CR}(P^+) \leq \mathrm{CR}(P^*)$ and the result follows. Next, we study how much closer the points are to q after the application of gttg. Initially, $P \subset B(q, \|q - \mathrm{CC}(P) + \mathrm{CR}(P))\|$. After the application of w_1, the configuration's circumcenter has not moved and the circumradius has decreased by δ_1, so $P^* \subset B(q, \|q - \mathrm{CC}(P) + \mathrm{CR}(P) - \delta_1)\|$. Then, after the application of w_2,

$$P^+ \subset B(q, \|q - NC^+ + \mathrm{CR}(P) - \delta_1)\|.$$

Combined with (3.5), the result follows. □

3.3.2 Proof of the main result

We are now ready to prove Theorem 3.3.1.

Proof of Theorem 3.3.1. In statement (i), the fact that there exists, with probability 1, a finite time after which all agents are in a goal coalition partition follows from Theorem 3.3.6. Proposition 3.3.8 allows us to upper bound the number of timesteps it takes for the circumradius of one of these coalitions to vanish by $\lceil \frac{\mathrm{diam}(Q)}{d_{\min}} \rceil$. This implies the fact that in finite time agents become coincident with its coalition members. Once coalitions form and all individual agents are coincident with the members of their respective coalitions, the collection of Voronoi

cells that the agents compute correspond to a correct Voronoi partition with $\lceil \frac{N}{\kappa} \rceil$ generators. Statement (ii) then follows from [12, Theorem 5.5]. □

3.4 Algorithm complexity analysis

This section investigates the time and communication complexity per time-step of the **Coalition Formation and Deployment Algorithm**.

3.4.1 Time complexity analysis

After having established in Section 3.3 the correctness of the **Coalition Formation and Deployment Algorithm**, here we analyze the expected completion time of the coalition formation dynamics. In general, this time depends on the specific probability law chosen. In this section, we bound the expected completion time for a specific switching probability law that we term **Proportional-to-Number-of-Unmatched-Agents**. Before specifying this law, let us introduce some useful notation. Given the network state at a certain time, let $N_{\text{left}} \leq N$ denote the number of agents not in a group of size κ at that moment. We assume that each agent i can estimate N^i_{left} within a constant factor of N_{left}, i.e.,

$$N_{\text{left}} \leq N^i_{\text{left}} \leq cN_{\text{left}} \tag{3.6}$$

uniformly in time, for some $c \in \mathbb{R}_{\geq 1}$. The **Proportional-to-Number-of-Unmatched-Agents** law is defined as the switching probability given by

$$p = \Big(\frac{1}{N^i_{\text{left}}}\Big)^{1+\gamma}, \quad \text{if } |C_i| \neq \kappa, \tag{3.7}$$

where $\gamma > 0$ is a design parameter.

Remark 3.4.1 (Determination of N_{left})**.** In the forthcoming analysis, we do not consider a specific way of estimating N_{left}. There are a number of ways to implement this. One possibility is for all agents to initially have an estimate of N.

If each time a coalition of size κ is formed, one of the agents pays the one-time broadcast cost to send a message of this to all agents in the environment, all the agents can update N_{left} to $N_{\text{left}} - \kappa$. •

Our strategy to characterize the algorithm's time complexity relies in measuring the effect that agents switching coalitions has on the function Ξ_ϵ, cf (3.3). When one agent switches coalitions, this action increases Ξ_ϵ. However, when multiple agents switch coalitions at the same time, it is possible that their joint actions decrease Ξ_ϵ. One example of this is when multiple agents join the same coalition, making it larger than size κ. The next result provides an upper bound on how much Ξ_ϵ might decrease when more than one agent switches per timestep. Its proof follows from over-approximating the decrease by removing two coalitions of size $\kappa - 1$ (one for the coalition left and joined) for each agent that is switching.

Lemma 3.4.2. *(Upper bound on decrease in Ξ_ϵ due to multiple switchers) In a non-goal coalition partition, if exactly $\phi > 1$ switch coalitions, the function Ξ_ϵ does not decrease by more than $2\phi(1+\epsilon)^{\kappa-1}$.*

Given $N_{\text{left}} \leq N$ agents not yet in a coalition of size κ, the next result shows that the expected number of timesteps until all agents are in coalitions of size κ can be upper bounded by a function of N_{left}.

Lemma 3.4.3. *(Convergence time for $N_{left} \leq N$ agents) The expected number of timesteps it takes $N_{left} \leq N$ agents not yet in a coalition of size κ to all be in κ-sized coalitions is upper bounded by $L_{left}(cN_{left})^{N_{left}(1+\gamma)L_{left}}$, with*

$$L_{left} = \frac{\lceil N_{left}/\kappa + 1 \rceil (1+\epsilon)^\kappa}{\epsilon^2}(\sqrt{cN_{left}} + 1) + \left\lfloor \frac{N_{left}}{\kappa} \right\rfloor,$$

under the bound (3.6)*, when agents switch using the* ***Proportional-to-Number-of-Unmatched-Agents*** *law, and each agent i's communication parameter is given by $\delta_i = diam(Q)/\sqrt{N^i_{left}}$.*

Proof. Following Lemma 3.3.3, Proposition 3.3.5, and Theorem 3.3.6 for the **Proportional-to-Number-of-Unmatched-Agents** switching law, one can define $\rho_{\text{left}} = (\frac{1}{cN_{\text{left}}})^{N_{\text{left}}(1+\gamma)}$ and change (3.4) to L_{left} to account for the estimate N^i_{left}

and δ_i's dependence on it. Then, the probability that all agents are in the goal coalition after L_{left} timesteps is at least $\rho_{\text{left}}^{L_{\text{left}}}$, independent of the network's state. Thus, the expected value of the first time the network is in the goal coalition is upper bounded by $\frac{L_{\text{left}}}{\rho_{\text{left}}^{L_{\text{left}}}}$, completing the result. □

The upper bound in Lemma 3.4.3 implies that for $N_{\text{left}} = \mathcal{O}(1)$, the time complexity is also $\mathcal{O}(1)$. We are now ready to upper bound the expected number of timesteps for all coalitions to form under **Coalition Formation and Deployment Algorithm**, executed over an arbitrary graph, when the switching probability is defined by (3.7).

Proposition 3.4.4. *(Time complexity on a generic graph) Under* ***Coalition Formation and Deployment Algorithm****, the expected number of timesteps for the network to enter the goal coalition partition is* $\mathcal{O}(N^{\frac{5}{2}+\gamma})$ *when agents switch using the* ***Proportional-to-Number-of-Unmatched-Agents*** *law, and each agent* i*'s communication parameter is given by* $\delta_i = diam(Q)/\sqrt{N_{left}^i}$.

Proof. Let S be the number of agents who wish to switch at a given timestep and s be the number of agents who actually do. Note that

$$\mathrm{P}\left(s = \phi \,|\, S = \varphi\right) = \binom{\varphi}{\phi} p^{\phi}(1-p)^{\varphi-\phi}.$$

Then, using (3.7), one can bound

$$\mathrm{P}\left(s = 1 \,|\, S = \varphi\right) \geq \frac{j}{(cN_{\text{left}})^{1+\gamma}}(1 - \frac{1}{2^{1+\gamma}})^2, \tag{3.8a}$$

$$\mathrm{P}\left(s = \phi \,|\, S = \varphi\right) \leq \frac{1}{\phi!}(\frac{\varphi}{N_{\text{left}}^{1+\gamma}})^{\phi}, \quad \forall 1 < \phi \leq N. \tag{3.8b}$$

For $\epsilon > 0$, using Lemmas 3.3.4 and 3.4.2, one can bound the expected change in Ξ_ϵ as a function of the number of agents that wish to switch by

$$\mathrm{E}[\Xi_\epsilon(\ell+1) - \Xi_\epsilon(\ell) | S(\ell) = j] \geq$$
$$\min\{\epsilon^2, 1+\epsilon\}\,\mathrm{P}\left(s = 1 \,|\, S = \varphi\right) - \sum_{\phi=2}^{\varphi} \mathrm{P}\left(s = \phi \,|\, S = \varphi\right) 2\phi(1+\epsilon)^{\kappa-1}.$$

Combining this with (3.8), we get

$$\mathrm{E}[\Xi_\epsilon(\ell+1)-\Xi_\epsilon(\ell)|S(\ell)=\varphi]\geq$$
$$\min\{\epsilon^2,1+\epsilon\}(1-\frac{1}{2^{1+\gamma}})^2\frac{\varphi}{(cN_{\text{left}})^{1+\gamma}}-2(1+\epsilon)^{\kappa-1}\sum_{\phi=2}^{\varphi}\frac{1}{(\phi-1)!}(\frac{\varphi}{N_{\text{left}}^{1+\gamma}})^\phi.$$

Using $\sum_{\phi=2}^{\infty}\frac{1}{(\phi-1)!}p^\phi=p(e^p-1)$, for all $|p|<1$, one gets

$$\mathrm{E}[\Xi_\epsilon(\ell+1)-\Xi_\epsilon(\ell)|S(\ell)=\varphi]\geq$$
$$\frac{\varphi}{N_{\text{left}}^{1+\gamma}}\Big(\frac{\min\{\epsilon^2,1+\epsilon\}(1-\frac{1}{2^{1+\gamma}})^2}{c^{1+\gamma}}-2(1+\epsilon)^{\kappa-1}(e^{\frac{j}{N_{\text{left}}^{1+\gamma}}}-1)\Big).$$

One can bound the expected change in Ξ_ϵ if $S>0$ by

$$\mathrm{E}[\Xi_\epsilon(\ell+1)-\Xi_\epsilon(\ell)|S(\ell)\geq 1]\geq$$
$$\frac{1}{N_{\text{left}}^{1+\gamma}}\Big(\frac{\min\{\epsilon^2,1+\epsilon\}(1-\frac{1}{2^{1+\gamma}})^2}{c^{1+\gamma}}-2(1+\epsilon)^{\kappa-1}(e^{\frac{1}{N_{\text{left}}^{\gamma}}}-1)\Big).$$

From this expression, one can see that, given A satisfying

$$0<A<\frac{\min\{\epsilon^2,1+\epsilon\}(1-\frac{1}{2^{1+\gamma}})^2}{c^{1+\gamma}},$$

one can find $N_{\text{crit}}(\epsilon,\gamma,c,A)$ such that for all $N_{\text{left}}\geq N_{\text{crit}}(\epsilon,\gamma,c,A)$, the following holds

$$\mathrm{E}[\Xi_\epsilon(\ell+1)-\Xi_\epsilon(\ell)|S(\ell)\geq 1]\geq\frac{A}{N_{\text{left}}^{1+\gamma}}.$$

From (3.3), note that the largest that Ξ_ϵ can be with $N_{\text{left}}\geq N_{\text{crit}}$ is

$$\Xi_{\epsilon,\text{crit}}=\frac{N-N_{\text{crit}}}{\kappa}(1+\epsilon)^\kappa+\frac{N_{\text{crit}}}{\kappa-1}(1+\epsilon)^{\kappa-1}.$$

Furthermore, once $N_{\text{left}}\leq N_{\text{crit}}$, it will be for all time after. From (3.7) and our choice of δ_i, there are at most $\sqrt{cN_{\text{left}}}$ timesteps between each time when at least one agent desires to switch. Therefore, one can say that

$$\mathrm{E}[N_{\text{left}}(\ell)]\leq N_{\text{crit}},\ \forall\ell\geq\ell_{\text{crit}}=\lceil\Xi_{\epsilon,\text{crit}}\sqrt{cN_{\text{left}}}\frac{N_{\text{left}}^{1+\gamma}}{A}\rceil.$$

By the definition of the expected value for a non-negative random variable, $\mathrm{P}\left(N_{\text{left}}(\ell) \leq N_{\text{crit}}\right) \geq \frac{1}{2}$, for all $\ell \geq \ell_{\text{crit}}$. Defining T_{crit} as the first time that $N_{\text{left}} \leq N_{\text{crit}}$, it is clear that $\mathrm{E}[T_{\text{crit}}] \leq \ell_{\text{crit}} + 1$.

Finally, define T to be the first time that all agents are in a goal coalition partition. By Lemma 3.4.3, $\mathrm{E}[|T|]$ is finite, for all finite N. With this condition satisfied, one can apply the law of total expectation [9] as well as Lemma 3.4.3 again and see that

$$\begin{aligned}\mathrm{E}[T] &= \mathrm{E}[\mathrm{E}[T \mid T_{\text{crit}}]] \leq \mathrm{E}[L_{\text{left}}(cN_{\text{crit}})^{N_{\text{crit}}(1+\gamma)L_{\text{left}}} + T_{\text{crit}}] \\ &\leq L_{\text{left}}(cN_{\text{crit}})^{N_{\text{crit}}(1+\gamma)L_{\text{left}}} + \ell_{\text{crit}} + 1.\end{aligned}$$

Finally, given that $N_{\text{left}} \leq N$, noting the order of ℓ_{crit} with respect to N finishes the result. □

Next, we show that the time complexity bound in Proposition 3.4.4 can be improved for the complete graph.

Proposition 3.4.5. *(Time complexity on the complete graph) Under the* ***Coalition Formation and Deployment Algorithm****, the expected number of timesteps for the network to enter the goal coalition partition is* $\mathcal{O}(N^{1+\gamma})$ *when agents switch using the* ***Proportional-to-Number-of-Unmatched-Agents*** *law and each agent can communicate with all other agents.*

Proof. The proof strategy is the same as for Proposition 3.4.4, so we only provide a sketch here. There are two differences between the generic case and the complete graph case. The first difference is that in a timestep where at least one agent wishes to switch coalitions, in the complete graph case, we can show that almost all agents wish to switch. More precisely, agents in coalitions larger than size κ have an incentive to at least form their own coalition. Of the coalitions less than size κ, agents desire to join the largest one. If two coalitions have the same cardinality and are both the largest coalition of size less than κ, they mutually want to join each other. This means that at least $N_{\text{left}} - \kappa + 1$ agents have an

incentive to switch coalitions. This affects the expected change in Ξ_ϵ as follows,

$$\mathrm{E}[\Xi_\epsilon(\ell+1) - \Xi_\epsilon(\ell) | S(\ell) \geq 1] \geq \frac{N_{\text{left}} - \kappa + 1}{N_{\text{left}}^{1+\gamma}} \Big(\frac{\min\{\epsilon^2, 1+\epsilon\}(1 - \frac{1}{2^{1+\gamma}})^2}{c^{1+\gamma}} - 2(1+\epsilon)^{\kappa-1}(e^{\frac{1}{N_{\text{left}}^{\gamma}}} - 1) \Big).$$

The second difference is that agents wish to switch at every timestep (instead of once every $\sqrt{cN_{\text{left}}}$ timesteps, as in Proposition 3.4.4, given the assumed δ_i and the **Proportional-to-Number-of-Unmatched-Agents** switching law). The result follows from propagating these changes through the proof of Proposition 3.4.4. □

3.4.2 Communication complexity per timestep

Here, we analyze the communication complexity per timestep of the **Coalition Formation and Deployment Algorithm**. We begin by stating our conventions regarding how messages are counted along the algorithm execution. First, we make the assumption that an identical message sent at a given moment by an agent to one or more other agents located within some distance of it counts as one. For instance, an omnidirectional communication model fits into this description.

Second, in several instances, the algorithm requires the location and identity of the neighbors of an agent. This information may be obtained via either communication or sensing. We assume this service is efficiently carried out by the network and do not count it toward the communication required per timestep.

Before stating our communication complexity characterization, we introduce one slight modification to step 2 of the **Best Neighbor Coalition Detection** that decreases the number of messages sent without affecting the overall algorithm execution. According to this modification, an agent, instead of querying all neighbors that are not in its coalition, will now query the closest neighbor who is not in its current coalition and also not in a coalition of size κ. This modification requires agents to know what nearby agents have already formed a coalition of the desired size. This can be addressed in at least one of the following two ways. One way is for agents to broadcast to the network that it and its coalition members are in a complete group. The other way is that when agents query the coalition size of

other agents (as in step 2 of the **Best Neighbor Coalition Detection**), if the queried agent is in a complete group, the querying agent notes the identities of all agents already in that complete group, and never needs to ask again.

We refer to the algorithm with this modification as the **Coalition Formation and Deployment Algorithm***. The modification does not affect the algorithm's correctness or time complexity bounds. The basic argument is that, even with the modification, in any network configuration, one can still guarantee that within $\text{diam}(Q)/\delta$ timesteps, at least one agent will have an incentive to join a more desirable coalition. This observation allows to reproduce the technical proofs given above to establish the same correctness and time complexity results. The next result characterizes the communication complexity per timestep of the algorithm.

Proposition 3.4.6. *(Communication complexity per timestep) Under the* ***Coalition Formation and Deployment Algorithm*****, the network of agents sends at most* $6N_{left}$ *messages per timestep and, hence, the communication complexity per timestep is* $\mathcal{O}(N)$*.*

Proof. We show the result by simply counting the number of messages sent per timestep. In steps 2 and 3 of the modified version of the **Best Neighbor Coalition Detection**, an agent not in a coalition of size κ sends one message to one neighbor and receives one back. In steps 2 and 4 of the **Coalition Switching**, when an agent switches coalitions it sends one broadcast message alerting its former coalition it is leaving, as well as one message to tell one member of its new coalition it is joining. This one member in the new coalition sends one broadcast message alerting the rest of its coalition of the new member, as specified in step 8. Finally, that member sends one message back to the joining member to alert it of any other agents who happened to join/leave in the exact same timestep, as specified in step 12. Thus, if an agent is joining another coalition, 4 messages are required and if the agent is forming its own coalition of size 1, only 1 message is required. The most messages would be sent if all agents switched at the same timestep. Since agents in coalitions of size κ will never switch, executing one timestep of the **Coalition Formation and Deployment Algorithm*** generates

at most $6N_{\text{left}}$ messages, and the result follows. □

Note that the upper bound in Proposition 3.4.6 is a function of the agents not in a completed coalition and, thus, monotonically decreasing as the algorithm evolves and completed coalitions form.

3.5 Simulations

This section presents several simulations of the **Coalition Formation and Deployment Algorithm**. In all simulations where they are relevant, $\delta = d_{\max} = \frac{.2}{\sqrt{2}}\frac{\text{diam}(Q)}{\sqrt{N}}$. We use the function

$$\phi(C_1, \ldots, C_N) = \frac{1}{N(\kappa - 1)} \sum_{i \in \mathcal{I}} ||C_i| - \kappa|, \tag{3.9}$$

to illustrate the coalition formation dynamics. This function measures the normalized average absolute difference between the agents' coalition size and the desired size κ.

We begin by illustrating the correctness of the algorithm, i.e., convergence to a desired goal coalition partition and the achievement of the deployment task. Figure 3.2(a)-(b) show an execution of the **Coalition Formation and Deployment Algorithm** on 21 agents forming coalitions of size 2 with **Proportional-to-Coalition-Size** switching law defined by

$$p = \begin{cases} 1 - (1-b)^{\frac{1}{|C_i|}}, & \text{if } |C_i| \neq \kappa, \\ 0, & \text{if } |C_i| = \kappa, \end{cases} \tag{3.10}$$

for some $b \in (0, 1)$. Note that this switching law satisfies (3.2). In this and other simulations where b is constant, we chose $b = 0.5$. The appeal of this switching law is that b is the probability that at least one agent in a coalition will switch, given that all coalition members wish to switch. This switching law makes it likely that several agents (most likely from different coalitions) will get the chance to switch coalitions at each timestep. One can observe in Figure 3.2(b) that the network converges to both correctly sized groups and coalitions optimally deployed

at their Voronoi cell's circumcenters. From Theorem 3.3.1, the final configuration optimizes $\mathcal{H}_{\mathrm{DC},11}$.

Figure 3.3(a) shows the number of coalition switches at each timestep for the same run. Many switches happen early, but decrease in frequency as agents form κ-sized coalitions. The evolution of ϕ depicted in Figure 3.3(b) confirms this by showing how agents join more desirable coalitions over time. It also shows the evolution of the objective function $\mathcal{H}_{N,N-1}$ that, in the language of Section 2.4, corresponds to the situation where $N-1$ of the sensors are working. This choice of function is motivated by the fact that, in one dimension, it is known that in such a case, forming coalitions of size 2 is optimal [15]. The bumps in the evolution of $\mathcal{H}_{21,20}$ occur when an agent with no nearby coalitions to join must increase its radius to join a group far away. $\mathcal{H}_{21,20}$ temporarily increases while these agents get together.

Figure 3.2(c) and (d) illustrate the robustness of the **Coalition Formation and Deployment Algorithm**. After agents have achieved the final optimal configuration seen in Figure 3.2(b), we let one agent fail and two new agents come into the picture. The agents adapt to the new network composition and optimally deploy according to the available resources.

Next, Figure 3.4 shows the average number of timesteps required for coalition formation for 4 different probabilistic switching laws under a generic communication topology, cf. (a), and the complete communication topology, cf. (b). For all network sizes, the desired coalition size is 4. Each point is the average of 50 runs, where the agents are initially randomly placed with uniform distribution in a unit square. The time complexity upper bounds in Section 3.4.1 are corroborated and the bound seems tight for the complete communication case.

Figure 3.5 illustrates the communication complexity analysis of Section 3.4.2. (a) shows the number of messages sent per timestep for one execution of 21 agents forming coalitions of size 3 with switching probability $p = .9$. As coalitions form, fewer messages are sent per timestep. (b) depicts the average number of messages sent per timestep as a function of the total network size for switching probability $p = .9$ and desired coalition size of 4. The plot validates

the $\mathcal{O}(N)$-characterization of the communication complexity per timestep stated in Proposition 3.4.6.

Finally, Figure 3.6 illustrates the dependency of the average coalition formation time on κ and b for the **Proportional-to-Coalition-Size** switching law. We focus on this law because it is the one that executes the fastest out of the probability laws illustrated in Figure 3.4. Each point is the average of 200 runs, where agents are initially uniformly randomly placed in a unit square. The error bars correspond to plus and minus one standard deviation. Figure 3.6(a) shows the average coalition formation convergence time for fixed $N = 20$ and varying κ. This time is roughly equal for all desired coalition sizes, until nearly all agents are joining one coalition, which takes less time on average. Figure 3.6(b) shows the average coalition formation time for 20 agents forming coalitions of size 4 as a function of b. For values of b far from 0 and 1, this time is roughly constant.

Chapter 3, in part, is a reprint of the material [65] as it appears in 'Hedonic coalition formation for optimal deployment' by M. Ouimet and J. Cortés in Automatica, to appear in 2013. The dissertation author was the primary investigator and author of this paper.

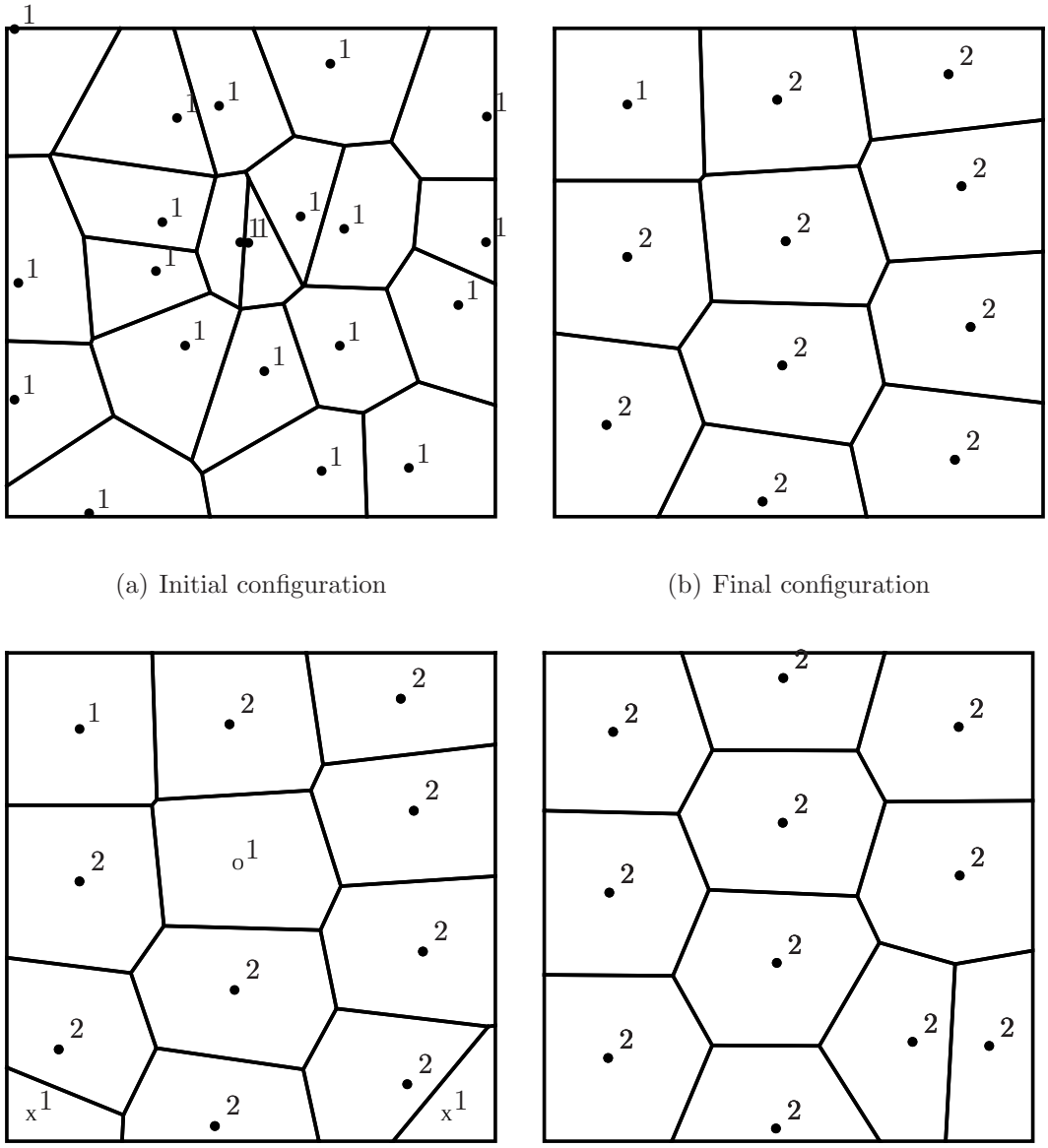

(a) Initial configuration

(b) Final configuration

(c) Agent addition and deletion

(d) New final configuration

Figure 3.2: Execution of the **Coalition Formation and Deployment Algorithm** with 21 agents and $\kappa = 2$ using the **Proportional-to-Coalition-Size** switching law (3.10). The network starts at (a) and converges to the configuration in (b) where all agents are in correctly-sized coalitions and these coalitions are optimally deployed. After this, (c) shows an agent failing in the coalition marked as 'o' and two agents, marked as 'x', joining the network. After the agent additions and subtractions, coalitions adapt and the network re-converges to the optimal deployment configuration in (d).

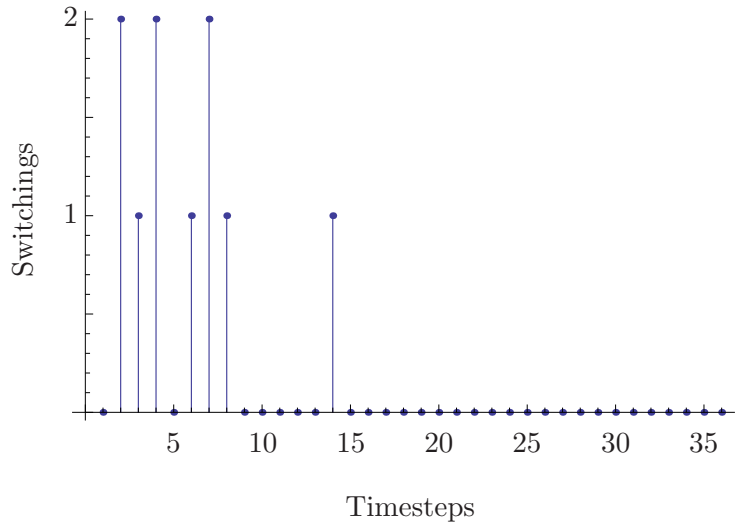

(a)

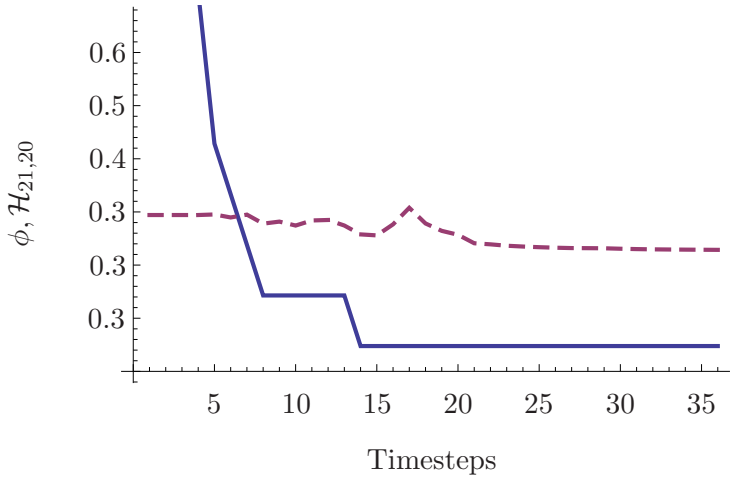

(b)

Figure 3.3: For the execution in Figure 3.2(a) and (b), (a) shows the number of agents switching coalitions at each timestep, and (b) shows the evolution of ϕ (solid line) as defined in (3.9) and $\mathcal{H}_{21,20}$ (dashed line) as defined in (2.1).

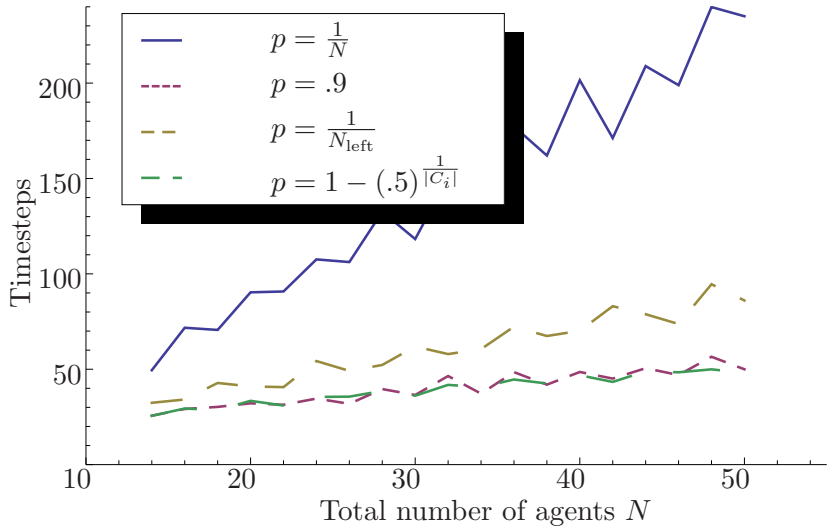

(a)

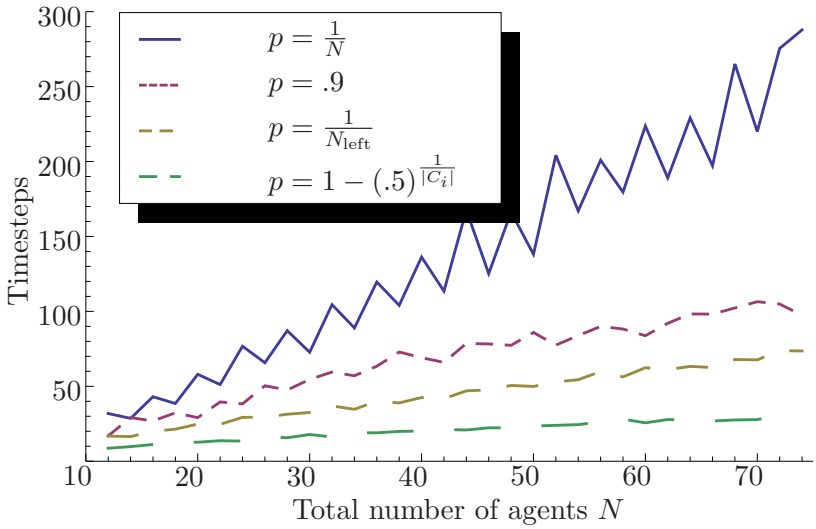

(b)

Figure 3.4: Average coalition formation time for 4 different probabilistic switching laws under (a) a generic communication topology and (b) the complete communication topology. Each point is the average of 50 runs, where the agents were initially randomly placed with uniform distribution in a unit square. The time complexity upper bounds in Section 3.4.1 are validated, and that the bound seems tight for the complete communication case.

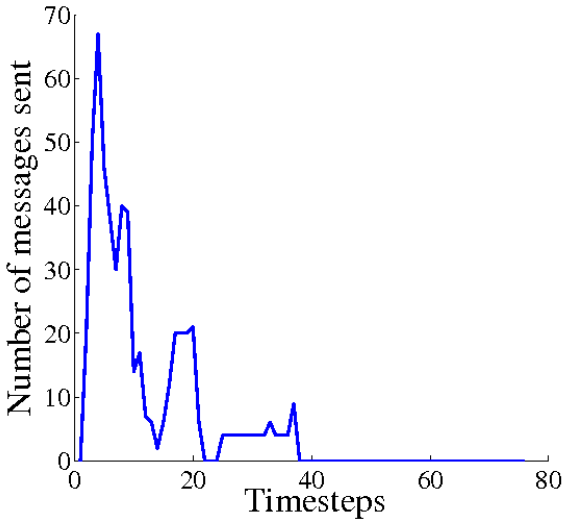

(a)

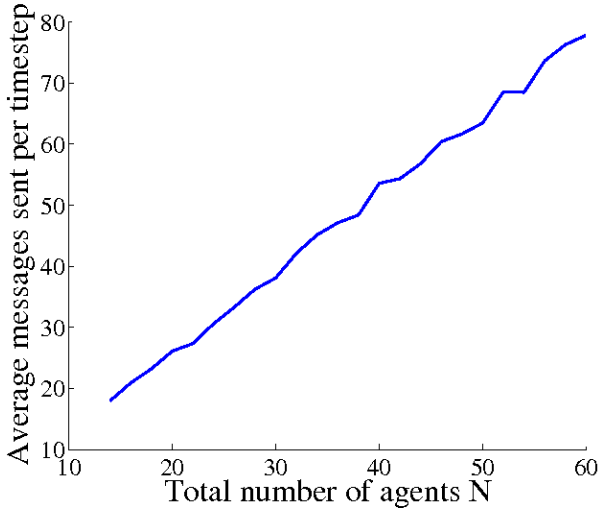

(b)

Figure 3.5: (a) depicts the number of messages sent per timestep for a run of 21 agents forming coalitions of size 3. (b) illustrates the average number of messages sent per timestep as a function of the network size. Both of these plots validate that the algorithm has an $\mathcal{O}(N)$ message complexity per timestep result, as in Proposition 3.4.6.

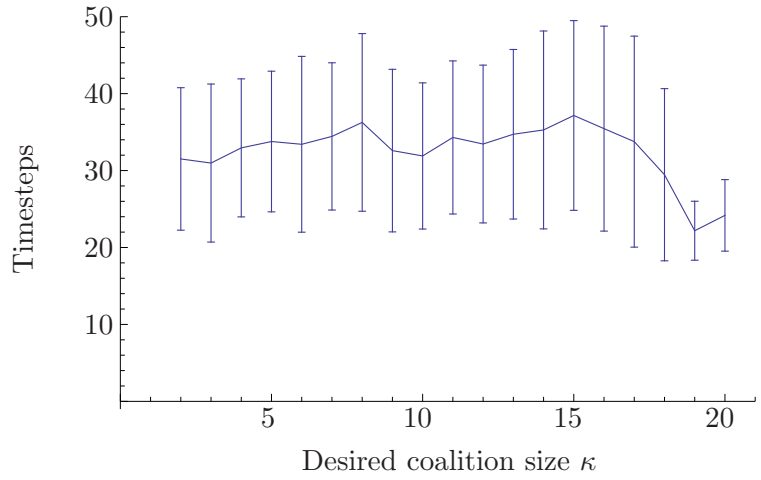

(a)

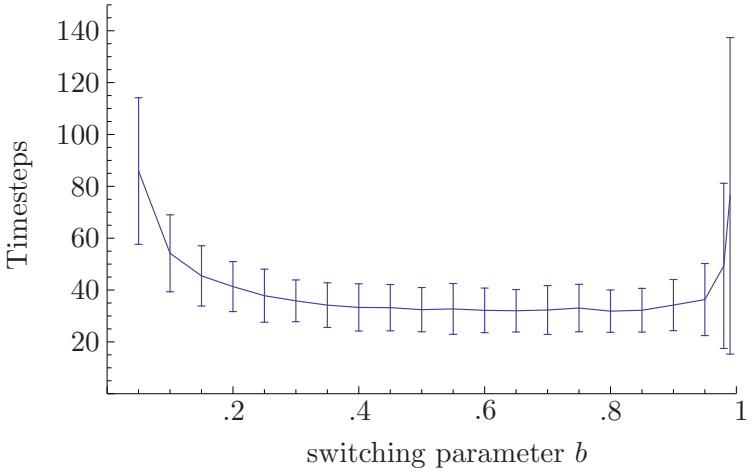

(b)

Figure 3.6: Average coalition formation time for 20 agents with the **Proportional-to-Coalition-Size** switching law (3.10) as a function of (a) the desired coalition size κ and (b) the parameter b (with coalitions of size 4). Each point is the average of 200 runs, where the agents were initially randomly placed with uniform distribution in a unit square. The error bars correspond to plus and minus one standard deviation.

Chapter 4

Estimation of linear internal waves

Internal waves are waves that propagate within a fluid, rather than on its surface. The type that we consider here corresponds to a moving oscillation in the boundary surface between two layers of a stratified fluid. In the ocean, these two layer fluids can occur at the mouth of large rivers where brackish (low salinity) water sits above sea water, for instance. Also, a continuously stratified fluid can be modeled as a two-layer fluid, where the interface, called pycnocline, is the surface of constant density where the vertical rate of change in density is largest. This class of internal waves can be broadly categorized into linear and nonlinear. Linear waves have amplitudes small relative to the depth of the water column. They are capable of moving around plankton, animal larvae, and other organisms, as well as creating mixing between the upper and lower layers. In contrast, nonlinear waves have larger amplitudes, allowing them to be an agent of transport of small oceanic life. Here, we consider linear waves modeled as a sinusoid which propagates along the pycnocline.

Traditional methods for studying internal waves have been satellite observations, acoustic tomography, conductance-temperature-depth (CTD) casts, and current meters on moorings. However, these methods lack the capability of real-time adaptability. Here, we tackle this problem using a group of drogues capable of drifting underwater near the internal wave's interface to determine the physical

parameters that define its motion. A drogue is a robotic Lagrangian drifter able to actuate its depth by changing its buoyancy. While underwater, drogues are subject to the flow induced by the motion of the internal wave and do not have access to exact location information. Figure 4.1 presents a pictorial illustration of the problem setup. The basic premise of this chapter is that the evolution of the inter-drogue distance and distance derivative measurements contains enough information for the drogues to be able to fully characterize the internal wave. To our knowledge, there is no algorithmic procedure available in the literature to solve this problem.

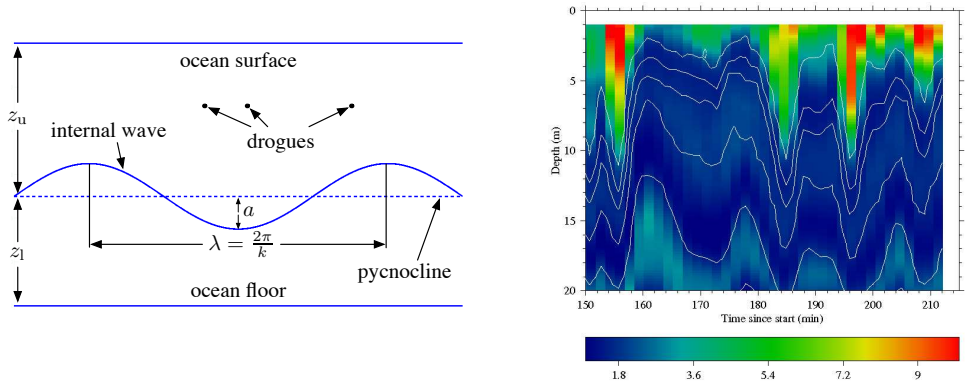

(a) Schematic of drogues and internal wave

(b) Plankton patchiness induced by internal wave

Figure 4.1: For a horizontally propagating ocean internal wave, (a) shows its spatial structure at a fixed instant of time whereas (b) shows its temporal structure at a fixed horizontal location. In (a), one can see a vertical cross-section of the ocean perpendicular to the wave propagation direction. A group of drogues float at a constant depth (but not necessarily along a straight line) and do not have access to exact location information. Our objective is to provide drogues with mechanisms that rely only on the relative measurements between them to determine the parameters that uniquely define the internal wave. In (b), one can see data at an anchor station off Mission Beach, CA, taken on April 19, 1997. The plankton's chlorophyll fluorescence (color scale) is depicted as a function of depth and time. Higher fluorescence corresponds to denser patches of plankton in the troughs of a horizontally propagating internal wave. Figure courtesy of Peter Franks, see [48] for additional information.

Internal waves are associated with high concentrations of various types of planktonic organisms and small fishes [94, 87], as well as an agent of lar-

val transport [73]. This makes their study important to oceanographers, see e.g. [27, 48, 90, 14]. In particular, striping of low/high densities in plankton can be well explained by small amplitude, linear internal waves [27]. Scientists widely use drogues drifting passively as monitoring platforms to gather relevant ocean data [71, 28, 38]. The use of autonomous underwater vehicles to detect and characterize internal waves is a relatively new approach. Whereas previous works use ocean measurements such as conductivity, temperature, pressure data [13, 72] or vertical flow velocity [95] to detect and analyze internal waves, our approach is unique in using inter-vehicles measurements. Recent work [44] explores the possibility of actively selecting tidal currents so that drogues can autonomously reach a desired destination. An increasing body of work in the systems and control literature deals with cooperative networks of agents estimating spatial natural phenomena, including ocean [49, 68, 33], river [78], and hurricane sampling [21]. In the problem considered here, drogues are able to actuate their depth through buoyancy changes, but are completely subject to the force of the internal wave in the flow-wise direction. Because of this, the task of determining the wave parameters can be seen as a data fitting problem [84, 83]. Due to the periodic nature of the inter-drogue distance trajectories, our problem has connections with least-squares spectral analysis problems [18, 24]. In general, however, the fact that the wave parameters appear nonlinearly makes the determination of the exact parameters challenging. Finally, since the presented algorithm can generate many independent estimates of the parameters. These parameter distributions are implicitly defined and non-Gaussian so we adopt a mixture distribution approach to express the distribution as a sum of simpler distributions [29].

4.1 Problem statement

This section formulates the problem under study. We begin by presenting the basic model for the motion of a linear internal wave. Then, we describe the capabilities of the group of drogues and discuss the effect that the internal wave has on their dynamics. With these ingredients in place, we formalize the distributed

parameter estimation problem.

4.1.1 Internal wave model

Let $\Sigma_g = (\mathbf{p}_g, \{\mathbf{e}_{x_g}, \mathbf{e}_{y_g}, \mathbf{e}_{z_g}\})$ be a global reference frame defined as follows: the origin p_g corresponds to an arbitrary point at the surface of the water; the vector $\mathbf{e}_{x_g}$ corresponds to the direction of wave propagation, which is parallel to the ocean bottom, and $\mathbf{e}_{z_g}$ is perpendicular to the ocean bottom, pointing from bottom to surface. Note that, with this convention, there is no wave motion in the $\mathbf{e}_{y_g}$-direction. The coordinates induced by Σ_g are denoted by $\{x, y, z\}$.

As in Figure 4.1, an internal wave is a wave which travels beneath the surface of the ocean, along a surface of constant water density called pycnocline. We consider an internal wave with amplitude a, frequency ω, propagating horizontally in the x-direction with horizontal wavenumber k, and at the mean depth $-z_{\mathrm{u}}$. The wave depth z_w as a function of x and t is

$$z_w(t, x) = -z_{\mathrm{u}} - a\sin(kx - \omega t + \phi).$$

The parameter ϕ, termed initial phase of the wave, effectively shifts the wave relative to the reference $(x, t) = (0, 0)$. Because of our choice of reference frame, there is no motion in the y-direction. The standard model [27, 48, 31] assumes that vertical velocity varies linearly with depth. This, coupled with the conservation of mass law for an incompressible fluid, gives rise to the following expressions for the horizontal u_{u} and vertical w_{u} velocities of the upper layer,

$$u_{\mathrm{u}}(t, x) = \frac{\omega a}{k z_{\mathrm{u}}} \sin(kx - \omega t + \phi), \tag{4.1a}$$

$$w_{\mathrm{u}}(t, x, z) = -\frac{z a \omega}{z_{\mathrm{u}}} \cos(kx - \omega t + \phi). \tag{4.1b}$$

Likewise, the horizontal u_{l} and vertical w_{l} velocities of the lower layer are

$$u_{\mathrm{l}}(t, x) = -\frac{\omega a}{k z_{\mathrm{l}}} \sin(kx - \omega t + \phi),$$

$$w_{\mathrm{l}}(t, x, z) = \frac{z + z_{\mathrm{u}} + z_{\mathrm{l}}}{z_{\mathrm{l}}} a\omega \cos(kx - \omega t + \phi).$$

Assumption 4.1.1 (Bounds on wave parameters)**.** The linear internal wave model is only accurate for $0 < a/z_{\mathrm{u}} \leq (a/z_{\mathrm{u}})_{\max} = 0.1$. Additionally, the spatial wavelengths of internal waves range from hundreds of meters to tens of kilometers [90]. Since k is inversely proportional to the spatial wavelength, we assume that there exists a bounded interval $[k_{\min}, k_{\max}]$ that k is guaranteed to be in. Finally, since the wave's speed is the ratio $\frac{\omega}{k}$, which physically must be bounded, we assume that there exists $\omega_{\max}$ such that $\omega \leq \omega_{\max}$. •

4.1.2 Drogue model

A drogue is a submersible buoy which can drift in the ocean, unattached to the ocean floor or a boat, and is able to change its depth in the water by controlling its buoyancy. A drogue can measure the relative distance, the distance derivative, and the orientation to other drogues, as well as depth through sensing (e.g., via acoustic or optical sensors and an onboard compass). However, it does not have access to absolute position because GPS is unavailable underwater.

We consider a group of N drogues. For each $i \in \{1, \ldots, N\}$, let $\Sigma_i = (\mathbf{p}_i, \{\mathbf{e}_{x_i}, \mathbf{e}_{y_i}, \mathbf{e}_{z_i}\})$ be a reference frame fixed to drogue i. The origin $\mathbf{p}_i$ corresponds to the location of the drogue. As in the global coordinate frame Σ_g, $\mathbf{e}_{z_i}$ is perpendicular to the ocean bottom, pointing from bottom to surface. The vectors $\mathbf{e}_{x_i}$ and $\mathbf{e}_{y_i}$ are parallel to the ocean floor, but neither is necessarily oriented in the direction of wave propagation. Thus, each drogue i must determine the angle between $\mathbf{e}_{x_i}$ and $\mathbf{e}_x$, which we denote by θ_i. Drogues are able to measure inter-drogue distances and distance derivatives. In our treatment, we deal separately with the case of noiseless and noisy measurements. We assume drogues take measurements at a sampling rate of f_s. Thus, at time $t \in \mathbb{R}_{>0}$, drogue i has measurements $\{(\mathbf{d}_{ij}(t_\kappa), \mathbf{d}'_{ij}(t_\kappa))\}_{\kappa \in \{0, \ldots, \lfloor f_s t \rfloor\}}$ at times $t_\kappa = \frac{\kappa}{f_s}$ and for drogues $j \in \{j_1, \ldots, j_M\}$, where these are the M drogues closest to i.

Consider the scenario where drogues move in the upper layer of the internal wave at a constant depth. There is no loss of generality in dealing with this situation, since drogues can control their depth through buoyancy changes. We make the simplifying assumption that the drogue dynamics under the linear in-

ternal wave is Lagrangian. In other words, the dynamics of the drogue position $\mathbf{p} = (p^x, p^y, p^z)$ in the global reference frame is given by

$$\mathbf{p}' = (p'^x, p'^y, p'^z) = (u_{\mathrm{u}}(t, p^x), 0, 0). \tag{4.2}$$

The absence of motion in the z-direction in this equation is due to the drogue's buoyancy control, which we assume is capable of counteracting the vertical forcing of the internal wave. Since the drogues can measure their depth, we assume there exists an underlying controller which uses these measurements to regulate the drogue at a desired depth. Figure 4.2 illustrates the time evolution of the x-component of inter-drogue distances as a function of the initial wave phase.

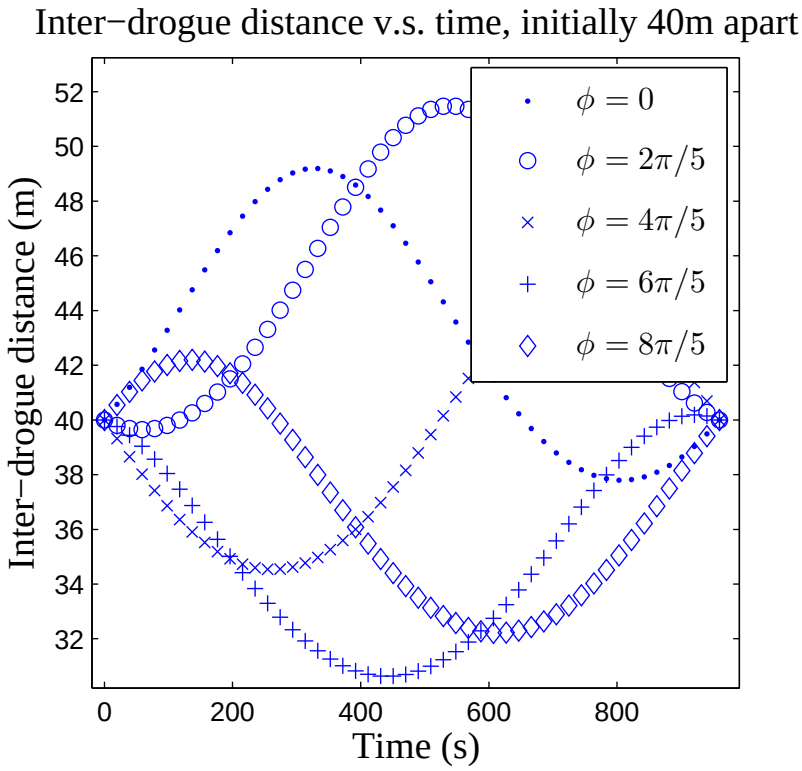

Figure 4.2: Inter-drogue distance evolution for drogues initially 40 meters apart, with different initial wave phases.

Remark 4.1.2 (Kinematic versus dynamical model)**.** The Lagrangian model for motion under the internal wave, cf. (4.2), is a simplification of the second-order

dynamic model, see e.g. [92],

$$mp''^x = -c_d\,|p'^x - u_{\mathrm{u}}(t,p^x)|(p'^x - u_{\mathrm{u}}(t,p^x)), \tag{4.3a}$$

$$p'^y = 0, \tag{4.3b}$$

$$mp''^z = -c_d\,|p'^z - w_{\mathrm{u}}(t,p^x,p^z)|(p'^z - w_{\mathrm{u}}(t,p^x,p^z)) + f, \tag{4.3c}$$

where m denotes the combined drogue mass and inertial added mass [11], c_d is the drag parameter, and f is the buoyancy control input. From this equation, one can derive

$$|u_u(t,p^x(t)) - p'^x(t)| \leq \sqrt{\frac{mu'_{\max}}{c_d}}\tanh(\sqrt{\frac{c_d u'_{\max}}{m}}t + \tanh^{-1}(\sqrt{\frac{c_d}{mu'_{\max}}}u_{\max})),$$

where $u_{\max} = \frac{\omega a}{kz_{\mathrm{u}}}$ and $u'_{\max} = \frac{\omega a}{kz_{\mathrm{u}}}(k\frac{\omega a}{kz_{\mathrm{u}}} + \omega)$ are bounds on the maximum velocity and acceleration according to the model (4.1). Following [27, 38], reasonable values for these quantities are $u_{\max} = .02\frac{\mathrm{m}}{\mathrm{s}}$, $u'_{\max} = .00014\frac{\mathrm{m}}{\mathrm{s}^2}$, $m = 1.5\mathrm{kg}$, and $c_d = 210\frac{\mathrm{Ns}^2}{m^2}$. For these values, the errors in the drogues' velocities will asymptotically be at most 5% of $u_{\max}$, leading us to favor the kinematic model over the dynamical one. Furthermore, we can see that in the worst case, with $p'^x(0) = 0$ when the drogues are dropped in the water and $u_u(0,p^x(0)) = u_{\max}$, after about 20 seconds, the drogues' velocities will be within 99% of their asymptotic behavior. Thus, after the drogues have been in the water for this long, the drogues' motion can be reasonably well modeled by the kinematic model. This analysis is illustrated in Figure 4.3. •

With our models now introduced, we are ready to state the problem of interest.

Problem statement: A team of N drogues is deployed in the ocean and their motion is governed by an internal wave. Since the drogues may control their depth, assume all are located at the same depth and each one can measure the relative distance, the distance derivative, and orientation to the closest M drogues in their own coordinate frame. The objective is to design a provably correct strategy that allows each drogue i to determine the parameters $\frac{a}{z_{\mathrm{u}}}$, k, ω, and θ_i, defining the motion of the internal wave with the limited information it possesses.

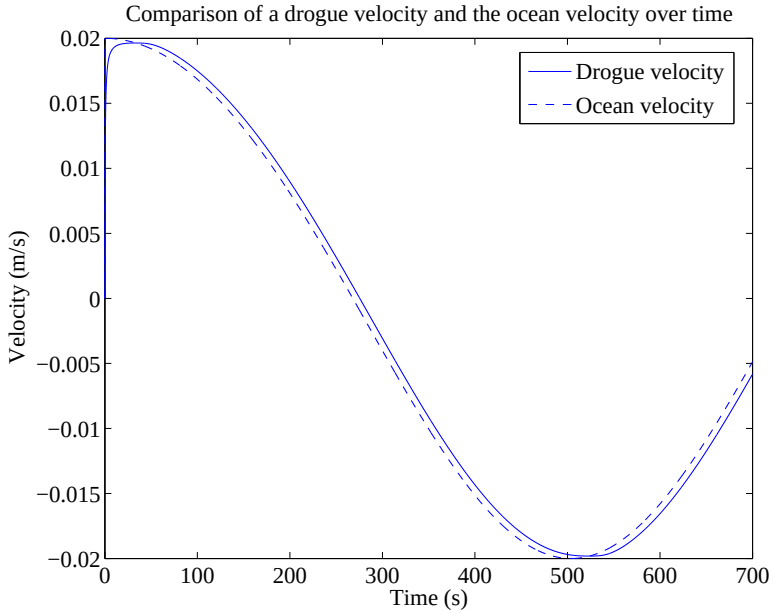

Figure 4.3: Comparison of the drogue's velocity as it moves according to the second-order dynamic model (4.3a) versus according to the kinematic model (4.2) corresponding to the ocean velocity. Quickly, the drogue's velocity becomes very close to the ocean velocity. The wave and drogue parameters are $k = \frac{2\pi}{200}\frac{1}{\mathrm{m}}$, $\omega = \frac{2\pi}{1000}\frac{1}{\mathrm{s}}$, $\frac{a}{z_{\mathrm{u}}} = .1$, $m = 1.5$ kg, and $c_d = 210\frac{\mathrm{Ns}^2}{\mathrm{m}^2}$.

4.2 Noise-free parameter estimation

We begin by noting that the dynamic evolution of a drogue under the linear internal wave can be explicitly described in the global reference frame. However, drogues cannot rely on this information as they do not have access to their global coordinates. This motivates our design of methods to determine the wave propagation direction and the internal wave parameters using the distance measurements available to the drogues. The following result shows that, remarkably, the drogue's dynamic evolution (4.2) can be described in an analytical way.

Proposition 4.2.1 (Drogue trajectory)**.** *The solution of* (4.2) *starting from* $\mathbf{p}(0)$

is

$$
\begin{aligned}
p^x(t) &= \frac{\omega}{k}\Big(1-\sqrt{1-(a/z_u)^2}\Big)t + \Xi(t) - \frac{\phi}{k},\\
\Xi(t) &= \frac{2}{k}\tan^{-1}\left(\frac{a}{z_u} - \sqrt{1-\left(\frac{a}{z_u}\right)^2}\tan\left(\frac{\pi t}{T}+\Lambda_0\right)\right)\\
&\quad - \frac{2\pi}{k}\left\lfloor \frac{t}{T} + \frac{\Lambda_0}{\pi} - \left\lfloor \frac{kp^x(0)+\phi+\pi}{2\pi}\right\rfloor + \frac{1}{2}\right\rfloor + \frac{2\pi}{kT}t,
\end{aligned}
$$

with

$$
\begin{aligned}
T &= \frac{2\pi}{\omega\sqrt{1-(a/z_u)^2}},\\
\Lambda_0 &= \tan^{-1}\left(\frac{1}{\sqrt{1-(a/z_u)^2}}\left(\frac{a}{z_u} - \tan\left(\frac{kp^x(0)+\phi}{2}\right)\right)\right).
\end{aligned}
$$

Proof. Let $\psi(t) = kp^x(t) - \omega t + \phi$ be the relative phase between the wave and drogue. Then (4.2) can be written as $\psi' = \omega\big(\frac{a}{z_u}\sin\psi - 1\big)$. Integrating, one gets

$$
\begin{aligned}
\int_{\psi_0}^{\psi} \frac{d\varsigma}{\frac{a}{z_u}\sin\varsigma - 1} &= \omega\int_0^t d\tau,\\
\frac{2}{\sqrt{1-(a/z_u)^2}}\tan^{-1}\left(\frac{a/z_u - \tan(\zeta/2)}{\sqrt{1-(a/z_u)^2}}\right)\Big|_{\psi_0}^{\psi} &= \omega t,
\end{aligned}
$$

where $\psi_0 = \psi(0) = kp^x(0) + \phi$. Manipulating the last expression, we arrive at

$$
\begin{aligned}
\psi(t) &= 2\tan^{-1}\left(\frac{a}{z_u} - \sqrt{1-\left(\frac{a}{z_u}\right)^2}\tan\left(\sqrt{1-(a/z_u)^2}\frac{\omega t}{2}+\Lambda_0\right)\right), \qquad (4.4)\\
\Lambda_0 &= \tan^{-1}\left(\frac{1}{\sqrt{1-(a/z_u)^2}}\left(\frac{a}{z_u} - \tan\left(\frac{kp^x(0)+\phi}{2}\right)\right)\right).
\end{aligned}
$$

Note that this function is discontinuous or, in other words, the expression for $\psi(t)$ above is only valid if the argument of the tangent function is in the interval $[-\frac{\pi}{2}, \frac{\pi}{2}]$. A general expression for $\psi(t)$ can be obtained as follows. Since the period of the tangent function is π, we deduce that the fundamental period of ψ is $T = \frac{2\pi}{\omega\sqrt{1-(a/z_u)^2}}$. Note that at $t^* = \frac{n\pi - 2\Lambda_0}{\omega\sqrt{1-(a/z_u)^2}}$, with $n \in \mathbb{Z}$ odd, one has that $\frac{\sqrt{1-(a/z_u)^2}}{2}\omega t^* + \Lambda_0 = \frac{n\pi}{2}$, and hence (4.4) jumps from $-\pi$ to π. To obtain

an expression of $\psi(t)$ which is valid in general, we need to subtract 2π from (4.4) every time t crosses one of the critical times (t^*) or, in other words, subtract the quantity

$$2\pi\left\lfloor \frac{t-\frac{1}{\omega\sqrt{1-(a/z_{\mathrm{u}})^2}}(\pi-2\Lambda_0)}{T}+1\right\rfloor = 2\pi\left\lfloor \frac{t}{T}+\frac{\Lambda_0}{\pi}+\frac{1}{2}\right\rfloor.$$

Finally, note that the initial condition Λ_0 jumps from $-\frac{\pi}{2}$ to $\frac{\pi}{2}$ at $kp^x(0)+\phi=n\pi$ for $n\in\mathbb{Z}$ odd. Thus, in order to make Λ_0 change continuously with the initial conditions, we subtract away from Λ_0 the quantity $\pi\left\lfloor\frac{kp^x(0)+\phi+\pi}{2\pi}\right\rfloor$. The result now follows. □

From Proposition 4.2.1, we see that the solution of (4.2) is the sum of a linear function in t and a periodic function Ξ with fundamental period T. Since the linear function does not depend on the initial condition, we deduce that the time evolution of the distance d_{ij}^x between any two drogues i and j is given by (with $\nu=\sqrt{1-(a/z_{\mathrm{u}})^2}$ for brevity)

$$\begin{aligned} d_{ij}^x(t) = {} & \frac{2}{k}\tan^{-1}\left(\frac{a}{z_{\mathrm{u}}}-\nu\tan\left(\frac{\nu\omega t}{2}+\Lambda_{0,j}\right)\right)-\frac{2\pi}{k}\left\lfloor\frac{t}{T}+\frac{\Lambda_{0,j}}{\pi}-\left\lfloor\frac{kp_j^x(0)+\phi+\pi}{2\pi}\right\rfloor+\frac{1}{2}\right\rfloor \\ & -\frac{2}{k}\tan^{-1}\left(\frac{a}{z_{\mathrm{u}}}-\nu\tan\left(\frac{\nu\omega t}{2}+\Lambda_{0,i}\right)\right)+\frac{2\pi}{k}\left\lfloor\frac{t}{T}+\frac{\Lambda_{0,i}}{\pi}-\left\lfloor\frac{kp_i^x(0)+\phi+\pi}{2\pi}\right\rfloor+\frac{1}{2}\right\rfloor, \end{aligned}$$

and is periodic with period T (as was numerically observed in Figure 4.2). However, from a drogue's viewpoint, two facts make this expression impractical: first, drogues do not have access to distances in the global reference frame and, second, since absolute position is not available, they are also unaware of their phase with respect to the internal wave. Even without these two hurdles, the highly nonlinear dependence of this expression on the parameters makes the results for standard least-squares data fitting methods [18, 24] not directly applicable.

These observations motivate the ensuing discussion describing a method to determine the internal wave parameters in the absence of measurement noise. Our treatment is presented for a generic drogue $i\in\{1,\ldots,N\}$ which requires inter-drogue distance and distance derivative measurements from its nearest 4 neighbors, denoted by $\{j_1,j_2,j_3,j_4\}$. Before getting into the details, we provide a brief overview of the algorithm design.

[Informal description]: Section 4.2.1 describes a method to determine the wave propagation direction. With this information available, drogues can project their inter-drogue measurements along the wave propagation direction. Section 4.2.2 uses relationships amongst the parameters to simplify the problem to first estimating one parameter. Specifically, it uses knowledge of the drogues' dynamics to define a function of the unknown horizontal wavenumber and the measurable inter-drogue data. Using this function and the data, the algorithm can determine the true value of the horizontal wavenumber. After this, Section 4.2.3 finds the amplitude ratio and frequency by solving equations derived from the drogue dynamics.

Remark 4.2.2 (Parameter estimation methodology)**.** The overall algorithm scheme involves simplifying the problem of estimating multiple parameters appearing nonlinearly by employing parametric relationships to allow the drogues to solve for one parameter first. The algorithm we propose here uses algebraic relationships to first find the wavenumber k. However, one could also utilize relationships generated from the data, for instance the drogue's period (see Proposition 4.2.1), to generate an algorithm which solves for the parameters in a different order. •

4.2.1 Wave propagation direction

Here we describe the method that drogues use to determine the wave propagation direction in their own body coordinates. Recall that the drogues are at the same depth but may be arbitrarily located in the $x-y$ plane. Consider the inter-drogue distance to the jth drogue, $j \in \{j_1, \ldots, j_4\}$, as measured by i in its own body coordinates,

$$\mathbf{d}_{ij} = \mathbf{p}_j - \mathbf{p}_i = (d_{ij}^{x_i}, d_{ij}^{y_i}, 0).$$

Figure 4.4 depicts the drogue i's own body coordinates, inter-drogue distance measurements, and the direction of wave propagation. For drogues undergoing motion purely caused by an internal wave, inter-drogue distances in their own body reference frame can be projected onto the global reference frame $\mathbf{d}_{ij}^g = Q_i^g \mathbf{d}_{ij}$ via the

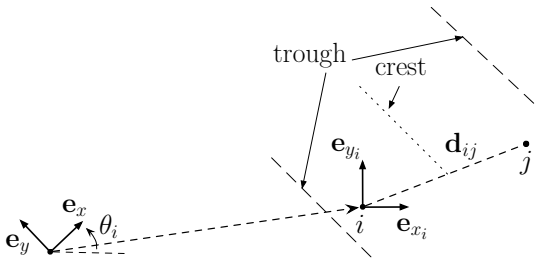

Figure 4.4: Drogue and wave orientations on the drogue's reference frame.

transformation matrix Q_i^g,

$$Q_i^g = \begin{bmatrix} \cos\theta_i & -\sin\theta_i & 0 \\ \sin\theta_i & \cos\theta_i & 0 \\ 0 & 0 & 1 \end{bmatrix}.$$

The global coordinate frame is useful because the inter-drogue distance in the y-direction is constant, i.e., $d_{ij}^{y'} = d_{ij}^{x_i\prime}\sin\theta_i + d_{ij}^{y_i\prime}\cos\theta_i = 0$. Since θ_i is constant, it can easily be found using the measurements available: $\theta_i = \tan^{-1}\left(\frac{-d_{ij}^{y_i\prime}}{d_{ij}^{x_i\prime}}\right)$.

Since both θ_i and $\theta_i + \pi$ fit this relation, we assume the drogues can differentiate the true θ_i. One way to accomplish this is to surface after at least one wave period and use GPS to determine which way the drogue has drifted.

4.2.2 Horizontal wavenumber via vanishing derivative

Here we describe a method to determine the horizontal wavenumber of the internal wave. Since the only dynamics are in the x-direction and each drogue i has determined θ_i as described in Section 4.2.1, from now on, we simply denote d_{ij}^x by d_{ij}. Thus, for each $i \in \{1, \ldots, N\}$, the following dynamics describe the drogues' motion in the x-direction,

$$d_{ij}' = 2\frac{\omega a}{k z_{\mathrm{u}}}\sin\Big(\frac{k d_{ij}}{2}\Big)\cos\Big(\frac{k d_{ij}}{2} + \psi_i\Big), \forall j \in \{j_1, \ldots, j_4\}, \tag{4.5a}$$

$$\psi_i' = \omega\Big(\frac{a}{z_{\mathrm{u}}}\sin(\psi_i) - 1\Big), \tag{4.5b}$$

where $\psi_i = k p_i^x - \omega t + \phi$ is the phase of the wave relative to drogue i, which is unmeasurable to it. We note that each inter-drogue distance equation (4.5a) contains

the unknowns ψ_i, $\frac{a}{z_u}$, ω, and k. Our strategy proceeds by deriving an equation which is only a function of measurement data and the horizontal wavenumber, and then determining conditions under which the correct value can be obtained. We later use this knowledge to determine the remaining parameters. In what follows, we make a notational distinction between $\mathcal{k}$ (the horizontal wavenumber interpreted as a variable) and k (the correct horizontal wavenumber that we seek to determine).

First, we show a result about the evolution of inter-drogue distances. This helps us formulate assumptions on the initial drogue locations to make the ensuing strategy applicable.

Lemma 4.2.3 (Inter-drogue distance bound)**.** *If at time t_0 the inter-drogue distance between i and j is bounded by $0 < |\frac{k}{2} d_{ij}(t_0)| < \frac{\pi}{2}$, then this bound holds for all $t \geq t_0$.*

Proof. We reason by contradiction. Assume there exists $t_* > t_0$ such that $|\frac{k}{2} d_{ij}(t_*)| \in \{0, \frac{\pi}{k}\}$. From (4.5a), we deduce that $d'_{ij}(t) = 0$ for all $t > t_*$, i.e., the inter-drogue distance stays constant. However, this contradicts the fact that the inter-drogue distances are periodic with period T. □

We present the assumptions on ordering of inter-drogue distances as well as bounds on initial inter-drogue distances.

Assumption 4.2.4 (Inter-drogue distance assumptions)**.** Without loss of generality, we assume $0 < d^x_{ij_1} < d^x_{ij_2} < d^x_{ij_3} < d^x_{ij_4}$. By Lemma 4.2.3, there exists an $\alpha > 0$ such that each drogue is at least α away from all other drogues in the x-direction, i.e.,

$$d^x_{ij}(t) > \alpha,\ \forall i \in \{1, \ldots, N\},\ \forall j \in \{j_1, j_2, j_3, j_4\},\ \forall t \geq t_0$$

We assume that initially drogue i and its 4 nearest neighbors are within one spatial wavelength of the internal wave, encapsulated by $d^x_{ij_4}(t_0) < \frac{2\pi}{k_{\max}}$, where k will be in $[k_{\min}, k_{\max}]$ by Assumption 4.1.1. Furthermore, by Lemma 4.2.3, this holds $\forall t \geq t_0$. Similarly, we assume that initially

$$d^x_{ij_2}(t_0) < \pi\left(\frac{1}{k_{\max}} - \frac{10}{99 k_{\min}}\right) - \alpha.$$

With the dynamics of (4.5a) and Assumption 4.1.1, this condition ensures that drogue i and its two closest neighbors are always within half a spatial wavelength minus α of each other. •

Unmeasurable relative phase

We begin by showing that the unmeasurable relative phase ψ_i can be explicitly expressed in terms of any two inter-drogue distances, which we choose as d_{ij_1} and d_{ij_2}, the distance derivatives d'_{ij_1} and d'_{ij_2}, and κ, as the sum of two functions:

$$\psi_i(\kappa, d_{ij_1}, d_{ij_2}, d'_{ij_1}, d'_{ij_2}) = \nu(\kappa, d_{ij_1}, d_{ij_2}, d'_{ij_1}, d'_{ij_2}) + \mu(\kappa, d_{ij_1}, d_{ij_2}, d'_{ij_1}, d'_{ij_2}). \quad (4.6)$$

The function ν captures the basic structure of ψ_i; it is derived by taking the quotient of two equations in the form of (4.5a) and solving for ψ_i. One loses information of the sign of d'_{ij_1} and d'_{ij_2} when one takes the ratio of them. Thus, $\{0, -\pi\}$-valued function μ determines which of the two solutions to $\tan(\psi_i) = C$ is the physically meaningful one. Specifically,

$$\nu(\kappa, d_{ij_1}, d_{ij_2}, d'_{ij_1}, d'_{ij_2}) = \tan^{-1}\left(\frac{d'_{ij_1}\sin(\frac{\kappa d_{ij_2}}{2})\cos(\frac{\kappa d_{ij_2}}{2}) - d'_{ij_2}\sin(\frac{\kappa d_{ij_1}}{2})\cos(\frac{\kappa d_{ij_1}}{2})}{d'_{ij_1}\sin^2(\frac{\kappa d_{ij_2}}{2}) - d'_{ij_2}\sin^2(\frac{\kappa d_{ij_1}}{2})}\right),$$

$$\mu(\kappa, d_{ij_1}, d_{ij_2}, d'_{ij_1}, d'_{ij_2}) = \begin{cases} 0, & \mathcal{F}(\kappa, d_{ij_2}, d'_{ij_2}, \nu) > 0 \vee \mathcal{F}(\kappa, d_{ij_1}, d'_{ij_1}, \nu) > 0, \\ -\pi, & \mathcal{F}(\kappa, d_{ij_2}, d'_{ij_2}, \nu) < 0 \vee \mathcal{F}(\kappa, d_{ij_1}, d'_{ij_1}, \nu) < 0, \end{cases}$$

where

$$\mathcal{F}(\kappa, d_{ij_2}, d'_{ij_2}, \nu) = \frac{d'_{ij_2}}{\cos(\frac{\kappa d_{ij_2}}{2} + \nu(\kappa, d_{ij_1}, d_{ij_2}, d'_{ij_1}, d'_{ij_2}))}.$$

Next, we present a result on the properties of ν, which are needed to determine k.

Lemma 4.2.5 (Smoothness properties of the relative phase)**.** *Under Assumption 4.2.4, the functions ν and $\partial_\kappa \nu$ are Lipschitz continuous with respect to $\frac{d'_{ij_1}}{d'_{ij_2}}$.*

Proof. One can show that ν and $\partial_\kappa \nu$ are differentiable with respect to $\frac{d'_{ij_1}}{d'_{ij_2}}$ if

$$0 < \frac{kd_{ij_1}}{2} < \frac{kd_{ij_2}}{2} < \frac{\pi}{2}. \quad (4.7)$$

By Assumption 4.2.4, the drogues will be in a compact subset of (4.7), which shows the result. □

We refer to the Lipschitz constants for $\boldsymbol{\nu}$ and $\partial_{\mathcal{k}}\boldsymbol{\nu}$ as $L_1(\alpha)$ and $L_2(\alpha)$, respectively. In general, ψ_i is a complex trigonometric function of $\mathcal{k}$. However, there are specific time instants for which its expression simplifies considerably, as the following result shows.

Lemma 4.2.6 (Simplifying expression of the relative phase)**.** *For time t_{cr}, let $d'_{ij}(t_{crit}) = 0$. Assume that drogues i and j are placed so that $0 < |\frac{k}{2}d_{ij}(t_{\mathrm{cr}})| < \frac{\pi}{2}$. Then $\psi_i(t_{\mathrm{cr}}) = \pm\frac{\pi}{2} - \frac{k}{2}d_{ij}(t_{\mathrm{cr}})$.*

Proof. The only thing that we need to justify is the existence of t_{cr}. Once this has been established, the explicit expression of $\psi_i(t_{\mathrm{cr}})$ readily follows from (4.5a). From Proposition 4.2.1, recall that d_{ij} is bounded and periodic. From (4.5b), we know that for any $t \in \mathbb{R}_{>0}$, $\psi_i'(t) \leq -\omega(1 - \frac{a}{z_{\mathrm{u}}}) < 0$, where we have used the fact that $\frac{a}{z_{\mathrm{u}}} \leq .1$. Therefore, looking at (4.5a), one can conclude the existence of t_{cr} within one period T when $d'_{ij}(t_{\mathrm{crit}}) = 0$. □

Recall that Lemma 4.2.3 guarantees that the assumptions of Lemma 4.2.6 are not difficult to ensure.

Distance rate quotient

Next, we note that the ratio of inter-drogue distance equations of the form (4.5a), say d'_{ij_3}/d'_{ij_4}, eliminates ω and a/z_{u}. These observations lead us to define the *distance rate quotient* function as follows. Let

$$\mathrm{dr}(\mathcal{k}, \psi_i, d_{ij}) = \sin\Big(\frac{\mathcal{k}d_{ij}}{2}\Big)\cos\Big(\frac{\mathcal{k}d_{ij}}{2} + \psi_i\Big).$$

Then, define $\mathrm{drq}(\mathcal{k}, \mathbf{D})$ as

$$\begin{aligned}\mathrm{drq}(\mathcal{k}, \mathbf{D}) &= \frac{\sin(\frac{\mathcal{k} d_{ij_3}}{2})\cos(\frac{\mathcal{k} d_{ij_3}}{2} + \psi_i(\mathcal{k}, d_{ij_1}, d_{ij_2}, d'_{ij_1}, d'_{ij_2}))}{\sin(\frac{\mathcal{k} d_{ij_4}}{2})\cos(\frac{\mathcal{k} d_{ij_4}}{2} + \psi_i(\mathcal{k}, d_{ij_1}, d_{ij_2}, d'_{ij_1}, d'_{ij_2}))} - \frac{d'_{ij_3}}{d'_{ij_4}} \\ &= \frac{\sin(\frac{\mathcal{k} d_{ij_3}}{2})\cos(\frac{\mathcal{k} d_{ij_3}}{2} + \boldsymbol{\nu}(\mathcal{k}, d_{ij_1}, d_{ij_2}, d'_{ij_1}, d'_{ij_2}))}{\sin(\frac{\mathcal{k} d_{ij_4}}{2})\cos(\frac{\mathcal{k} d_{ij_4}}{2} + \boldsymbol{\nu}(\mathcal{k}, d_{ij_1}, d_{ij_2}, d'_{ij_1}, d'_{ij_2}))} - \frac{d'_{ij_3}}{d'_{ij_4}} \\ &= \frac{\mathrm{dr}(\mathcal{k}, \boldsymbol{\nu}(\mathcal{k}, d_{ij_1}, d_{ij_2}, d'_{ij_1}, d'_{ij_2}), d_{ij_3})}{\mathrm{dr}(\mathcal{k}, \boldsymbol{\nu}(\mathcal{k}, d_{ij_1}, d_{ij_2}, d'_{ij_1}, d'_{ij_2}), d_{ij_4})} - \frac{d'_{ij_3}}{d'_{ij_4}}, \end{aligned} \tag{4.8}$$

where $\mathbf{D} = (d_{ij_1}, d_{ij_2}, d_{ij_3}, d_{ij_4}, d'_{ij_1}, d'_{ij_2}, d'_{ij_3}, d'_{ij_4})$ is the collection of all 4 inter-drogue distances and distance derivatives. The second equality comes from noting that drq takes the same value for either value that the function μ takes. By definition, $\mathcal{k} = k$ satisfies

$$\mathrm{drq}(k, \mathbf{D}) = 0. \tag{4.9}$$

In principle, there could be additional roots to this equation. This is what we investigate next.

Determining the horizontal wavenumber

Our goal now is to determine conditions that guarantee that only k is a solution to (4.9). The following result precisely characterizes how small the ratio d'_{ij_1}/d'_{ij_2} should be in order to guarantee that k is the unique value that satisfies (4.9).

Proposition 4.2.7. *(Range of suitable derivative ratios for determining k) Assuming internal wave parameters are within the bounds in Assumption 4.1.1, consider noiseless inter-drogue distance and distance derivative measurements* $\mathbf{D}$ *satisfying Assumption 4.2.4 and* $\left|\frac{d'_{ij_1}}{d'_{ij_2}}\right| < \delta(\alpha, k_{min})$*, where*

$$\delta(\alpha, k_{min}) = \min\left\{ \sin^2\left(\frac{k_{min}\alpha}{2}\right), \epsilon_{max}(k_{min}\alpha, L_1(\alpha), L_2(\alpha))\right\}$$

is positive, and the function ϵ_{max} *is defined in* (4.10)*. Then, only* k *satisfies* (4.9)*.*

The following auxiliary result is needed before we present the proof of Proposition 4.2.7. We begin by defining $\epsilon_{\max} : \mathbb{R}^3_{>0} \to \mathbb{R}_{>0}$,

$$\epsilon_{\max}(x, C_1, C_2) = \max_{\gamma \in [0, \Gamma(x)]} \mathcal{R}(x, \gamma, C_1, C_2) > 0, \tag{4.10}$$

with $\Gamma(x) = x - \sin(x)\cos(x)$ and

$$\mathcal{R}(x, \gamma, C_1, C_2) = \begin{cases} \min\left\{ \frac{\frac{1}{2}\arcsin(2(x-\gamma))-x}{C_1}, \frac{\gamma}{C_2} \right\}, & \frac{\pi}{4} > x - \gamma > 0, \\ \frac{x-\gamma-\frac{1}{2}}{C_2}, & 2\pi > x - \gamma > \frac{\pi}{4}. \end{cases}$$

Lemma 4.2.8. *$\forall x \in (0, 2\pi)$, $C_1, C_2 \in \mathbb{R}_{>0}$, $\epsilon \in (-\epsilon_{max}(x, C_1, C_2), \epsilon_{max}(x, C_1, C_2))$,*

$$\frac{1}{2}\sin(2(x + C_1\epsilon)) - x + C_2\epsilon \leq 0, \tag{4.11}$$

Proof. Note that for any $x > 0$, $\gamma \in (0, \Gamma(x))$ and $C_1, C_2 \in \mathbb{R}_{>0}$, $R(x, \gamma, C_1, C_2) > 0$, ensuring that $\epsilon_{\max}(x, C_1, C_2) > 0$ as well. For γ such that $x - \gamma > \frac{\pi}{4}$, we know that for any $\epsilon \in [-\mathcal{R}(x, \gamma, C_1, C_2), \mathcal{R}(x, \gamma, C_1, C_2)]$,

$$\frac{1}{2}\sin(2(x + C_1\epsilon)) - x + C_2\epsilon \leq \frac{1}{2} - x + \frac{C_2(x - \gamma - \frac{1}{2})}{C_2} = -\gamma \leq 0.$$

For γ such that $0 < x - \gamma \leq \frac{\pi}{4}$, note that for any $\epsilon \in [-\mathcal{R}(x, \gamma, C_1, C_2), \mathcal{R}(x, \gamma, C_1, C_2)]$,

$$\frac{1}{2}\sin(2(x + C_1\epsilon)) - x + C_2\epsilon \leq \frac{1}{2}\sin(2(x + C_1\frac{\frac{1}{2}\arcsin(2(x-\gamma)) - x}{C_1})) - x + \gamma = 0,$$

which completes the result. □

Proof of Proposition 4.2.7. The proof proceeds by establishing $\partial_{\mathsf{k}} \operatorname{drq}(\mathsf{k}, \mathbf{D}) > 0$, for all $\mathsf{k} \in [k_{\min}, k_{\max}]$. Once this is shown, it is easy to see that only k satisfies (4.9) since drq is strictly increasing as a function of k. To prove this fact about drq, it is enough to establish that

$$\frac{\partial_{\mathsf{k}} \operatorname{dr}(\mathsf{k}, \boldsymbol{\nu}(\mathsf{k}, d_{ij_1}, d_{ij_2}, d'_{ij_1}, d'_{ij_2}), d_{ij_3})}{\operatorname{dr}(\mathsf{k}, \boldsymbol{\nu}(\mathsf{k}, d_{ij_1}, d_{ij_2}, d'_{ij_1}, d'_{ij_2}), d_{ij_3})} > \frac{\partial_{\mathsf{k}} \operatorname{dr}(\mathsf{k}, \boldsymbol{\nu}(\mathsf{k}, d_{ij_1}, d_{ij_2}, d'_{ij_1}, d'_{ij_2}), d_{ij_4})}{\operatorname{dr}(\mathsf{k}, \boldsymbol{\nu}(\mathsf{k}, d_{ij_1}, d_{ij_2}, d'_{ij_1}, d'_{ij_2}), d_{ij_4})},$$

as long as

$$\operatorname{sgn}(\operatorname{dr}(\mathsf{k}, \boldsymbol{\nu}(\mathsf{k}, d_{ij_1}, d_{ij_2}, d'_{ij_1}, d'_{ij_2}), d_{ij_3})) = \operatorname{sgn}(\operatorname{dr}(\mathsf{k}, \boldsymbol{\nu}(\mathsf{k}, d_{ij_1}, d_{ij_2}, d'_{ij_1}, d'_{ij_2}), d_{ij_4})), \tag{4.12}$$

which corresponds to

$$\nu \in \Big(\frac{-\pi}{2} - \frac{\kappa d_{ij_3}}{2}, \frac{\pi}{2} - \frac{\kappa d_{ij_4}}{2}\Big) \bigcup \Big(\frac{\pi}{2} - \frac{\kappa d_{ij_3}}{2}, \frac{3\pi}{2} - \frac{\kappa d_{ij_4}}{2}\Big).$$

This set admits all $\frac{d'_{ij_1}}{d'_{ij_2}} \in \Big(-\infty, \frac{\sin(\frac{\kappa d_{ij_1}}{2})\sin(\frac{\kappa}{2}(d_{ij_4}-d_{ij_1}))}{\sin(\frac{\kappa d_{ij_2}}{2})\sin(\frac{\kappa}{2}(d_{ij_4}-d_{ij_2}))}\Big)$. By hypothesis, $\frac{d'_{ij_1}}{d'_{ij_2}}$ is in this range and hence (4.12) holds. Since $d_{ij_3} < d_{ij_4}$, its sufficient to show that

$$\partial_{d_{ij_3}}\left(\frac{\partial_\kappa \operatorname{dr}(\kappa, \nu(\kappa, d_{ij_1}, d_{ij_2}, d'_{ij_1}, d'_{ij_2}), d_{ij_3})}{\operatorname{dr}(\kappa, \nu(\kappa, d_{ij_1}, d_{ij_2}, d'_{ij_1}, d'_{ij_2}), d_{ij_3})}\right) < 0.$$

After some calculations, we obtain

$$\partial_{d_{ij_3}}\left(\frac{\partial_\kappa \operatorname{dr}(\kappa, \nu(\kappa, d_{ij_1}, d_{ij_2}, d'_{ij_1}, d'_{ij_2}), d_{ij_3})}{\operatorname{dr}(\kappa, \nu(\kappa, d_{ij_1}, d_{ij_2}, d'_{ij_1}, d'_{ij_2}), d_{ij_3})}\right) = \frac{\sin\left(\frac{\kappa d_{ij_3}}{2}\right)\cos\left(\frac{\kappa d_{ij_3}}{2}\right) - \frac{\kappa d_{ij_3}}{2}}{2\sin^2\left(\frac{\kappa d_{ij_3}}{2}\right)} - \frac{\sin\left(\frac{\kappa d_{ij_3}}{2} + \nu\right)\cos\left(\frac{\kappa d_{ij_3}}{2} + \nu\right) + \kappa\left(\frac{d_{ij_3}}{2} + \partial_\kappa \nu\right)}{2\cos^2\left(\frac{\kappa d_{ij_3}}{2} + \nu\right)}. \quad (4.13)$$

From Lemma 4.2.6, when $\frac{d'_{ij_1}}{d'_{ij_2}} = 0$, then $\nu = \frac{\pi}{2} - \frac{\kappa d_{ij_1}}{2}$ and $\partial_\kappa \nu = -\frac{d_{ij_1}}{2}$, and so (4.13) becomes

$$\partial_{d_{ij_3}}\left(\frac{\partial_\kappa \operatorname{dr}(\kappa, \nu(\kappa, d_{ij_1}, d_{ij_2}, d'_{ij_1}, d'_{ij_2}), d_{ij_3})}{\operatorname{dr}(\kappa, \nu(\kappa, d_{ij_1}, d_{ij_2}, d'_{ij_1}, d'_{ij_2}), d_{ij_3})}\right) = \frac{\sin\left(\frac{\kappa d_{ij_3}}{2}\right)\cos\left(\frac{\kappa d_{ij_3}}{2}\right) - \frac{\kappa d_{ij_3}}{2}}{2\sin^2\left(\frac{\kappa d_{ij_3}}{2}\right)} + \frac{\sin\left(\frac{\kappa(d_{ij_3}-d_{ij_1})}{2}\right)\cos\left(\frac{\kappa(d_{ij_3}-d_{ij_1})}{2}\right) - \kappa\frac{(d_{ij_3}-d_{ij_1})}{2}}{2\sin^2\left(\frac{\kappa(d_{ij_3}-d_{ij_1})}{2}\right)},$$

where both summands of which are clearly negative ensuring the desired partial derivative is negative. With this in mind, we write in general that $\nu = \frac{\pi}{2} - \frac{\kappa d_{ij_1}}{2} + \epsilon_1$ and $\partial_\kappa \nu = -\frac{d_{ij_1}}{2} + \epsilon_2$. Similarly, we rewrite (4.13) as

$$\partial_{d_{ij_3}}\left(\frac{\partial_\kappa \operatorname{dr}(\kappa, \nu(\kappa, d_{ij_1}, d_{ij_2}, d'_{ij_1}, d'_{ij_2}), d_{ij_3})}{\operatorname{dr}(\kappa, \nu(\kappa, d_{ij_1}, d_{ij_2}, d'_{ij_1}, d'_{ij_2}), d_{ij_3})}\right) = \frac{\sin\left(\frac{\kappa d_{ij_3}}{2}\right)\cos\left(\frac{\kappa d_{ij_3}}{2}\right) - \frac{\kappa d_{ij_3}}{2}}{2\sin^2\left(\frac{\kappa d_{ij_3}}{2}\right)} + \frac{\sin\left(\frac{\kappa(d_{ij_3}-d_{ij_1})}{2} + \epsilon_1\right)\cos\left(\frac{\kappa(d_{ij_3}-d_{ij_1})}{2} + \epsilon_1\right) - \kappa\frac{(d_{ij_3}-d_{ij_1})}{2} + \kappa\epsilon_2}{2\sin^2\left(\frac{\kappa(d_{ij_3}-d_{ij_1})}{2} + \epsilon_1\right)}.$$

The unchanged, first summand is still negative. A sufficient condition for the whole expression being negative is that the sum of the second and third summands is

negative too. Using Lemma 4.2.8, we can ensure that (4.13) is negative when $\left|\frac{d'_{ij_1}}{d'_{ij_2}}\right| < \epsilon_{\max}\left(\frac{\kappa(d_{ij_3}-d_{ij_1})}{2}, L_1, L_2\right)$, which completes the expression for δ. The fact that $\delta > 0$ is seen from the definition of $\epsilon_{\max}$ and the assumption that $\kappa \leq \frac{2\pi}{d_{ij_4}}$. □

Note that the conditions of Proposition 4.2.7 are satisfied by data obtained at time t_{cr} with $d'_{ij_1}(t_{\text{cr}}) = 0$, as in Lemma 4.2.6. Now, the question is what is the interval around t_{cr} where the measured data still satisfies the conditions of Proposition 4.2.7. Among other things, this issue is important in order to determine acceptable sampling rates for the drogues. The next result answers this question.

Corollary 4.2.9 (Range of suitable times for determining k)**.** *Assuming internal wave parameters are within the bounds in Assumption 4.1.1, consider noiseless inter-drogue distance and distance derivative measurements at t_{cr} such that $d'_{ij_1}(t_{\text{cr}}) = 0$ and initial conditions satisfying Assumption 4.2.4. Then, k uniquely satisfies* (4.9) *with data $\mathbf{D}(t)$, for all $t \in (t_{\text{cr}} - \Delta, t_{\text{cr}} + \Delta)$, where $\Delta(\delta, L_3, L_4) = \frac{L_4}{L_3}\frac{\delta}{1+\delta}$, δ is given in Proposition 4.2.7, $L_3 \geq 2\frac{\omega a}{k z_u}(\frac{\omega a}{z_u} + \omega)$, and $0 < L_4 \leq |d'_{ij_2}(t_{\text{cr}})|$.*

Proof. The magnitude of the second time derivative of any inter-drogue distance is bounded by $2\frac{\omega a}{k z_{\text{u}}}(\frac{\omega a}{z_{\text{u}}} + \omega)$. Thus,

$$|d'_{ij_1}(t) - d'_{ij_1}(t_{\text{cr}})| \leq L_3|t - t_{\text{cr}}|,$$
$$|d'_{ij_2}(t) - d'_{ij_2}(t_{\text{cr}})| \leq L_3|t - t_{\text{cr}}|.$$

From the analysis in Proposition 4.2.7, for a set of inter-drogue measurements there exists an open interval $(-\delta, \delta)$ in $\frac{d'_{ij_1}}{d'_{ij_2}}$ containing 0 where drq is strictly increasing. Thus, by the assumption that $t \in (t_{\text{cr}} - \Delta, t_{\text{cr}} + \Delta)$, we have the following,

$$\left|\frac{d'_{ij_1}(t + t_{\text{cr}})}{d'_{ij_2}(t + t_{\text{cr}})}\right| \leq \frac{L_3|t - t_{\text{cr}}|}{L_4 - L_3|t - t_{\text{cr}}|} < \frac{\frac{L_4\delta}{1+\delta}}{L_4(1 - \frac{\delta}{1+\delta})} = \delta,$$

which proves the result. □

Using Corollary 4.2.9 and the assumptions in Assumptions 4.1.1 and 4.2.4, the following result gives a sufficient sampling rate to satisfy the conditions of Corollary 4.2.9.

Lemma 4.2.10 (Minimum sampling rate)**.** *If internal wave parameters satisfy Assumption 4.1.1 and given $\alpha > 0$ from Assumption 4.2.4, a bound on the minimum sampling rate for Corollary 4.2.9 is*

$$f_{s,min} > \frac{(1 + (\frac{a}{z_u})_{max})\omega_{max} \csc^2(\frac{k_{min}\alpha}{2})}{\min\{\sin^2(\frac{k_{min}\alpha}{2}), \epsilon_{max}(\frac{k_{min}\alpha}{2}, L_1(\alpha), L_2(\alpha))\}}. \tag{4.14}$$

4.2.3 Amplitude ratio and frequency via data fitting

In this section, we discuss how once the true horizontal wavenumber k is known, the parameters $\frac{a}{z_u}$ and ω can also be found as described in the following result.

Lemma 4.2.11 (Determination of $\frac{a}{z_u}$ and ω)**.** *Assume k is known. For $t_{\xi_1} < t_{\xi_2} < t_{\xi_3}$ with $t_{\xi_3} - t_{\xi_1} < T$, compute noiseless measurements of ψ_i and ψ_i' at these times by evaluating* (4.6) *and using the method described in Section 2.3. Then, ω and $\frac{a}{z_u}$ can be found from*

$$\begin{bmatrix}\beta_1 \\ \beta_2\end{bmatrix} = \begin{bmatrix}\sin(\psi_i(t_\varpi)) & 1 \\ \sin(\psi_i(t_\aleph)) & 1\end{bmatrix}^{-1} \begin{bmatrix}\psi_i'(t_\varpi) \\ \psi_i'(t_\aleph)\end{bmatrix} \tag{4.15a}$$

$$\omega = -\beta_2, \quad \frac{a}{z_u} = \frac{-\beta_1}{\beta_2}, \tag{4.15b}$$

where $\varpi, \aleph \in \{\xi_1, \xi_2, \xi_3\}$ so that $\sin(\psi_i(t_\varpi)) \neq \sin(\psi_i(t_\aleph))$.

Proof. First, given that $\psi_i' < 0$ and $\psi_i(t+T) = \psi_i(t) - 2\pi$, $\sin(\psi_i(t_\varpi)) \neq \sin(\psi_i(t_\aleph))$ for some $t_\varpi, t_\aleph \in \{t_{\xi_1}, t_{\xi_2}, t_{\xi_3}\}$. Using the values of ψ_i and ψ_i' at these two timesteps, one can solve for $\frac{a}{z_u}$ and ω using (4.5b) as described in (4.15). □

Remark 4.2.12 (Minimum sampling rate)**.** For Lemma 4.2.11 to hold, one needs $f_{s,\min} > \frac{3}{T}$. Comparing this to Lemma 4.2.10, one can see that if (4.14) is enforced, then the assumptions of both Corollary 4.2.9 and Lemma 4.2.11 hold. •

4.2.4 Vanishing Distance Derivative Detection Strategy

We gather the discussion above into Algorithm 4.1.

For Step **3**, any root finder method can find k uniquely; one suitable method, for instance, is gradient descent. The following result establishes the

Table 4.1: **Vanishing Distance Derivative Detection Strategy**

Assumptions: $f_s \geq f_{s,\min}$, initial distances satisfy Assumption 4.2.4 for some $\alpha > 0$, internal wave parameters within bounds in Assumption 4.1.1

run at time $t_\kappa = \frac{\kappa}{f_s}$, for some $\kappa \in \mathbb{Z}_{\geq 1}$

1: calculate wave propagation direction, $\theta_i = \tan^{-1}(-d_{ij_1}^{y_i\prime}(t_\kappa)/d_{ij_1}^{x_i\prime}(t_\kappa))$

2: **if** $\left|\frac{d'_{ij_1}(t_\kappa)}{d'_{ij_2}(t_\kappa)}\right| < \min\left\{\sin^2\left(\frac{k_{\min}\alpha}{2}\right), \epsilon_{\max}(k_{\min}\alpha, L_1(\alpha), L_2(\alpha))\right\}$ **then**

3: find k by solving $\mathrm{drq}(\mathcal{k}, \mathbf{D}(t_\kappa)) = 0$

4: compute $\psi_i(t_\xi)$ (via (4.6)) and $\psi_i'(t_\xi)$ (via Section 2.3), for $\xi \in \{\kappa-2, \kappa-1, \kappa\}$

5: choose $\varpi, \aleph \in \{\kappa-2, \kappa-1, \kappa\}$ such that $\sin(\psi_i(\varpi)) \neq \sin(\psi_i(\aleph))$ and solve

$$\begin{bmatrix}\beta_1\\ \beta_2\end{bmatrix} = \begin{bmatrix}\sin(\psi_i(\varpi)) & 1\\ \sin(\psi_i(\aleph)) & 1\end{bmatrix}^{-1}\begin{bmatrix}\psi_i'(\varpi)\\ \psi_i'(\aleph)\end{bmatrix}$$

6: set $\omega = -\beta_2$ and $\frac{a}{z_u} = \frac{-\beta_1}{\beta_2}$

7: **end if**

correctness of this strategy, which follows from Corollary 4.2.9, Lemma 4.2.11, and Remark 4.2.12.

Proposition 4.2.13 (Conditions for determining all parameters)**.** *Assuming that $f_s \geq f_{s,min}$, internal wave parameters are within bounds in Assumption 4.1.1, and that the initial drogue locations satisfy Assumption 4.2.4, then drogue i can uniquely determine the parameters θ_i, $\frac{a}{z_u}$, ω, and k using the* ***Vanishing Distance Derivative Detection Strategy****.*

4.3 Robustness of parameter estimation to error

Here, we consider the effect of error in measurements on the application of the **Vanishing Distance Derivative Detection Strategy**. Section 4.3.1 describes some of the sources of error which occur during an ocean implementation of the proposed algorithm. Section 4.3.2 shows that the **Vanishing Distance Derivative Detection Strategy** is able to get a parameter estimates when the data has sufficiently small errors. This motivates our results in Section 4.3.3, which bound the errors in estimates of k, $\frac{a}{z_u}$, and ω as a function of the errors in the measured quantities. Finally, in Section 4.3.4, we devise a method for aggregating noisy parameter estimates from different timesteps.

4.3.1 Sources of error from algorithm implementation

Here, we describe some of the sources of error which occur in the algorithm's implementation.

Noise in measurements: In practice measurements collected by sensors contain noise. We assume this noise is unbiased, Gaussian, and that the noise at different time instances and for different measurements is uncorrelated.

Model uncertainty: The problem setup described in Section 4.1.2 assumes that drogues are Lagrangian. However, as seen in Remark 4.1.2, drogues have a finite mass and drag coefficient making them not perfectly Lagrangian, leading to a difference between the actual drogue's velocity and the ocean

velocity. One can treat this mismatch as an unknown but nonrandom error in the measurements of inter-drogue distances and distance derivatives.

Drogues not maintaining depth: We assume that the drogues have a controller that uses feedback on depth measurements to maintain a desired depth. Due to noisy depth measurements and a desire to minimize actuation cost, instead we assume that the drogues will be within an interval around the desired depth. Although depth is not directly used by the proposed algorithm, this inaccuracy affects inter-drogue distance measurements. As above, one can treat this as an unknown but nonrandom error in the inter-drogue distance measurements.

4.3.2 Existence of parameter estimates under error

Here we show that the **Vanishing Distance Derivative Detection Strategy** is able to estimate the parameters from measurements with sufficiently small error. We begin our study with the horizontal wavenumber k because an estimate of it is needed for estimates of the other parameters. The next result establishes the analytic character of the function drq. The proof follows from the known fact, see e.g., [45], that sums, products, and compositions of analytic functions are analytic, and quotients of analytic functions are analytic provided the denominator does not vanish.

Lemma 4.3.1 (drq is analytic)**.** *For any $k \in [k_{min}, k_{max}]$,* drq *is analytic on the set $\mathcal{D}_{altc}(k)$:*

$$\mathcal{D}_{altc}(k) = \{\mathbf{D} \mid d'_{ij_1}\sin^2(\frac{kd_{ij_2}}{2}) - d'_{ij_2}\sin^2(\frac{kd_{ij_1}}{2}) \neq 0, d'_{ij_4} \neq 0, \\ \cos\Big(\frac{kd_{ij_4}}{2} + \psi_i(k, d_{ij_1}, d_{ij_2}, d'_{ij_1}, d'_{ij_2})\Big) \neq 0, \sin\Big(\frac{kd_{ij_4}}{2}\Big) \neq 0\}.$$

We now introduce two sets which help define the set of distances and distance derivatives $\mathbf{D}$ where estimates of k can be found in a neighborhood around $\mathbf{D}$.

Let

$$\mathcal{D}_{\text{real}}(\mathbf{\Phi}) = \big\{\mathbf{D} \mid 0 < d_{ij_1} < d_{ij_2} < d_{ij_3} < d_{ij_4} < \frac{2\pi}{k},$$
$$d'_{ij} = 2\frac{\omega a}{k z_{\text{u}}} \sin\Big(\frac{k d_{ij}}{2}\Big)\cos\Big(\frac{k d_{ij}}{2} + \psi_i(k, d_{ij_1}, d_{ij_2}, d'_{ij_1}, d'_{ij_2})\Big),\ j \in \{j_1, \ldots, j_4\}\big\}.$$

be the set of all inter-drogue measurements $\mathbf{D}$ that can come from one instantiation of $\mathbf{\Phi} = (\frac{a}{z_{\text{u}}}, \omega, k)$. Let $\mathcal{D}_{\text{diff}}(k) = \{\mathbf{D} \mid \partial_k \operatorname{drq}(k, \mathbf{D}) \neq 0\}$. Combining Lemma 4.3.1 with the Analytic Implicit Function Theorem [45] yields the existence of the implicit function for estimates of k.

Lemma 4.3.2. *(Existence of estimates of horizontal wavenumber) For any* $\mathbf{D} \in \mathcal{D}_{real}(\mathbf{\Phi}) \cap \mathcal{D}_{diff}(k) \cap \mathcal{D}_{altc}(k)$*, there is a neighborhood of* $\mathbf{D}$*,* $\mathcal{N}_{\mathbf{D}}(\mathbf{\Phi}) \subset \mathbb{R}^8$ *for which there exists an analytic function* $\mathbf{k_D} : \mathbb{R}^8 \to \mathbb{R}$ *which satisfies*

$$\operatorname{drq}(\mathbf{k_D}(\tilde{\mathbf{D}}), \tilde{\mathbf{D}}) = 0, \text{ for } \tilde{\mathbf{D}} \in \mathcal{N}_{\mathbf{D}}(\mathbf{\Phi}).$$

The existence of the function $\mathbf{k_D}$ guarantees that k can be estimated from inter-drogue measurements containing errors, when the errors are sufficiently small.

Remark 4.3.3. *(Frequency and amplitude ratio estimates from measurements with errors)* From (4.6), given an estimate of k and measurements with errors, one can get an estimate of ψ_i. Furthermore, using the method outlined in Section 2.3, one can also estimate ψ'_i. Thus, using (4.15), estimates for ω and $\frac{a}{z_{\text{u}}}$ exist as long as $\sin(\tilde{\psi}_i(t_\varpi)) \neq \sin(\tilde{\psi}_i(t_\aleph))$. •

4.3.3 Robustness to error

In this section we bound the error in estimates of the horizontal wavenumber k, amplitude ratio $\frac{a}{z_{\text{u}}}$, and frequency ω as a function of the error in the measurements.

Horizontal wavenumber

From the analysis in Section 4.3.2, for a fixed set of noiseless measurements $\mathbf{D} \in \mathcal{D}_{\text{real}}(\mathbf{\Phi}) \cap \mathcal{D}_{\text{diff}}(k) \cap \mathcal{D}_{\text{altc}}(k)$, the corresponding noisy estimate of k in a neighborhood around $\mathbf{D}$, $\mathcal{N}_{\mathbf{D}}(\mathbf{\Phi})$, is given by the function $\mathbf{k_D}$. We wish to now restrict

ourselves to a set where changes in the function $\mathbf{k_D}$ are bounded. Specifically, let $U_{\text{bnd-drv}} > 0$ and define

$$\mathcal{D}_{\text{deriv},U_{\text{bnd-drv}}}(\mathbf{\Phi}) = \{\mathbf{D} \in \mathcal{D}_{\text{real}}(\mathbf{\Phi}) \cap \mathcal{D}_{\text{diff}}(k) \cap \mathcal{D}_{\text{altc}}(k) \mid \max_{r\in\{1,\ldots,8\}} |\partial_{\text{cpnt}_r(\mathbf{D})}\mathbf{k_D}(\mathbf{D})| < U_{\text{bnd-drv}}\}.$$

For each $\mathbf{D} \in \mathcal{D}_{\text{deriv},U_{\text{bnd-drv}}}(\mathbf{\Phi})$, by the analyticity of $\mathbf{k_D}$, one can construct a neighborhood $\mathcal{N}_{\mathbf{D},U_{\text{bnd-drv}}}(\mathbf{\Phi})$ such that for $\max_{r\in\{1,\ldots,8\}} |\partial_{\text{cpnt}_r(\mathbf{D})}\mathbf{k_D}(\tilde{\mathbf{D}})| < U_{\text{bnd-drv}}$ for any $\tilde{\mathbf{D}} \in \mathcal{N}_{\mathbf{D},U_{\text{bnd-drv}}}(\mathbf{\Phi})$. The set of measurements with small enough error are $\tilde{\mathcal{D}}_{U_{\text{bnd-drv}}}(\mathbf{\Phi}) = \bigcup_{\mathbf{D}\in\mathcal{D}_{\text{deriv},U_{\text{bnd-drv}}}} \mathcal{N}_{\mathbf{D},U_{\text{bnd-drv}}}(\mathbf{\Phi})$.

The next result provides bounds on the error in estimating k by the error in the measurements. The proof is a combination of the Mean Value Theorem and the Cauchy-Schwartz inequality [79].

Lemma 4.3.4. *(Bounds for errors in k as function of errors in measurements) Given noisy measurements of inter-drogue distances and distance derivatives $\tilde{\mathbf{D}} \in \tilde{\mathcal{D}}_{U_{bnd\text{-}drv}}(\mathbf{\Phi})$ for some $U_{bnd\text{-}drv} > 0$, then the error between the estimated $\hat{k}$ produced by the **Vanishing Distance Derivative Detection Strategy** and k can be bounded by*

$$|\hat{k} - k| = |\mathbf{k_D}(\tilde{\mathbf{D}}) - k| \leq \sqrt{8}U_{bnd\text{-}drv}||\tilde{\mathbf{D}} - \mathbf{D}||.$$

Amplitude ratio and frequency

As seen in Lemma 4.2.11, with noiseless measurements, two measurements of ψ_i and ψ_i' are sufficient to exactly determine $\frac{a}{z_{\text{u}}}$ and ω. However, with noisy measurements, the question that naturally arises is whether there is a benefit to using more than 2 measurements. This is what we explore next.

Given n noisy measurements of ψ_i',

$$\tilde{\psi}_i'(t_{\kappa_q}) = \psi_i'(t_{\kappa_q}) + \epsilon_{\psi_i'}(t_{\kappa_q}), \quad \forall q \in \{1, \ldots, n\},$$

we construct estimates of $\frac{a}{z_{\text{u}}}$ and ω using least-squares techniques on the ψ_i dy-

namics in (4.5b),

$$\underbrace{\begin{bmatrix}\psi_i'(t_{\kappa_1})\\ \vdots \\ \psi_i'(t_{\kappa_n})\end{bmatrix}}_{\psi_i'} = \underbrace{\begin{bmatrix}\sin(\psi_i(t_{\kappa_1})) & 1\\ \vdots & \\ \sin(\psi_i(t_{\kappa_n})) & 1\end{bmatrix}}_{W} \underbrace{\begin{bmatrix}\beta_1\\ \beta_2\end{bmatrix}}_{\beta},$$

$$\beta_1 = \frac{\omega a}{z_{\mathrm{u}}}, \quad \beta_2 = -\omega,$$

mimicking (4.15). The least-squares estimates are

$$\begin{aligned}\hat{\beta} &= (W^TW)^{-1}W^T\tilde{\psi}_i' = (W^TW)^{-1}W^T(\psi_i' + \epsilon_{\psi_i'})\\ &= \beta_{\text{true}} + \underbrace{(W^TW)^{-1}W^T\epsilon_{\psi_i'}}_{\beta_{\text{error}}}.\end{aligned}$$

Explicitly, β_{error} is given by

$$\begin{aligned}\text{cpnt}_1(\beta_{\text{error}}) &= \frac{\sum_{q=1}^n \epsilon_q(\sum_{r=1}^n \sin(\psi_i(t_{\kappa_q})) - \sin(\psi_i(t_{\kappa_r})))}{\sum_{q=1}^n \sin(\psi_i(t_{\kappa_q}))(\sum_{r=1}^n \sin(\psi_i(t_{\kappa_q})) - \sin(\psi_i(t_{\kappa_r})))},\\ \text{cpnt}_2(\beta_{\text{error}}) &= \frac{\sum_{q=1}^n \epsilon_q(\sum_{r=1}^n \sin(\psi_i(t_{\kappa_r}))(\sin(\psi_i(t_{\kappa_r})) - \sin(\psi_i(t_{\kappa_q}))))}{\sum_{q=1}^n \sin(\psi_i(t_{\kappa_q}))(\sum_{r=1}^n \sin(\psi_i(t_{\kappa_q})) - \sin(\psi_i(t_{\kappa_r})))}.\end{aligned}$$

The error β_{error} is a complex function of the distribution of ψ_i' as well as the sampling pattern (both spacing and the number of samples). Because the distribution of ψ_i' is non-Gaussian and unknown, we consider the case that all errors in ψ_i' are at most ϵ. Furthermore, we assume that the sampling pattern is uniform, meaning that

$$\begin{aligned}\sin(\psi_i(t_{\kappa_q})) = \frac{q-1}{n-1}\Big(\sin(\psi_i(t_{\kappa_n})) - \sin(\psi_i(t_{\kappa_1}))\Big) + \\ \sin(\psi_i(t_{\kappa_1})), \quad \forall q \in \{2, n-1\}. \quad (4.16)\end{aligned}$$

Let WLS be the *Worst-case Least Squares* error (for estimating ω) defined by,

$$\begin{aligned}&\text{WLS}(n, \sin(\psi_i(t_{\kappa_1})), \sin(\psi_i(t_{\kappa_n})), \epsilon)\\ &\qquad = \epsilon\frac{\sum_{q=1}^n |(\sum_{r=1}^n \sin(\psi_i(t_{\kappa_r}))(\sin(\psi_i(t_{\kappa_r})) - \sin(\psi_i(t_{\kappa_q}))))|}{\sum_{q=1}^n \sin(\psi_i(t_{\kappa_q}))(\sum_{r=1}^n \sin(\psi_i(t_{\kappa_q})) - \sin(\psi_i(t_{\kappa_r})))}.\end{aligned}$$

In the right-hand side, we use (4.16) to express $\{\sin(\psi_i(t_{\kappa_q}))\}_{q=2}^{n-1}$ in terms of $\sin(\psi_i(t_{\kappa_1}))$ and $\sin(\psi_i(t_{\kappa_n}))$. Note that WLS is an upper bound of $\text{cpnt}_2(\beta_{\text{error}})$. Even though the asymptotic dependence of WLS on n is difficult to characterize, the next result provides bounds that are sufficient to answer the question that motivates this section.

Lemma 4.3.5. *(Worst-case estimation error grows with number of measurements) Consider any maximum error $\epsilon > 0$, wave parameters $\frac{a}{z_u}, \omega \in \mathbb{R}$, number of measurements $n \in \mathbb{Z}_{\geq 1}$, and range of measurements $\sin(\psi_i(t_{\kappa_1})) < \sin(\psi_i(t_{\kappa_n})) \in [-1, 1)$. If the set of measurements of ψ_i are distributed according to* (4.16) *and the errors in ψ_i' are bounded by ϵ, i.e., $|\tilde{\psi}_i'(t_{\kappa_q}) - \psi_i'(t_{\kappa_q})| < \epsilon$, for all $q \in \{1, \ldots, n\}$, then* WLS *can be bounded between two increasing functions of n as*

$$\epsilon \frac{3 \max\{|\sin(\psi_i(t_{\kappa_1}))|, |\sin(\psi_i(t_{\kappa_n}))|\}(n-1)}{(\sin(\psi_i(t_{\kappa_n})) - \sin(\psi_i(t_{\kappa_1})))n} \geq$$
$$\text{WLS}(n, \sin(\psi_i(t_{\kappa_1})), \sin(\psi_i(t_{\kappa_n})), \epsilon) \geq B_n,$$

where $B_n = \epsilon$ if $-1 < \sin(\psi_i(t_{\kappa_1})) \leq 0$ and

$$B_n = \epsilon \max\Big(\frac{3 \sin(\psi_i(t_{\kappa_1}))(n+3)(n-2)}{2(\sin(\psi_i(t_{\kappa_n})) - \sin(\psi_i(t_{\kappa_1})))n(n+1)}, 1\Big),$$

if $0 < \sin(\psi_i(t_{\kappa_1})) < 1$.

Proof. To reduce the length of expressions in the proof, we rewrite the data with the following notation,

$$\tilde{y}_q = \beta_1 x_q + \beta_2 + \epsilon_q, \quad x_q = \frac{q-1}{n-1}(x_n - x_1) + x_1,$$

for $q \in \{1, \ldots, n\}$, where

$$x_1 = \sin(\psi_i(t_{\kappa_1})), \quad x_n = \sin(\psi_i(t_n)), \quad x_q = \sin(\psi_i(t_{\kappa_q})),$$
$$\tilde{y}_q = \tilde{\psi}_i'(t_{\kappa_q}), \qquad \epsilon_q = \tilde{\psi}_i'(t_{\kappa_q}) - \psi_i'(t_{\kappa_q}),$$

and $\beta_1 = \frac{\omega a}{z_{\mathrm{u}}}$ and $\beta_2 = -\omega$. Then,

$$\begin{aligned}
\mathrm{WLS}(n, x_1, x_n, \epsilon) &= \epsilon \frac{\sum_{q=1}^{n} \left| \frac{x_n - x_1}{n-1} \sum_{r=1}^{n} (\frac{r-1}{n-1}(x_n - x_1) + x_1)(q-r) \right|}{\sum_{q=1}^{n} \left((\frac{q-1}{n-1}(x_n - x_1) + x_1)(\frac{x_n - x_1}{n-1} \sum_{r=1}^{n} (q-r)) \right)} \\
&\leq \frac{\epsilon \frac{x_n - x_1}{n-1} \max\{|x_1|, |x_n|\} \sum_{q=1}^{n} \sum_{r=1}^{n} \left| q - r \right|}{\frac{1}{12} \frac{(x_n - x_1)^2}{n-1} n^2 (n+1)} \\
&= \epsilon \frac{3 \max\{|x_1|, |x_n|\}(n-1)}{(x_n - x_1)n},
\end{aligned}$$

which is strictly increasing in n because $\sum_{q=1}^{n} \sum_{r=1}^{n} |r - q| = \frac{n(n+1)(n-1)}{3}$. WLS can be bounded below by

$$\mathrm{WLS}(n, x_1, x_n, \epsilon) \geq \frac{\epsilon |\sum_{q=1}^{n} (\sum_{r=1}^{n} x_r (x_r - x_q))|}{\sum_{q=1}^{n} x_q (\sum_{r=1}^{n} x_q - x_r)} = \epsilon$$

for any $x_1 < x_n \in [-1, 1)$. Also, for any $0 < x_1 < x_n < 1$,

$$\begin{aligned}
\mathrm{WLS}(n, x_1, x_n, \epsilon) &= \epsilon \frac{\frac{x_n - x_1}{n-1}}{\sum_{q=1}^{n} \left((\frac{q-1}{n-1}(x_n - x_1) + x_1)(\frac{x_n - x_1}{n-1} \sum_{r=1}^{n} (q-r)) \right)} \cdot \\
&\quad \cdot \Big(\sum_{q=1}^{n} \Big| \sum_{r=1}^{q-1} (\frac{r-1}{n-1}(x_n - x_1) + x_1)(q-r) + \\
&\qquad \sum_{r=q+1}^{n} (\frac{r-1}{n-1}(x_n - x_1) + x_1)(q-r) \Big| \Big) \\
&\geq \epsilon \frac{\frac{x_n - x_1}{n-1} \sum_{q=1}^{\frac{n}{2}-1} \left| \sum_{r=2q}^{n} x_1 (q-r) \right|}{\sum_{q=1}^{n} \left((\frac{q-1}{n-1}(x_n - x_1) + x_1)(\frac{x_n - x_1}{n-1} \sum_{r=1}^{n} (q-r)) \right)} \\
&= \epsilon \frac{|x_1| \frac{x_n - x_1}{n-1} \frac{n(n+3)(n-2)}{8}}{\frac{1}{12} \frac{(x_n - x_1)^2}{n-1} n^2 (n+1)} = \epsilon \frac{3|x_1|(n+3)(n-2)}{2(x_n - x_1)n(n+1)},
\end{aligned}$$

which completes the result. □

Lemma 4.3.5 is validated by Figure 4.5, which shows that WLS is an increasing function of n under uniformly distributed measurements. Given that the drogues' measurements are roughly uniformly distributed, that the distribution of errors in ψ_i' is non-Gaussian and not necessarily unbiased, and Lemma 4.3.5, we use two as the number of measurements to estimate ω and $\frac{a}{z_{\mathrm{u}}}$.

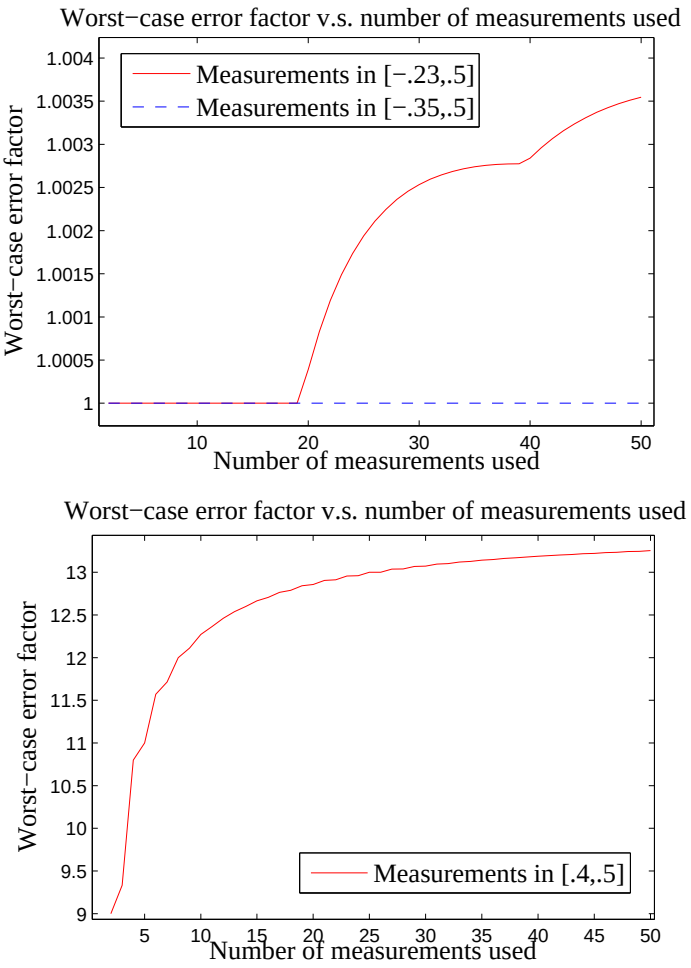

Figure 4.5: In the uniformly distributed measurements case, the worst case error factor (amount multiplying ϵ) is an increasing function of n.

4.3.4 Parameter estimate aggregation

In this section we consider the task of aggregating parameter estimates. Before we can tackle this, we must define the distributions for measurements. Here, we assume that the the non-random errors stemming from the dynamical assumptions are small relative to the random sensor noise. As seen in Remark 4.1.2, the mismatch in dynamical models rapidly becomes small. The error associated with the depth mismatch can be made small by choosing a tighter depth-keeping interval. Thus, given an inter-drogue distance d and distance derivative d', we let $\tilde{d}$, $\tilde{d'}$, denote the measurements of d and d' by a drogue, with the following Gaussian error model

$$\tilde{d} = d + \epsilon_d, \qquad \epsilon_d \sim \mathcal{N}(0, \sigma_d^2), \tag{4.17a}$$

$$\tilde{d'} = d' + \epsilon_{d'}, \quad \epsilon_{d'} \sim \mathcal{N}(0, \sigma_{d'}^2). \tag{4.17b}$$

We assume that the variances are a function of the specific sensors used and are known.

Within one period of the wave, the **Vanishing Distance Derivative Detection Strategy** generates many estimates of the parameters (an estimate is generated every time that the condition in Step **2** of Algorithm 4.1 is satisfied). Furthermore, drogues may be sampling over the course of several periods. Therefore, it makes sense to improve the estimation by fusing together estimates obtained at different timesteps. However, the synthesis of the appropriate fusion mechanism is challenging because the distribution of estimates of the parameters is non-Gaussian due to the nonlinearity of the dynamics and the operations within the algorithm. This is the problem that we tackle next, beginning with an informal description.

> *[Informal description]:* Because the parameters' distributions are only implicitly defined and non-Gaussian, we create an approximation up to a desired order $p \in \mathbb{Z}_{\geq 1}$. Using on the fact that measurements are Gaussian, we compute the expectation and variance of this approximate distribution and them to properly fuse parameter estimates.

Since $\mathbf{k_D}$ is analytic on $\mathcal{N}_{\mathbf{D}}(\mathbf{\Phi})$, we use Taylor series to generate approximations of arbitrary order. Formally, given an arbitrary analytic function

$\mathbf{pr}_{\mathbf{D}} : \mathbb{R}^8 \to \mathbb{R}$ with $\mathbf{pr}_{\mathbf{D}}(\mathbf{D}) = \text{pr}$, the pth-order Taylor series expression around $\mathbf{D}$ is

$$\mathbf{pr}_{\mathbf{D}}(\tilde{\mathbf{D}}) = \text{pr} + T^p_{\mathbf{D}}(\tilde{\mathbf{D}}) + R^p_{\mathbf{D}}(\tilde{\mathbf{D}}), \tag{4.18}$$

where

$$T^p_{\mathbf{D}}(\tilde{\mathbf{D}}) = \sum_{q=1}^{p} \frac{1}{q!} \mathbf{pr}^{(q)}_{\mathbf{D}}(\mathbf{D}; \tilde{\mathbf{D}} - \mathbf{D}),$$
$$R^p_{\mathbf{D}}(\tilde{\mathbf{D}}) = \mathbf{pr}^{(p+1)}_{\mathbf{D}}(\mathbf{D}^*; \tilde{\mathbf{D}} - \mathbf{D}),$$

for some $\mathbf{D}^* \in [\tilde{\mathbf{D}}, \mathbf{D}]$ and parameter value pr, where

$$\mathbf{pr}^{(q)}_{\mathbf{D}}(\mathbf{D}; \tilde{\mathbf{D}} - \mathbf{D}) = \sum_{r_1=1}^{8} \cdots \sum_{r_q=1}^{8} \frac{\partial^q \mathbf{pr}_{\mathbf{D}}(\tilde{\mathbf{D}})}{\partial_{\text{cpnt}_{r_1}(\mathbf{D})} \cdots \partial_{\text{cpnt}_{r_q}(\mathbf{D})}} \cdot$$
$$(\text{cpnt}_{r_1}(\tilde{\mathbf{D}}) - \text{cpnt}_{r_1}(\mathbf{D})) \ldots (\text{cpnt}_{r_q}(\tilde{\mathbf{D}}) - \text{cpnt}_{r_q}(\mathbf{D})).$$

For $\mathbf{pr}_{\mathbf{D}} = \mathbf{k}_{\mathbf{D}}$, equation (4.18) represents the noisy parameter calculated from a set of noisy measurements $\tilde{\mathbf{D}}$. Since Taylor's Theorem provides existence of the truncation term but no constructive way to determine it, we seek to investigate how accurate the pth order approximation $T^p_{\mathbf{D}}(\tilde{\mathbf{D}})$ is. Specifically, the form of the function, along with knowing the Gaussian distribution of the measurements, allows one to calculate the expectation and variance of this (approximate) distribution of the parameter. In practice, one cannot quite calculate these quantities, because they require partial derivatives which must be evaluated at the noiseless measurements $\mathbf{D}$, which are not available. However, by using $\tilde{\mathbf{D}}$ one may approximately determine these quantities.

Determining the expectation and variance of individual parameter estimates with the method described above allows us to devise a strategy to fuse them to get a more accurate approximation.

We are now ready to define the **pth-Order Parameter Fusion** procedure. Given a sequence of noisy parameter estimates $\{(\hat{\text{pr}}_\ell, \tilde{\mathbf{D}}_\ell) \mid \ell \in \mathbb{Z}_{\geq 1}\}$ determined from noisy measurements, $\hat{\text{pr}}_\ell = \mathbf{pr}_{\mathbf{D}_\ell}(\tilde{\mathbf{D}}_\ell)$, this procedure generates a sequence of

estimates $\{\widehat{\mathrm{pr}}_\ell^p \mid \ell \in \mathbb{Z}_{\geq 1}\}$ by means of the following iterative aggregation process

$$(\widehat{\mathrm{pr}}_{\ell+1}^p, \mathrm{Var}[\widehat{\mathrm{pr}}_{\ell+1}^p]) = \mathrm{OptAgg}\Big(\widehat{\mathrm{pr}}_\ell^p, \mathrm{Var}[\widehat{\mathrm{pr}}_\ell^p], \widehat{\mathrm{pr}}_{\ell+1} - \mathrm{E}[T^p_{\mathbf{D}_{\ell+1}}(\tilde{\mathbf{D}}_{\ell+1})], \mathrm{Var}[T^p_{\mathbf{D}_{\ell+1}}(\tilde{\mathbf{D}}_{\ell+1})]\Big), \quad (4.19)$$

where $\widehat{\mathrm{pr}}_1^p = \hat{\mathrm{pr}}_1 - \mathrm{E}[T^p_{\mathbf{D}_1}(\tilde{\mathbf{D}}_1)]$ and $\mathrm{Var}[\widehat{\mathrm{pr}}_1^p] = \mathrm{Var}[T^p_{\mathbf{D}_1}(\tilde{\mathbf{D}}_1)]$. According to this procedure, the pth-order estimate $\widehat{\mathrm{pr}}^p$ is sequentially updated by optimally combining the previous aggregated value with the next parameter estimate (after the expected bias has been removed). The next result establishes its convergence under suitable conditions on the pth-order approximation of $\mathbf{pr}$.

Proposition 4.3.6 (pth-order aggregation)**.** *For noisy inter-drogue measurements* $\{\tilde{\mathbf{D}}_\ell \mid \ell \in \mathbb{Z}_{\geq 1}\}$ *containing additive Gaussian noise according to* (4.17)*, assume there exist* $\epsilon_E \geq 0$ *and* $\epsilon_V \geq 0$ *such that the following bounds hold uniformly for all* $\ell \in \mathbb{Z}_{\geq 1}$*,*

$$|\,\mathrm{E}[\mathbf{pr}_{\mathbf{D}_\ell}(\tilde{\mathbf{D}}_\ell) - T^p_{\mathbf{D}_\ell}(\tilde{\mathbf{D}}_\ell)] - \mathrm{pr}\,| \leq \epsilon_E,\ \mathrm{Var}[\mathbf{pr}_{\mathbf{D}_\ell}(\tilde{\mathbf{D}}_\ell)] \leq \epsilon_V.$$

Then, the iterates (4.19) *generated by p**th-Order Parameter Fusion** satisfy*

$$\lim_{\ell\to\infty} \Pr[|\widehat{\mathrm{pr}}_\ell^p - \mathrm{pr}\,| \leq \epsilon_E + \epsilon] = 1, \quad \forall \epsilon > 0.$$

Proof. First, we note that $\widehat{\mathrm{pr}}_{\ell+1}^p$ can be written in the following non-recursive way:

$$\widehat{\mathrm{pr}}_{\ell+1}^p = \frac{\sum_{q=1}^{\ell+1} \frac{\mathbf{pr}_{\mathbf{D}_q}(\tilde{\mathbf{D}}_q) - \mathrm{E}[T^p_{\mathbf{D}_q}(\tilde{\mathbf{D}}_q)]}{\mathrm{Var}[T^p_{\mathbf{D}_q}(\tilde{\mathbf{D}}_q)]}}{\sum_{q=1}^{\ell+1} \frac{1}{\mathrm{Var}[T^p_{\mathbf{D}_q}(\tilde{\mathbf{D}}_q)]}}.$$

Thus, the variance of $\widehat{\mathrm{pr}}_{\ell+1}^p$ is

$$\begin{aligned}\mathrm{Var}[\widehat{\mathrm{pr}}_{\ell+1}^p] &= \frac{\sum_{q=1}^{\ell+1} \frac{\mathrm{Var}\,[\mathbf{pr}_{\mathbf{D}_q}(\tilde{\mathbf{D}}_q) - \mathrm{E}[T^p_{\mathbf{D}_q}(\tilde{\mathbf{D}}_q)]]}{\mathrm{Var}[T^p_{\mathbf{D}_q}(\tilde{\mathbf{D}}_q)]^2}}{(\sum_{q=1}^{\ell+1} \frac{1}{\mathrm{Var}[T^p_{\mathbf{D}_q}(\tilde{\mathbf{D}}_q)]})^2} \\ &= \frac{\sum_{q=1}^{\ell+1} \frac{\mathrm{Var}\,[\mathbf{pr}_{\mathbf{D}_q}(\tilde{\mathbf{D}}_q)]}{\mathrm{Var}[T^p_{\mathbf{D}_q}(\tilde{\mathbf{D}}_q)]^2}}{(\sum_{q=1}^{\ell+1} \frac{1}{\mathrm{Var}[T^p_{\mathbf{D}_q}(\tilde{\mathbf{D}}_q)]})^2} \leq \frac{\epsilon_V \sum_{q=1}^{\ell+1} \frac{1}{\mathrm{Var}[T^p_{\mathbf{D}_q}(\tilde{\mathbf{D}}_q)]^2}}{(\sum_{q=1}^{\ell+1} \frac{1}{\mathrm{Var}[T^p_{\mathbf{D}_q}(\tilde{\mathbf{D}}_q)]})^2}.\end{aligned}$$

From there, we notice that $\lim_{\ell\to\infty} \mathrm{Var}[\widehat{\mathrm{pr}}_\ell^p] = 0$. Now we bound the expected value of $\widehat{\mathrm{pr}}^p - \mathrm{pr}$:

$$
\begin{aligned}
|\,\mathrm{E}[\widehat{\mathrm{pr}}_{\ell+1}^p - \mathrm{pr}]| &= \left| \mathrm{E}\left[\sum_{q=1}^{\ell+1} \frac{\frac{\mathbf{pr}_{\mathbf{D}_\ell}(\tilde{\mathbf{D}}_q) - \mathrm{E}(T^p_{\mathbf{D}_q}(\tilde{\mathbf{D}}_q))}{\mathrm{Var}(T^p_{\mathbf{D}_q}(\tilde{\mathbf{D}}_q))}}{\sum_{q=1}^{\ell+1} \frac{1}{\mathrm{Var}(\tilde{\mathbf{pr}}_{\mathbf{D}_q}(\tilde{\mathbf{D}}_q))}} - \mathrm{pr} \right] \right| \\
&\leq \sum_{q=1}^{\ell+1} \frac{\frac{|\,\mathrm{E}[\mathbf{pr}_{\mathbf{D}_\ell}(\tilde{\mathbf{D}}_q) - \mathrm{E}(T^p_{\mathbf{D}_q}(\tilde{\mathbf{D}}_q)) - \mathrm{pr}]|}{\mathrm{Var}[T^p_{\mathbf{D}_q}(\tilde{\mathbf{D}}_q)]}}{\sum_{q=1}^{\ell+1} \frac{1}{\mathrm{Var}[\tilde{\mathbf{pr}}_{\mathbf{D}_q}(\tilde{\mathbf{D}}_q)]}} \leq \epsilon_E,
\end{aligned}
$$

implying $\forall \epsilon > 0$, $\lim_{\ell\to\infty} \Pr[|\widehat{\mathrm{pr}}_\ell^p - \mathrm{E}[\widehat{\mathrm{pr}}_\ell^p]| < \epsilon] = 1$. Also,

$$
\begin{aligned}
\Pr[|\widehat{\mathrm{pr}}_\ell^p - \mathrm{E}[\widehat{\mathrm{pr}}_\ell^p]| < \epsilon] &\leq \Pr[|\widehat{\mathrm{pr}}_\ell^p - \mathrm{E}[\widehat{\mathrm{pr}}_\ell^p| + |\,\mathrm{E}[\widehat{\mathrm{pr}}_\ell^p - \mathrm{pr}]|] < \epsilon + \epsilon_E], \\
&= \Pr[|\widehat{\mathrm{pr}}_\ell^p - \mathrm{E}[\widehat{\mathrm{pr}}_\ell^p| + |\,\mathrm{E}[\widehat{\mathrm{pr}}_\ell^p] - \mathrm{pr}\,|] < \epsilon + \epsilon_E], \\
&\leq \Pr[|\widehat{\mathrm{pr}}_\ell^p - \mathrm{pr}\,| < \epsilon + \epsilon_E],
\end{aligned}
$$

which shows the convergence result. □

Note that for $p = 1$, one is estimating the distribution of the parameter as a sum of Gaussian distributions because there are only first-order terms in the function T^1 in (4.18). Similarly for $p = 2$, the distribution is the sum of Gaussian distributions plus second-order Chi-squared distributions. Chi-squared distributions have non-zero expectation, and so, the **Second-Order k Fusion** outperforms the **First-Order k Fusion** because it estimates what the distribution's bias is and subtracts this from individual parameter estimates before fusing them.

Figure 4.6(a) shows the evolution of **pth-Order Parameter Fusion** for $p = 1$ and $p = 2$ for estimates of k generated by the **Vanishing Distance Derivative Detection Strategy**. The x-axis corresponds to the number of estimates of k fused together. Each k estimate is obtained at a different instant of time. Note that both evolutions, after only a small number of fusions, have a smaller error than the individual measurements, and that the evolution corresponding to $p = 2$ has a smaller asymptotic error. Note that Proposition 4.3.6 is not directly applicable to make guarantees on convergence because the implicit functions that give estimates of k (cf. Lemma 4.3.2) and ω and $\frac{a}{z_{\mathrm{u}}}$ (cf. Remark 4.3.3) have domains that are not all $\mathbb{R}^8$. This implies that the Gaussian noise may occasionally be too

large to produce estimates. However, as the standard deviation of the measurement noise get smaller, the fraction of acceptable noisy measurements increases and so the execution of the p**th-Order Parameter Fusion** more closely mirrors Proposition 4.3.6. One can see that the simulations are in line with the result.

Figure 4.6(b) shows the absolute error of p**th-Order Parameter Fusion** for $p = 1$ and $p = 2$, using k estimates from the **Vanishing Distance Derivative Detection Strategy**, as a function of the standard deviation in inter-drogue distance and distance derivatives measurements, which depicts that $p = 2$ outperforms $p = 1$.

Finally, Figure 4.7 compares an inter-drogue trajectory generated from true wave parameters with the trajectory that would have occurred from estimated parameters. Specifically, the **Vanishing Distance Derivative Detection Strategy** and the **Second-Order** k **Fusion** method are used to generate and fuse estimates of k after which the other parameters are estimated. One can see that the trajectory closely tracks the true trajectory.

Chapter 4, in part, is a reprint of the material [66] as it appears in 'Robust, distributed estimation of internal wave parameters via inter-drogue measurements' by M. Ouimet and J. Cortés in IEEE Transactions on Control Systems Technology, to appear in 2014. The dissertation author was the primary investigator and author of this paper.

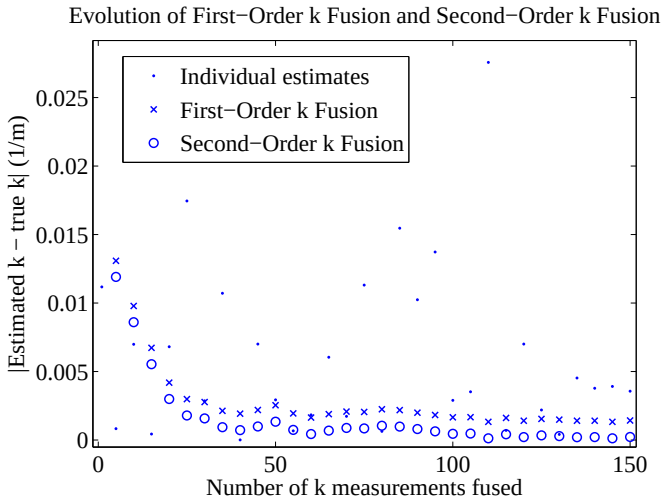

(a)

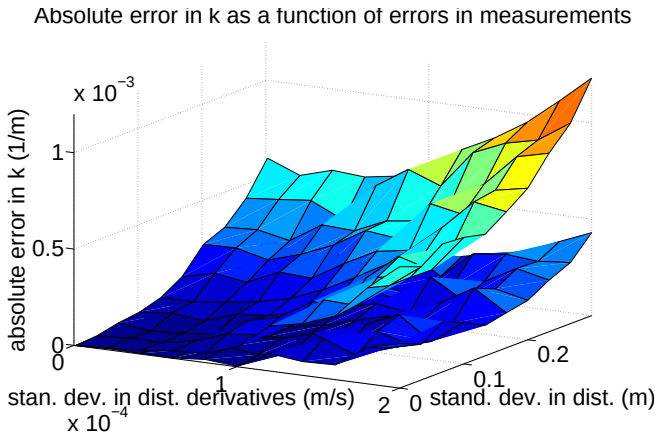

(b)

Figure 4.6: (a) shows p**th-Order Parameter Fusion** applied to estimates of k from **Vanishing Distance Derivative Detection Strategy**, for $p = 1$ and $p = 2$. After only a few estimates are fused, the error is already much smaller than the individual estimates. Also, $p = 2$ converges to a smaller error than $p = 1$. (b) shows the absolute error of p**th-Order Parameter Fusion** applied to estimates of k from **Vanishing Distance Derivative Detection Strategy** as a function of the standard deviations in measurement noise, highlighting how $p = 2$ outperforms $p = 1$. In both figures the parameter values, taken from [48], are $k = \frac{2\pi}{190}\frac{1}{m}$, $\frac{a}{z_u} = \frac{1}{7}$, and $\omega = \frac{2\pi}{960}\frac{1}{s}$. The drogues are in a line, initially $10m$ apart from the closest drogues on either side. In (a), the standard deviations in distances and distance derivatives are $.01m$ and $.0005\frac{m}{s}$, respectively. In (b) for each set of standard deviations, $10,000$ estimates were fused.

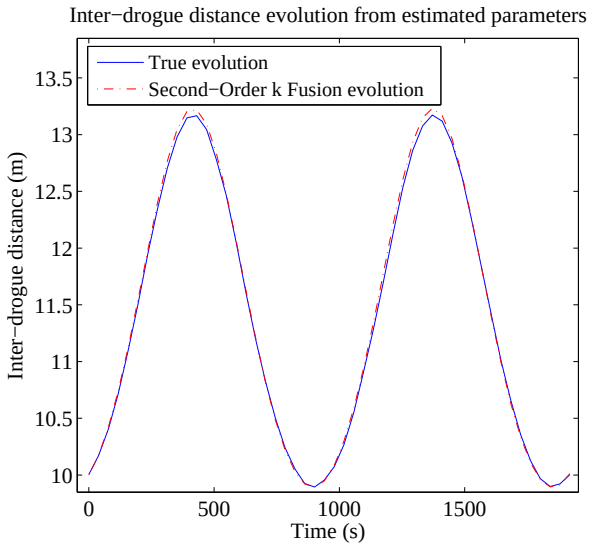

Figure 4.7: Comparison between inter-drogue trajectories generated from a set of true wave parameters and from the parameters estimated by the **Vanishing Distance Derivative Detection Strategy** and the **Second-Order k Fusion** method. Here, the standard deviations in distances and distance derivatives are $.01m$ and $.0001\frac{m}{s}$, respectively. The estimated trajectory closely matches the true trajectory.

Chapter 5

Estimation of nonlinear internal waves

This chapter solves a problem very similar to the Chapter 4. The difference is that in this chapter, we seek to estimate a nonlinear wave, rather than a linear one. Linear waves have amplitudes small relative to the depth of the water column. They are capable of moving around plankton, animal larvae, and other organisms, as well as creating mixing between the upper and lower layers. In contrast, nonlinear waves have larger amplitudes, allowing them to be an agent of transport of small oceanic life [73].Many models exist for nonlinear waves [37, 39] to account for the wide variety of conditions and bathymetries found in the ocean. Here, we consider nonlinear waves modeled as solitons, which are stable, solitary peaks (or troughs) which propagate along the pycnocline.

As explained in Chapter 4, traditional methods for studying internal waves have been satellite observations, acoustic tomography, conductance-temperature-depth (CTD) casts, and current meters on moorings. However, these methods lack the capability of real-time adaptability. Here, we tackle this problem using a group of drogues capable of drifting underwater near the internal wave's interface to determine the physical parameters that define its motion. A drogue is a robotic Lagrangian drifter able to actuate its depth by changing its buoyancy. While underwater, drogues are subject to the flow induced by the motion of the internal wave and do not have access to exact location information. Figure 5.1 presents a

pictorial illustration of the problem setup. The basic premise is that the evolution of the inter-drogue distance and distance derivative measurements contains enough information for the drogues to be able to fully characterize the internal wave. The method proposed here is inspired by the algorithm introduced in Chapter 4.

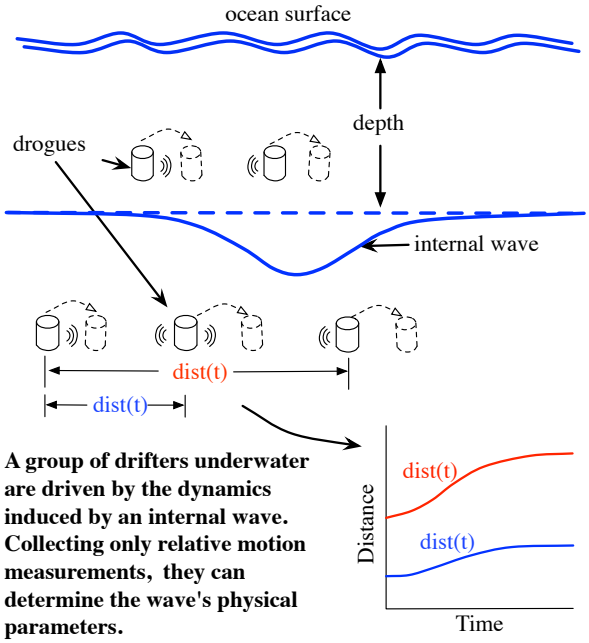

Figure 5.1: For an ocean nonlinear internal wave, this figure show a vertical cross-section of the ocean perpendicular to the wave propagation direction at a fixed instant in time. A group of drogues float at constant depths (but not necessarily along a straight line) and do not have access to exact location information. Our objective is to provide drogues with mechanisms that rely only on the relative measurements to determine the parameters that uniquely define the internal wave.

5.1 Problem statement

This section contains the nonlinear internal wave model used, the model for the drogue drifters and their interaction with the internal wave, and a formalized problem statement.

5.1.1 Nonlinear internal wave model

Let $\Sigma_g = (\mathbf{p}_g, \{\mathbf{e}_{x_g}, \mathbf{e}_{y_g}, \mathbf{e}_{z_g}\})$ be a global reference frame defined as follows: the origin p_g corresponds to an arbitrary point at the ocean surface; the vector $\mathbf{e}_{x_g}$ corresponds to the direction of wave propagation, which is parallel to the ocean bottom and assumed to be constant, and $\mathbf{e}_{z_g}$ is perpendicular to the ocean bottom, pointing from bottom to surface. For convenience, the coordinates induced by Σ_g are denoted by $\{x, y, z\}$.

As shown in Figure 5.1, an internal wave is a wave which travels beneath the surface of the ocean, along a surface of constant water density called a pycnocline. When the amplitude of the wave becomes a large enough fraction of the water column, the wave begins to 'feel' the surface and bottom of the ocean and nonlinear terms of the governing PDE must be included. One classical equation used to model weakly nonlinear long internal waves is the Korteweg-de Vries (KdV) equation, see e.g., [39]:

$$\frac{\partial \eta}{\partial t} - \frac{3}{2} c \frac{h_l - h_u}{h_u h_l} \eta \frac{\partial \eta}{\partial x} + \frac{1}{6} c h_u h_l \frac{\partial^3 \eta}{\partial x^3} = 0, \tag{5.1}$$

where η is the distance that the internal wave is displacing the pycnocline, $c = \sqrt{g \frac{|\rho_l - \rho_u|}{\rho_l} \frac{h_u h_l}{h_u + h_l}}$, ρ_u, h_u and ρ_l, h_l are the density and depth of the upper and lower layers, respectively, and g is the acceleration due to gravity. In the absence of an internal wave, the pycnocline is at depth h_u. The stable soliton solution to (5.1) is, cf. [37],

$$\eta(x,t) = -\frac{2Ch_u h_l}{h_l - h_u} \operatorname{sech}^2\Big(\frac{1}{2}\sqrt{\frac{6C}{ch_u h_l}}(x - Ct - \chi_0)\Big) = A \operatorname{sech}^2\big(k(x - \chi_0) - \omega t\big), \tag{5.2}$$

where

$$A = -\frac{2Ch_u h_l}{h_l - h_u} \quad k = \frac{1}{2}\sqrt{\frac{6C}{ch_u h_l}}, \quad \omega = \frac{1}{2}\sqrt{\frac{6C}{ch_u h_l}} C,$$

are the amplitude, wavenumber, and temporal frequency, respectively, $C = \frac{\omega}{k}$ is the celerity (speed) of the wave, and χ_0 is the initial location of the center of the wave. As the wave propagates, it induces motion in the nearby water. The standard model assumes that the vertical velocity varies linearly with depth. Coupled with the conservation of mass law for an incompressible fluid, one can

derive the following expressions for the horizontal u_u and vertical v_u velocities of the upper layer

$$u_u(x,t) = -\frac{2CA}{h_u}\operatorname{sech}^2(k(x-\chi_0)-\omega t),$$
$$v_u(x,z,t) = \frac{2\omega A z}{h_u}\operatorname{sech}^2(k(x-\chi_0)-\omega t)\tanh(k(x-\chi_0)-\omega t).$$

Likewise, the horizontal u_l and vertical v_l velocities of the lower layer are

$$u_l(x,t) = \frac{2CA}{h_l}\operatorname{sech}^2(k(x-\chi_0)-\omega t),$$
$$v_l(x,z,t) = 2\omega A\frac{h_u+h_l-z}{h_l}\operatorname{sech}^2(k(x-\chi_0)-\omega t)\tanh(k(x-\chi_0)-\omega t).$$

For convenience, we define the upper and lower velocity amplitudes as $B_u = -\frac{2CA}{h_u}$ and $B_l = \frac{2CA}{h_l}$.

Remark 5.1.1. *(Bounds on wave parameters)* We assume that, for each wave parameter, there exists a closed and bounded interval in $\mathbb{R}_{>0}$ that the parameter is guaranteed to fall within. This is reasonable because natural parameters, such as an object's size or speed, cannot be arbitrarily small or large. We refer to a parameter's bounds with subscripts min and max. •

5.1.2 Drogue model

A drogue is a submersible buoy which can drift in the ocean, unattached to the ocean floor or a boat, and is able to change its depth in the water by controlling its buoyancy. While underwater, a drogue can measure the relative distance, distance derivative, and orientation in space to other drogues through sensing (e.g., via acoustic or optical sensors and an onboard compass). A drogue can also measure its depth. However, it does not have access to absolute position because GPS is unavailable underwater.

Consider a group of N drogues, each with a reference frame

$$\Sigma_i = (\mathbf{p}_i, \{\mathbf{e}_{x_i}, \mathbf{e}_{y_i}, \mathbf{e}_{z_i}\}), \qquad i \in \{1,\dots,N\},$$

attached to it. The origin $\mathbf{p}_i$ corresponds to the location of the drogue. As in the global coordinate frame Σ_g, $\mathbf{e}_{z_i}$ is perpendicular to the ocean bottom, pointing

from bottom to surface. The vectors $\mathbf{e}_{x_i}$ and $\mathbf{e}_{y_i}$ are parallel to the ocean floor, but neither is necessarily oriented in the wave propagation direction. We assume here for simplicity that this direction, θ_i, is known, so that each drogue may rotate its own coordinates to the one aligned with the wave direction. Although not necessary, this assumption simplifies the ensuing exposition considerably. Section 4.2.1 shows how each drogue i can determine θ_i using relative distance and distance derivative measurements.

We make the simplifying assumption that the drogues' dynamics are Lagrangian, i.e., the drogue's velocity is equal to ocean's velocity at its current location. Furthermore, we assume that the drogues maintain the same prescribed depth by means of buoyancy control. Thus, without loss of generality, the dynamics of drogue $i \in \{1, \ldots, N\}$ in the upper layer is

$$\dot{\mathbf{p}}_i = (\dot{x}_i, \dot{y}_i, \dot{z}_i) = (u_u(x,t), 0, 0)$$

and can be similarly defined for drogues in the lower layer. Drogue i senses inter-drogue measurements with the M closest drogue neighbors. For each neighbor j, drogue i has access to

$$\begin{aligned}\mathbf{d}_{i,j} &= (d^x_{i,j}, d^y_{i,j}, 0) = \mathbf{x}_j - \mathbf{x}_j,\\ \dot{\mathbf{d}}_{i,j} &= (\dot{d}^x_{i,j}, 0, 0) = \dot{\mathbf{x}}_j - \dot{\mathbf{x}}_j.\end{aligned}$$

We assume the drogues have continuous access to these quantities. In Section 5.2, we elaborate on the fact that a large enough, finite sampling rate will also produce noiseless parameter estimates. Since the internal wave causes no motion in the y-direction (due to choice of coordinates), we ease notation by letting $d_{i,j} = d^x_{i,j}$ and $\dot{d}_{i,j} = \dot{d}^x_{i,j}$.

Remark 5.1.2. *(Kinematic versus dynamical model)* The Lagrangian dynamics is a simplification of the second-order dynamical model, see e.g. [92],

$$m\ddot{x} = -c_d\,|\dot{x} - u_{\mathrm{u}}(t,x)|(\dot{x} - u_{\mathrm{u}}(t,x)), \tag{5.3a}$$

$$\dot{y} = 0, \tag{5.3b}$$

$$m\ddot{z} = -c_d\,|\dot{z} - w_{\mathrm{u}}(t,x,z)|(\dot{z} - w_{\mathrm{u}}(t,x,z)) + f, \tag{5.3c}$$

where m denotes the combined drogue mass and inertial added mass [11], c_d is the drag parameter, and f is the buoyancy control input. Following [27, 38], reasonable values for wave/ocean parameters are $h_u = 10$ m, $h_l = 60$ m, $C = .1\frac{\text{m}}{\text{s}}$, and $\frac{|\rho_l - \rho_u|}{\rho_l} = .002$ and drogue parameters are $m = 1.5$kg, and $c_d = 210\frac{\text{Ns}^2}{m^2}$. Figure 5.2 depicts the position, inter-drogue distance, and velocity evolution for a pair of drogues initially at rest 50 m and 55 m from the crest of the internal wave. In these simulations, the spatial wavelength is about 250 m. In Figure 5.2(a), one can see that the Lagrangian model approximates well the second-order one, with the drogue's position error on the order of .1 m. In Figure 5.2(b), one can see that since drogues are close relative to the spatial wavelength, their position errors are roughly the same, causing the errors in distance to be of the order .01 m. This comparison provides a good justification for the use of the simpler Lagrangian model. In Section 5.2, we revisit the effect of this approximation when discussing the sources of errors present in realistic implementations. •

5.1.3 Problem description

A team of N drogues is deployed in the ocean and their motion is governed by an internal wave. The drogues may control their depth through buoyancy changes, and each one can measure the relative distance and orientation to the closest M drogues in their own coordinate frame. Our objective is to design an algorithm that allows the drogues to collectively determine the physical parameters C, $\frac{|\rho_u - \rho_l|}{\rho_l}$, h_u, and h_l which define the internal wave through (5.2).

5.2 Parameter Determination Strategy

In this section, we define a strategy, termed the **Parameter Determination Strategy**, to estimate the nonlinear wave parameters. The following informal rationale describes the basic idea behind its design.

> *[Rationale]: The strategy for determining the physical parameters which define the internal wave are based on first determining the phase of the wave relative to the drogues at some time. Our method leverages the*

fact that, when the crest of the wave is directly between two drogues, their inter-drogue distance derivative momentarily becomes zero and the drogues can then determine the phase. Using this insight, one can create equations between inter-drogue measurements and the parameters of interest. The crux of the analysis is to ensure that only the true set of parameters solve the constructed set of equations.

The algorithm requires the capability for measuring both inter-drogue distance and its derivative. It is written in terms of drogue i using measured inter-drogue data between itself and nearest neighbors with identities j_1, j_2, j_3, j_4, j_5, and j_6. Before introducing the algorithm, we comment briefly on some assumptions on drogue locations which make the presentation easier.

Remark 5.2.1. *(Assumptions on drogue locations)* For concreteness in the presentation of the algorithm, we make the assumption that drogues i, j_1, j_2, j_3 j_4 are in the same ocean layer. The algorithm also requires at least one drogue in the lower layer and one in the upper layer, which for concreteness we assume are drogues j_5 and j_6, respectively. •

5.2.1 Determination of the wavenumber

Because drogues do not have absolute measurements, we write their dynamics in terms of the inter-distance between them. To completely describe the drogues evolution, we also need to add the state v_i, which is the position of the wave relative to drogue i,

$$v_i = k(x - \chi_0) - \omega t,$$

Thus, the dynamics are

$$\dot{d}_{i,j_m} = B(\operatorname{sech}^2(kd_{i,j_m} + v_i) - \operatorname{sech}^2(v_i)),\ \forall m \neq i \tag{5.4a}$$

$$\dot{v_i} = Bk \operatorname{sech}^2(v_i) - \omega. \tag{5.4b}$$

The relative phase v_i is unobservable, however, at times when inter-drogue distance derivatives momentarily vanish, one can gain insight, as the following result shows. Furthermore, at all other times, there exists an implicit function that describes the relative phase.

Lemma 5.2.2. *(Relative wave position when distance derivative vanishes) For three drogues i, j_1 and j_2 at initial positions $x_i(0) \neq x_{j_1}(0) \neq x_{j_2}(0)$, if $x_i(0)$, $x_j(0) > \chi_0$, then there exists time $t_{\text{cr}} > 0$ when $\dot{d}_{i,j}(t_{\text{cr}}) = 0$ and*

$$v_i(t_{\text{cr}}) = -\frac{k d_{i,j_1}(t_{\text{cr}})}{2}. \tag{5.5}$$

Furthermore, for all times $t > 0$, there exists an implicit function for $v_i(k, d_{i,j_1}, d_{i,j_2}, \dot{d}_{i,j_1}, \dot{d}_{i,j_2})$ determined by the equation

$$\frac{\dot{d}_{i,j_1}}{\dot{d}_{i,j_2}} - \frac{\operatorname{sech}^2(k d_{i,j_1} + v_i) - \operatorname{sech}^2(v_i)}{\operatorname{sech}^2(k d_{i,j_2} + v_i) - \operatorname{sech}^2(v_i)} = 0. \tag{5.6}$$

From the Lagrangian drogue model (5.4), the dynamics of an inter-drogue distance between drogues i and j in the wave propagation direction contain the unknown parameters B and k, as well as unmeasurable state v_i. However, using Lemma 5.2.2 to write the ratio of two equations in (5.4a) for i,j_3 and i,j_4 specifically at the t_{cr} when $\dot{d}_{i,j_1}(t_{\text{cr}}) = 0$, one gets

$$\frac{\dot{d}_{i,j_3}}{\dot{d}_{i,j_4}} - \frac{\operatorname{sech}^2(k(d_{i,j_3} - \frac{d_{i,j_1}}{2})) - \operatorname{sech}^2(k\frac{d_{i,j_1}}{2})}{\operatorname{sech}^2(k(d_{i,j_4} - \frac{d_{i,j_1}}{2})) - \operatorname{sech}^2(k\frac{d_{i,j_1}}{2})} = 0,$$

and, more generally, for all times,

$$\frac{\dot{d}_{i,j_3}}{\dot{d}_{i,j_4}} - \frac{\operatorname{sech}^2(k d_{i,j_3} - v_i) - \operatorname{sech}^2(v_i)}{\operatorname{sech}^2(k d_{i,j_4} - v_i) - \operatorname{sech}^2(v_i)} = 0,$$

which is now only a function of the unknown parameter k (because $v_i = v_i(k, d_{i,j_1}, d_{i,j_2}, \dot{d}_{i,j_1}, \dot{d}_{i,j_2})$, as implicitly defined in Lemma 5.2.2). We now wish to show that only the actual value of k satisfies this equation. With this in mind, we define the function f as

$$\begin{aligned}\mathrm{f}(\mathcal{k}, d_{i,j_3}, d_{i,j_4}, \dot{d}_{i,j_3}, \dot{d}_{i,j_4}, v_i(\mathcal{k}, d_{i,j_1}, d_{i,j_2}, \dot{d}_{i,j_1}, \dot{d}_{i,j_2})) = \\ \frac{\dot{d}_{i,j_3}}{\dot{d}_{i,j_4}} - \frac{\operatorname{sech}^2(k d_{i,j_3} - v_i) - \operatorname{sech}^2(v_i)}{\operatorname{sech}^2(k d_{i,j_4} - v_i) - \operatorname{sech}^2(v_i)}\end{aligned} \tag{5.7}$$

and examine the number of roots in the next result.

Lemma 5.2.3. *(Uniqueness of spatial wavenumber) Given noiseless measurements of $d_{i,j}(t)$ and $\dot{d}_{i,j}(t)$, for $j \in \{j_1, j_2, j_3, j_4\}$, where t is sufficiently close to t_{cr}, the time when $\dot{d}_{i,j_1}(t_{\text{cr}}) = 0$. If $d_{i,j_1}(t)$ is sufficiently small, then $\mathcal{k} = k$ is the only root to (5.7).*

Proof. One can take the derivative of f with respect to $\mathcal{k}$. We consider the limiting case when $t = t_{\text{cr}}$ (i.e. $v_i = \frac{-\mathcal{k} d_{i,j_1}}{2}$) and $d_{i,j_1} = 0$. By taking the derivative of (5.6), one can calculate the derivative of v_i with respect to $\mathcal{k}$. Note that it is 0 when evaluated at the limiting case. Thus, for this limiting case,

$$\frac{\partial \mathrm{f}}{\partial \mathcal{k}} = \tanh(\mathcal{k} d_{i,j_3}) \operatorname{sech}^2(\mathcal{k} d_{i,j_3}) \coth(\mathcal{k} d_{i,j_4}) \cdot \operatorname{csch}^2(\mathcal{k} d_{i,j_4})(d_{i,j_3} \sinh(2\mathcal{k} d_{i,j_4}) - d_{i,j_4} \sinh(2\mathcal{k} d_{i,j_3})),$$

Showing that $\frac{\partial \mathrm{f}}{\partial \mathcal{k}}$ is either strictly positive or strictly negative ensures that only $\mathcal{k} = k$ is a root of (5.7). In fact, $\frac{\partial \mathrm{f}}{\partial \mathcal{k}}$ is strictly positive if $d_{i,j_3} < d_{i,j_4}$ and strictly negative if $d_{i,j_3} > d_{i,j_4}$, for all $\mathcal{k} > 0$. This shows that $\mathcal{k} = k$ is the unique root of (5.7) when $t = t_{\text{cr}}$ and $d_{i,j_1}(t_{\text{cr}}) = 0$. Furthermore, by continuity of $\frac{\partial \mathrm{f}}{\partial \mathcal{k}}$, for t close enough to t_{cr} and $d_{i,j_1}(t)$ close enough to 0, $\frac{\partial \mathrm{f}}{\partial \mathcal{k}}$ is either strictly positive or strictly negative (dependent on the sign of $d_{i,j_2} - d_{i,j_3}$), which completes the result. □

5.2.2 Correctness analysis

Once k has been determined, we wish to leverage it to calculate other parameters. This is what the **Parameter Determination Strategy** accomplishes using the dynamics that defines the internal wave. The strategy is formally presented in Algorithm 5.1. We also refer back to Remark 5.2.1, which explains the assumptions on drogue locations, which are needed to make the algorithm more concrete.

The following result establishes the correctness of the algorithm. Its proof follows from Lemma 5.2.3, as well as the form of the inter-drogue distance derivative equation, and algebraic relations between parameters in the nonlinear soliton model in Section 5.1.1.

Proposition 5.2.4. *(Correctness of **Parameter Determination Strategy**) At times t sufficiently close to t_{cr} when $\dot{d}_{i,j_1} = 0$ and if $d_{i,j_1}(t)$ is sufficiently small, then given noiseless knowledge of $d_{i,j_m}(t)$ and $\dot{d}_{i,j_m}(t)$ for all $m \in \{j_1, j_2, j_3, j_4, j_5, j_6\}$, the **Parameter Determination Strategy**, presented in Algorithm 5.1, can be used to determine all of the internal wave physical parameters.*

Table 5.1: **Parameter Determination Strategy**

1: Set $\theta_i = \tan^{-1}\left(-\dot{d}^{y_i}_{i,j_1}/\dot{d}^{x_i}_{i,j_1}\right)$

2: Set t such that $\dot{d}_{i,j_1}(t)$ sufficiently close to 0

3: k uniquely solves $\mathrm{f}(k,d_{i,j_3},d_{i,j_4},\dot{d}_{i,j_3},\dot{d}_{i,j_4},v_i(k,d_{i,j_1},d_{i,j_2},\dot{d}_{i,j_1},\dot{d}_{i,j_2}))=0$

4: Set $v_i(t) = v_i(k, d_{i,j_1}(t), d_{i,j_2}(t), \dot{d}_{i,j_1}(t), \dot{d}_{i,j_2}(t))$

5: Set $B_l = \frac{\dot{d}_{i,j_5}(t)}{\mathrm{sech}^2(kd_{i,j_5}(t)+v_i(t))-\mathrm{sech}^2(v_i(t))}$

6: Set $B_u = \frac{\dot{d}_{i,j_6}(t)+B_l\,\mathrm{sech}^2(v_i(t))}{\mathrm{sech}^2(kd_{i,j_6}(t)+v_i(t))}$

7: Set t_2 not equal to t

8: Set $v_i(t_2) = v_i(k, d_{i,j_1}(t_2), d_{i,j_2}(t_2), \dot{d}_{i,j_1}(t_2), \dot{d}_{i,j_2}(t_2))$

9: Set $\omega = \frac{k(d_{i,j_1}(t_2)-d_{i,j_1}(t))-v_i(t_2)+v_i(t)}{t_2-t}$

10: Set $C = \frac{\omega}{k}$

11: Set $h_u = \frac{h_{\mathrm{ocean}}}{1-\frac{B_u}{B_l}}$

12: Set $h_l = h_{\mathrm{ocean}} - h_u$

13: Set $c = \frac{3C}{2k^2h_uh_l}$

14: Set $\frac{|\rho_l-\rho_u|}{\rho_l} = \frac{c^2h_{\mathrm{ocean}}}{gh_uh_l}$

Note that Step 3 can be solved using a variety of root-finding methods. Since f is a monotonic function in k, a gradient descent method would be sufficient, for example.

Having established the correctness of the algorithm under perfect measurements, let us briefly comment on its performance when errors are present. The fact that all the functions that appear in the equations employed in Algorithm 5.1 have a continuous dependence on the variables makes the **Parameter Determination Strategy** naturally robust against errors, in the sense that the estimated parameters are still unique and remain close to the true parameters for small enough errors. For completeness, we discuss the sources of error that arise in practical implementations of the algorithm.

Noise in measurements: In practice one can expect noise in the measurements collected from sensors. We assume that this noise is unbiased, additive, and Gaussian with variance proportional to the measured quantities, and that the noise at different time instances and for different measurements are uncorrelated.

Groups of nonlinear waves: In reality, nonlinear internal waves travel in ordered groups by speed, with the larger amplitude, faster moving ones at the front. As time goes on, the distance between the waves increases. Although our model assumes only one wave is present, it is possible to instead consider the case when the waves in the group are far enough apart that their relative effect is negligible.

Model uncertainty: The problem setup described in Section 5.1.2 assumes that drogues are Lagrangian. In practice, drogues have a finite mass and drag coefficient making them not perfectly Lagrangian, leading to a difference between the actual drogue's velocity and the ocean velocity. One can treat this mismatch as an unknown but nonrandom error in the measurements of inter-drogue distances and distance derivatives.

Drogues not maintaining depth: We assume that the drogues have a controller that uses feedback on depth measurements to maintain a desired

depth. Due to noisy depth measurements and a desire to minimize actuation cost, instead we assume that the drogues will be within an interval around the desired depth. Although depth is not directly used by the proposed algorithm, this inaccuracy affects inter-drogue distance measurements. As above, one can treat this as an unknown but nonrandom error in the inter-drogue distance measurements.

Figure 5.3 depicts an actual Lagrangian drogue trajectory along with trajectories generated from the parameters estimated from the **Parameter Determination Strategy** with measurement error of 1% and .1%. As the error in measurements decreases, the algorithm estimates the wave parameters more accurately, which produces trajectories closer to the true trajectory. The spatial wavelength $\frac{2\pi}{k}$ in this case is about 290 m, and therefore, the trajectory errors relative to the wave's scale are really small.

Remark 5.2.5 (Robustness against noise)**.** Here we briefly comment on the algorithm performance when errors are present, specifically noise in the sensor measurements. We assume that this noise is unbiased, Gaussian, and that noise at different time instances and for different measurements are uncorrelated. As stated above, the fact that all of the functions that appear in the equations employed in Algorithm 5.1 have a continuous dependence on the variables makes the **Parameter Determination Strategy** naturally robust against errors, in the sense that the estimated parameters are still unique and remain close to the true parameters for small enough errors. Figure 5.4 illustrates the algorithm robustness for three different initial drogue configurations. Note that our method has a linear on a log-log plot relationship between relative errors in measurements and relative errors in the wavenumber. This figure also investigates the effect that the largest inter-drogue distance has in the estimation of the wavenumber. Three drogues are located at 0, 1, and 2 meters and the fourth drogue's position varies; in three trials it is located at 10, 100, and 200 meters. One can see that as the largest inter-drogue distance grows, the algorithm robustness improves. •

5.3 Aggregation of estimates

The **Parameter Determination Strategy** can be executed at various instants of times, as described in the previous section. Each execution gives rise to an estimate of the parameters. Therefore, a natural question is whether drogues could aggregate their individual estimates, as well as potentially use multiple sets of data from many different waves, to improve estimates of the parameters. Since the parameters are solutions to (implicit) nonlinear equations, even with the assumption of Gaussian measurements, the resulting distributions of the parameters are, in general, non-Gaussian and only implicitly defined. Therefore, we employ a Mixture Distribution approach to represent each parameter's distribution as a truncated Taylor series expansion. For concreteness and simplicity, we define the procedure for aggregating estimates of one parameter, the wavenumber k.

Using (5.7) and the implicit function theorem, one can guarantee that in a neighborhood around true measurements, noisy measurements produce a unique estimate of the wavenumber. Since this function is only implicitly defined, one can resort to calculating successive terms of its Taylor series expansion. In this way, we estimate the implicit distribution of the wavenumber as a function of the errors in our measurements.

Letting $D = (d_{i,j_1}, d_{i,j_2}, d_{i,j_3}, d_{i,j_4}, \dot{d}_{i,j_1}\dot{d}_{i,j_2}, \dot{d}_{i,j_3}, \dot{d}_{i,j_4})$, we substitute the implicit function $k(D)$ into (5.7) and differentiate with respect to D, which yields

$$\frac{\partial k(D)}{\partial D} = \frac{-\frac{\partial \mathrm{f}(k,D)}{\partial D}}{\frac{\partial \mathrm{f}(k,D)}{\partial k}}$$

Therefore, for a set of noisy measurements $\hat{D}$, we have the following distribution

$$k_D(\hat{D}) = k + \frac{\partial k(D)}{\partial D}(\hat{D} - D) + \mathcal{O}((\hat{D} - D)^2).$$

Repeated differentiation of (5.7) can produce higher-order terms in this Taylor series expansion. For simplicity, we consider only the first-order term. Then, our approximation of this distribution is

$$\hat{k}_D(\hat{D}) = k + \frac{\partial k(D)}{\partial D}(\hat{D} - D) = k + \hat{e}_D(\hat{D}).$$

By assumption, $\hat{D} - D$ is a zero-mean, Gaussian random variable with a diagonal covariance matrix, making our approximation of the parameter's distribution a sum of Gaussian distributions. Given parameter estimates $\{k_\ell^{\text{est}} \mid \ell \in \mathbb{Z}_{\geq 1}\}$ and measurements $\{\hat{D}_\ell \mid \ell \in \mathbb{Z}_{\geq 1}\}$, we define the following aggregation scheme:

$$(k_{\ell+1}^{\text{agg}}, \text{Var}[k_{\ell+1}^{\text{agg}}]) = \text{OptAgg}\Big(k_\ell^{\text{agg}}, \text{Var}[k_\ell^{\text{agg}}], \\ k_{\ell+1}^{\text{est}} - \text{E}[\hat{e}_{D_{\ell+1}}(\hat{D}_{\ell+1})], \text{Var}[\hat{e}_{D_{\ell+1}}(\hat{D}_{\ell+1})]\Big), \quad (5.8)$$

where $k_1^{\text{agg}} = k_1^{\text{est}} - \text{E}[\hat{e}_D(\hat{D}_1)]$ and $\text{Var}[k_1^{\text{agg}}] = \text{Var}[\hat{e}_D(\hat{D}_1)]$. The following result is now a consequence of Proposition 4.3.6.

Proposition 5.3.1 (Wavenumber aggregation)**.** *Given a sequence of noisy measurements $\{\hat{D}_\ell \mid \ell \in \mathbb{Z}_{\geq 1}\}$, assume there exist $\epsilon_E \geq 0$ and $\epsilon_V \geq 0$ such that the following bounds hold uniformly for all $\ell \in \mathbb{Z}_{\geq 1}$*

$$|\,\text{E}[k_{D_\ell}(\hat{D}_\ell) - \hat{e}_{D_\ell}(\hat{D}_\ell)] - k| \leq \epsilon_E \quad \text{Var}[k_{D_\ell}(\hat{D}_\ell)] \leq \epsilon_V.$$

Then, with the estimates $\{k_\ell^{\text{est}} \mid \ell \in \mathbb{Z}_{\geq 1}\}$ generated by the **Parameter Determination Strategy** *using $\{\hat{D}_\ell\}$, the iterates $\{k_\ell^{\text{agg}} \mid \ell \in \mathbb{Z}_{\geq 1}\}$ of the aggregation scheme defined in* (5.8) *satisfy the following:*

$$\lim_{\ell \to \infty} \Pr[|k_\ell^{\text{agg}} - k| \leq \epsilon_E + \epsilon] = 1 \quad \forall \epsilon > 0.$$

Figure 5.5 depicts the aggregation method discussed above. It plots the relative error in estimates of the wavenumber, both for individual estimates and the aggregated estimate. Note that the aggregated estimate converges to a relative error significantly smaller than the individual estimates.

5.4 Extension to two nonlinear waves

In this section, we discuss how our previous algorithm design and analysis can be extended to situations where two nonlinear internal waves are simultaneously present. The basic idea relies on choosing a coordinate system such that, in one of the directions, the drogues only feel the effect of one of the two waves. One

can apply the extended **Parameter Determination Strategy** in the direction where only one wave is felt to solve for the parameters of that wave. Once that wave has been characterized, its effect can be removed from the drogue's measurements, allowing one to again apply the **Parameter Determination Strategy** to determine the other wave's parameters.

Consider the situation where a drogue is floating in the presence of two nonlinear internal waves, each with its own set of wave parameters and propagation directions. As before, assume that these propagation directions are known a priori. Choosing a horizontal $x-y$ coordinate system with the x-direction aligned with wave 1's direction makes $\theta_1 = 0$. Summing each wave's individual effect yields the following planar dynamics for drogue i,

$$\begin{aligned}\dot{x}_i &= \sum_{n=1}^{2} -\frac{2C_nA_n}{h_u}\operatorname{sech}^2(k_n(x_i\cos(\theta_n)+y_i\sin(\theta_n)-\chi_{0n})-\omega_n t)\cos(\theta_n),\\ \dot{y}_i &= -\frac{2C_2A_2}{h_u}\operatorname{sech}^2(k_2(x_i\cos(\theta_2)+y_i\sin(\theta_2)-\chi_{02})-\omega_2 t)\sin(\theta_2).\end{aligned}$$

Note that in the y direction, the drogue only feels the effect of the second wave.

Writing the dynamics for the y direction in terms of inter-drogue distances between drogue i and j as well as the relative phase v_i gives

$$\begin{aligned}\dot{d}^y_{i,j_1} = -\frac{2C_2A_2}{h_u}\sin(\theta_2)\cdot&\\ \big(\operatorname{sech}^2(k_2(d^x_{i,j}\cos(\theta_2)+d^y_{i,j}\sin(\theta_2)+v_i^2)-\omega_2 t)-\operatorname{sech}^2(v_i^2)\big),&\end{aligned}$$

where $v_i^2 = k_2(x_i\cos(\theta_2)+y_i\sin(\theta_2)-\chi_{02})-\omega_2 t$.

Now, the **Parameter Determination Strategy** can be used to determine the parameters of internal wave 2, which we state in the following result.

Proposition 5.4.1 (Determination of wave 2)**.** *At times t sufficiently close to t_{cr} when $\dot{d}^y_{i,j_1}(t_{\text{cr}}) = 0$, if $\|d_{i,j_1}(t)\|$ is sufficiently small, then given noiseless knowledge of $d^y_{i,j_m}(t)$ and $\dot{d}^y_{i,j_m}(t)$ for all $m \in \{j_1, j_2, j_3, j_4, j_5, j_6\}$, the* **Parameter Determination Strategy***, presented in Algorithm 5.1, can be used to determine all of the internal wave physical parameters of internal wave 2.*

With the internal wave 2's parameters known, we define

$$\begin{aligned}\widetilde{\dot{d}^x_{i,j_1}} &= \dot{d}^x_{i,j_1} - \dot{d}^y_{i,j_1}\cot(\theta)\\ &= -\frac{2C_1A_1}{h_u}\big(\operatorname{sech}^2(k_1 d^x_{i,j} + v^1_i) - \operatorname{sech}^2(v^1_i)\big),\end{aligned}$$

as the component of the distance derivative in the x-direction that is due to the internal wave 1. Here, $v^1_i = k_1(x_i - \chi_{01}) - \omega_1 t$.

Again, one can now apply the **Parameter Determination Strategy** to show the following result.

Proposition 5.4.2 (Determination of wave 1)**.** *At times t_2 sufficiently close to $t_{\mathrm{cr}2}$ when $\widetilde{\dot{d}^x_{i,j_1}}(t_{\mathrm{cr}2}) = 0$, if $\|d_{i,j_1}(t_2)\|$ is sufficiently small, then given noiseless knowledge of $d^x_{i,j_m}(t_2)$ and $\widetilde{\dot{d}^x_{i,j_m}}(t_2)$ for all $m \in \{j_1, j_2, j_3, j_4, j_5, j_6\}$, the* **Parameter Determination Strategy***, presented in Algorithm 5.1, can be used to determine all of the internal wave physical parameters of internal wave* 1*.*

The combination of Propositions 5.4.1 and 5.4.2 yields the following result.

Proposition 5.4.3 (Determination of both waves)**.** *At times t and t_2 sufficiently close to t_{cr} when $\dot{d}^y_{i,j_1}(t_{\mathrm{cr}}) = 0$ and $t_{\mathrm{cr}2}$ when $\widetilde{\dot{d}^x_{i,j_1}}(t_{\mathrm{cr}2}) = 0$, respectively, if $\|d_{i,j_1}(t)\|$, $\|d_{i,j_1}(t_2)\|$ are sufficiently small, then given noiseless knowledge of $d^y_{i,j_m}(t)$, $\dot{d}^y_{i,j_m}(t)$, $d^x_{i,j_m}(t_2)$, and $\widetilde{\dot{d}^x_{i,j_m}}(t_2)$ for all $m \in \{j_1, j_2, j_3, j_4, j_5, j_6\}$, the* **Parameter Determination Strategy***, presented in Algorithm 5.1, can be used to determine all of the internal wave physical parameters of both internal waves.*

5.5 Alternate wavenumber determination method

In this section, we define an alternative method for determining the wavenumber k, which is based on utilizing the analytic form of the change in inter-drogue distance after the wave has completely passed. Thus, we begin with analyzing the motion of a drifter under the presence of a nonlinear internal wave. After that we introduce the proposed method.

5.5.1 Analyzing the motion of the Lagrangian drifter

Here, we analyze the dynamics of a depth-maintaining drogue that moves under the influence of an internal wave. We begin by defining the speed ratio

$$D = \sqrt{\Big|\frac{B}{B-C}\Big|},$$

which measures the ratio of the maximum water velocity to the difference between the wave velocity and maximum water velocity. The following result describes the drogue's trajectory in implicit form.

Lemma 5.5.1. *(Implicit expression of the drogue trajectory) Let $B \in \mathbb{R}$, $k, \omega \in \mathbb{R}_{>0}$, and $t_0 \in \mathbb{R}_{\geq 0}$. The solution of*

$$\dot{x} = B\,\mathrm{sech}^2(k(x-\chi_0)-\omega t),$$

starting at time t_0 can be implicitly described by

$$\begin{aligned} D\Big(&\tanh^{-1}\Big(D\tanh(k(x(t)-\chi_0)-\omega t)\Big) - \\ &\tanh^{-1}\Big(D\tanh(k(x(t_0)-\chi_0)-\omega t_0)\Big)\Big) = -k(x(t)-x(t_0)), \end{aligned} \tag{5.9}$$

if $0 < kB < \omega$ and otherwise by

$$\begin{aligned} D\Big(&\tanh^{-1}\Big(D\tanh(k(x(t)-\chi_0)-\omega t)\Big) - \\ &\tanh^{-1}\Big(D\tanh(k(x(t_0)-\chi_0)-\omega t_0)\Big)\Big) = k(x(t)-x(t_0)). \end{aligned} \tag{5.10}$$

Proof. Let $z = k(x-\chi_0)-\omega t$. In this new coordinate, the dynamics can be expressed as

$$\dot{z} = kB\,\mathrm{sech}^2(z) - \omega.$$

Integrating both sides,

$$\int_{z_0}^{z} \frac{d\beta}{kB\,\mathrm{sech}^2(\beta)-\omega} = \int_{t_0}^{t} d\tau.$$

yields

$$D\tanh^{-1}\Big(D\tanh(z)\Big) - D\tanh^{-1}\Big(D\tanh(z_0)\Big) + z_0 - z = \omega(t-t_0).$$

The second case follows from substituting the definition of z. From there, the first case follows from the identity that $\sqrt{-1}\tanh^{-1}(\sqrt{-1}f(x)) = -\tan^{-1}(f(x))$. □

From Section 5.1.1, note that the sign of B is different for the upper and lower layer, and the sign that each takes is dependent on the relative ocean layer thicknesses. Consequently the form of the drogue trajectory is dependent on whether the drogue is in the upper or lower layer as well as on the sign of $h_u - h_l$. For the rest of this section, we assume that the drogues are in the ocean layer which makes B negative. Similar results hold in the opposite case which we omit for the sake of clarity.

Since absolute position information is unavailable, the following result expands on Lemmas 5.5.1 and 5.2.2 to only use inter-drogue distance information.

Corollary 5.5.2. *(Change in inter-drogue distance after wave passes) For any drogues i, j and $B < 0$, the following holds*

$$d_{i,j}(\infty) - d_{i,j}(t_{\text{cr}}) = -\frac{2D}{k} \tanh^{-1}\big(D \tanh(k\frac{d_{i,j}(t_{\text{cr}})}{2})\big). \tag{5.11}$$

Proof. Note that for any $x_i(t_0)$ finite, $x_i(\infty)$ is finite, as well. Letting $t_0 = t_{\text{cr}}$, $t = \infty$ in (5.10), and applying (5.5) one obtains the following equation for drogue i:

$$D\Big(\tanh^{-1}\big(-D\big) - \tanh^{-1}\big(D \tanh(\frac{-kd_{i,j}(t_{\text{cr}})}{2})\big)\Big) = k(x_i(\infty) - x_i(t_{\text{cr}})). \tag{5.12}$$

One can create a similar equation to (5.12) for drogue j. Subtracting the two yields the result. □

5.5.2 Passing wave method

This section defines another method for determining the wave's spatial wavenumber and speed ratio. It requires inter-drogue distance measurements and the ability to detect when a distance derivative is zero, but does not need distance derivative values, unlike the **Parameter Determination Strategy**. It is written in terms of drogue i using measured inter-drogue data between itself and drogues j_1 and j_2.

Building on (5.11), we define g as follows,

$$\mathrm{g}(\mathcal{k}, \mathcal{D}, d_{i,j_1}(t_{\mathrm{cr}}), d_{i,j_1}(\infty)) = d_{i,j_1}(\infty) - d_{i,j_1}(t_{\mathrm{cr}}) + \frac{2\mathcal{D}}{\mathcal{k}} \tanh^{-1}\left(\mathcal{D}\tanh(\mathcal{k}\frac{d_{i,j_1}(t_{\mathrm{cr}})}{2})\right). \quad (5.13)$$

Equation (5.13) contains 2 unknowns: k and D. It is unclear how many $(\mathcal{k}, \mathcal{D})$ roots there are to two equations of that form. With this in mind, the next result transforms those equations into a more easily analyzable form.

Lemma 5.5.3. *(1-1 correspondence for change of variables) Let $t_{\mathrm{cr},1}$ and $t_{\mathrm{cr},2}$ be the times when $\dot{d}_{i,j_1}(t_{\mathrm{cr},1}) = 0$ and $\dot{d}_{i,j_2}(t_{\mathrm{cr},2}) = 0$, respectively. For $k \in \mathbb{R}_{>0}$, $0 < D < 1$ and measurements $d_{i,j_1}(t_{\mathrm{cr},1}), d_{i,j_1}(\infty), d_{i,j_2}(t_{\mathrm{cr},2}), d_{i,j_2}(\infty)$, the (k, D) pairs which solve*

$$2D\tanh^{-1}\left(D\tanh(k\frac{d_{i,j_1}(t_{\mathrm{cr},1})}{2})\right) + k(d_{i,j_1}(\infty) - d_{i,j_1}(t_{\mathrm{cr},1})) = 0, \quad (5.14a)$$

$$2D\tanh^{-1}\left(D\tanh(k\frac{d_{i,j_2}(t_{\mathrm{cr},2})}{2})\right) + k(d_{i,j_2}(\infty) - d_{i,j_2}(t_{\mathrm{cr},2})) = 0. \quad (5.14b)$$

have a $1-1$ correspondence to the (X, Y) roots of

$$X\tanh(X) - YR_1\tanh(Y) = 0, \quad (5.15a)$$

$$X\tanh(R_2X) - YR_1\tanh(R_3Y) = 0, \quad (5.15b)$$

where

$$R_1 = \frac{d_{i,j_1}(t_{\mathrm{cr},1})}{d_{i,j_1}(t_{\mathrm{cr},1}) - d_{i,j_1}(\infty)}, \quad R_2 = \frac{d_{i,j_2}(t_{\mathrm{cr},2})}{d_{i,j_1}(t_{\mathrm{cr},1})}, \quad R_3 = \frac{d_{i,j_2}(t_{\mathrm{cr},2}) - d_{i,j_2}(\infty)}{d_{i,j_1}(t_{\mathrm{cr},1}) - d_{i,j_1}(\infty)}.$$

The correspondence is defined by $X = k\frac{d_{i,j_1}(t_{\mathrm{cr},1})}{2}$ and $Y = \frac{k}{2D}(d_{i,j_1}(t_{\mathrm{cr},1}) - d_{i,j_1}(\infty))$.

Proof. We begin using trigonometric identities to put (5.14) into a more palatable form. Noting that

$$\tanh(A+B) = \frac{\tanh(A) + \tanh(B)}{1 + \tanh(A)\tanh(B)},$$

(5.14) is equivalent to the expressions

$$\frac{D\tanh\left(k\frac{d_{i,j_1}(t_{\mathrm{cr},1})}{2}\right)+\tanh\left(\frac{k}{2D}(d_{i,j_1}(\infty)-d_{i,j_1}(t_{\mathrm{cr},1}))\right)}{1+D\tanh\left(k\frac{d_{i,j_1}(t_{\mathrm{cr},1})}{2}\right)\tanh\left(\frac{k}{2D}(d_{i,j_1}(\infty)-d_{i,j_1}(t_{\mathrm{cr},1}))\right)},$$
$$\frac{D\tanh\left(k\frac{d_{i,j_2}(t_{\mathrm{cr},2})}{2}\right)+\tanh\left(\frac{k}{2D}(d_{i,j_2}(\infty)-d_{i,j_2}(t_{\mathrm{cr},2}))\right)}{1+D\tanh\left(k\frac{d_{i,j_2}(t_{\mathrm{cr},2})}{2}\right)\tanh\left(\frac{k}{2D}(d_{i,j_2}(\infty)-d_{i,j_2}(t_{\mathrm{cr},2}))\right)},$$

both vanishing. Since $0 < D < 1$, the denominators of these equations are strictly positive and hence its roots are the same as those of

$$D\tanh\left(k\frac{d_{i,j_1}(t_{\mathrm{cr},1})}{2}\right)-\tanh\left(\frac{k}{2D}(d_{i,j_1}(t_{\mathrm{cr},1})-d_{i,j_1}(\infty))\right)=0, \tag{5.16a}$$

$$D\tanh\left(k\frac{d_{i,j_2}(t_{\mathrm{cr},2})}{2}\right)-\tanh\left(\frac{k}{2D}(d_{i,j_2}(t_{\mathrm{cr},2})-d_{i,j_2}(\infty))\right)=0. \tag{5.16b}$$

The result follows by substituting for X and Y and noting that the (k, D) to (X, Y) transformation is $1-1$ for $k, D > 0$. □

The next result identifies conditions for when there exists one unique solution to (5.15).

Lemma 5.5.4. *(Uniqueness for small Y) For fixed $R_1 > 1$, $R_3^3 > R_2 > R_3 > 1$ and for a small enough interval in Y, there exists at most one pair (X, Y) which solves* (5.15).

Proof. For each equation of (5.15), there exists a positive implicit function for X as a function of Y, which we term $\mathbf{X}_1$ and $\mathbf{X}_2$. Since $\mathbf{X}_1$ and $\mathbf{X}_2$ are only implicitly defined, we determine a Taylor series expansion around $Y = 0$. Given that $\mathbf{X}_1$ corresponds to $\mathbf{X}_2$ with $R_2 = R_3 = 1$, we consider the Taylor series approximation of $\mathbf{X}_2$,

$$\mathbf{X}_2(Y) = a_1Y + a_2Y^2 + a_3Y^3 + a_5Y^5 + \mathcal{O}(Y^7), \tag{5.17}$$

where

$$a_1 = \sqrt{\frac{R_1R_3}{R_2}}, \quad a_2 = 0, \quad a_3 = \frac{R_3}{6}\sqrt{\frac{R_1R_3}{R_2}}(R_1R_2 - R_3).$$

Table 5.2: **Passing Wave Method**

1: Let $t_{\text{cr},1}$ such that $\dot{d}_{i,j_1}(t_{\text{cr},1}) = 0$
2: Let $t_{\text{cr},2}$ such that $\dot{d}_{i,j_2}(t_{\text{cr},2}) = 0$
3: Set $R_1 = \frac{d_{i,j_1}(t_{\text{cr},1})}{d_{i,j_1}(t_{\text{cr},1}) - d_{i,j_1}(\infty)}$, $R_2 = \frac{d_{i,j_2}(t_{\text{cr},2})}{d_{i,j_1}(t_{\text{cr},1})}$, and $R_3 = \frac{d_{i,j_2}(t_{\text{cr},2}) - d_{i,j_2}(\infty)}{d_{i,j_1}(t_{\text{cr},1}) - d_{i,j_1}(\infty)}$
4: Solve for the unique (X, Y) that satisfies

$$X \tanh(X) + Y R_1 \tanh(Y) = 0,$$
$$X \tanh(R_2 X) + Y R_1 \tanh(R_3 Y) = 0.$$

5: Set $k = \frac{2X}{d_{i,j_1}(t_{\text{cr},1})}$
6: Set $D = \frac{k}{2Y}(d_{i,j_1}(t_{\text{cr},1}) - d_{i,j_1}(\infty))$

A sufficient condition to guarantee the existence of at most one unique solution pair (X, Y) is that $\frac{d^2 \mathbf{X}_2 - \mathbf{X}_1}{dY^2} > 0$. Looking at the third order expansion of $\mathbf{X}_2 - \mathbf{X}_1$,

$$\mathbf{X}_2(Y) - \mathbf{X}_1(Y) = \Big(\sqrt{\frac{R_1 R_3}{R_2}} - \sqrt{R_1}\Big) Y + \Big(\frac{R_3}{6}\sqrt{\frac{R_1 R_3}{R_2}}(R_1 R_2 - R_3) - \frac{1}{6}\sqrt{R_1}(R_1 - 1)\Big) Y^3,$$

one can see $\mathbf{X}_2 - \mathbf{X}_1$ is convex for small Y, given the assumptions on R_1, R_2, and R_3, which completes the result. □

Based on the above discussion, we present formally the **Passing Wave Method** as Algorithm 5.2. The following remark provides a justification for its design rationale.

Remark 5.5.5. *(Justification for **Passing Wave Method**)* From Lemma 5.5.3, given knowledge of $d_{i,j_1}(t_{\text{cr},1}) - d_{i,j_1}(\infty)$, one must only search for roots to (5.15) in the Y interval of $[0, \frac{k_{\max}}{D_{\min}} d_{i,j_1}(t_{\text{cr},1}) - d_{i,j_1}(\infty)]$. By controlling where the drogues are deployed, one has approximate control over $d_{i,j_1}(t_{\text{cr},1})$, and therefore $d_{i,j_1}(t_{\text{cr},1}) - d_{i,j_1}(\infty)$. By Lemma 5.5.4, for small enough Y and fixed coefficients R_1, R_2, and R_3 there exists a unique (X, Y). Thus a reasonable to strategy is to choose $d_{i,j_1}(t_{\text{cr},1})$

small so that the true (X, Y) root is within the range where there is at most one root. However, the coefficients R_1, R_2, and R_3 are themselves functions of $d_{i,j_1}(t_{\mathrm{cr},1})$, and so one cannot easily guarantee that the true root is in the range of at most one root. Nevertheless, simulations appear to show that there is always one unique root. •

Remark 5.5.6. The proposed algorithm requires knowledge of inter-drogue distances after the wave has completely passed by, i.e., nominally at $t = \infty$. However, in practice one only needs to wait until the wave is sufficiently far away. For instance, when the distance between the drogue and the crest of the wave is 5 spatial wavelengths apart, the effect of the wave is reduced to .02% of its maximum. Not waiting until $t = \infty$ induces a non-random error in the measurements. •

Chapter 5, in part, is a reprint of the material [64] as it appears in 'Collective estimation of ocean nonlinear internal waves using robotic underwater drifters' by M. Ouimet and J. Cortés in IEEE Access 1 in 2013 as well as the material [67] titled 'Robust estimation and aggregation of ocean internal wave parameters using Lagrangian drifters' by M. Ouimet and J. Cortés which was accepted to the American Controls Conference 2014. The dissertation author was the primary investigator and author of this paper and unpublished material.

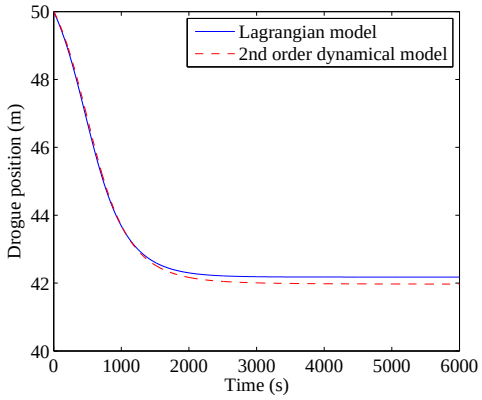

(a) Position evolution

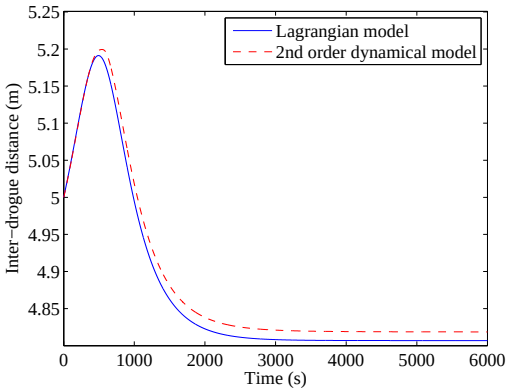

(b) Inter-drogue distance evolution

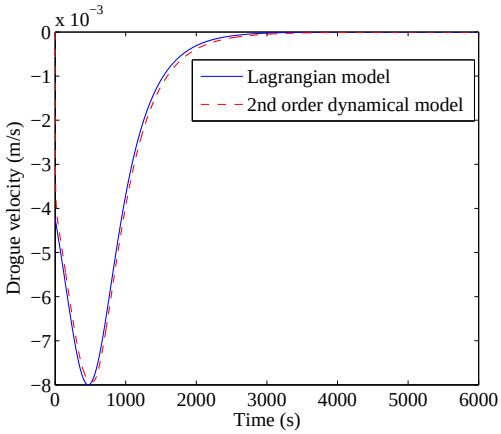

(c) Velocity evolution

Figure 5.2: The plots show the position, inter-drogue distance, and velocity evolution of drogues in the presence of a nonlinear internal wave for the Lagrangian and second-order dynamical models. The closeness of the two models justifies the use of the simpler Lagrangian model. The wave/ocean parameters are $h_u = 10$ m, $h_l = 60$ m, $C = .1\frac{\text{m}}{\text{s}}$, and $\frac{|\rho_l - \rho_u|}{\rho_l} = .002$ (implying a spatial wavelength of about 250 m) and the drogue parameters are $m = 1.5$kg, and $c_d = 210\frac{\text{Ns}^2}{m^2}$

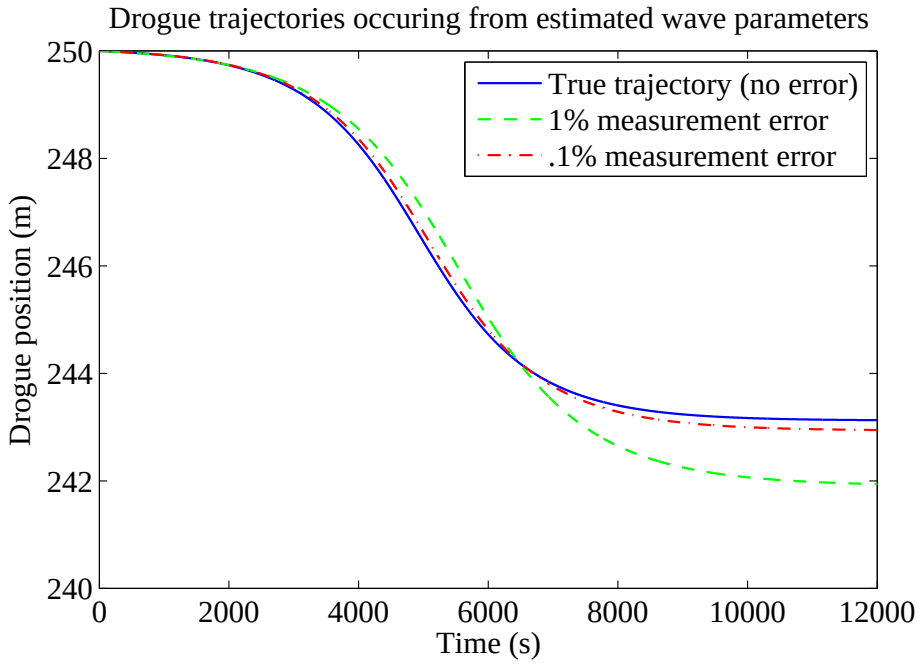

Figure 5.3: True Lagrangian drogue trajectory and two trajectories generated from using the parameters estimated by the **Parameter Determination Strategy** with 1% and .1% measurement error. As the measurement error decreases, the trajectories more closely match the true one. The wave/ocean parameters used are $h_u = 10$ m, $h_l = 60$ m, $C = .05\frac{\text{m}}{\text{s}}$, and $\frac{|\rho_l - \rho_u|}{\rho_l} = .002$.

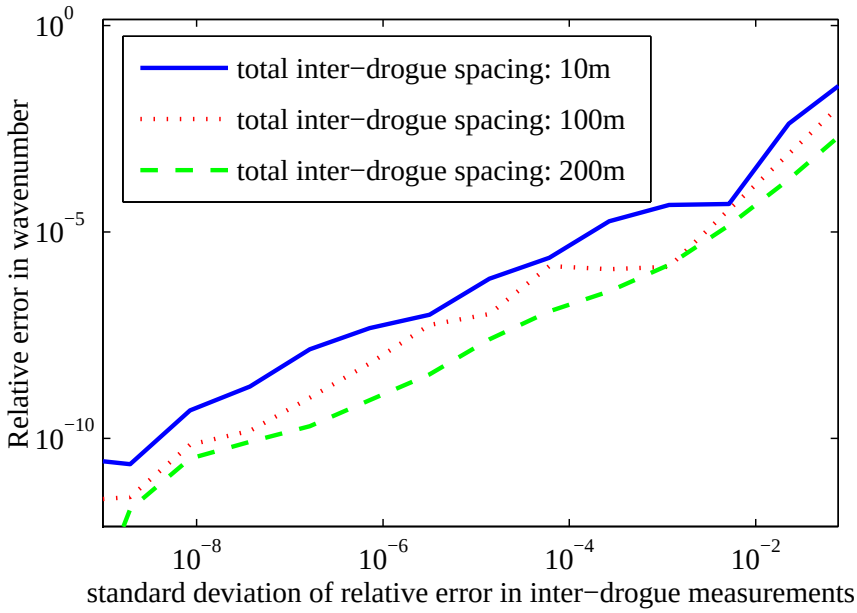

Figure 5.4: Plot of the relative error in estimates of the wavenumber as a function of the relative errors in the inter-drogue distance and its derivative measurements for several different initial drogue locations. Specifically, it shows the effect of changing the largest inter-drogue distance on the performance of **Parameter Determination Strategy**. The true value of the wavenumber is $k = .0065\frac{1}{m}$ and the first three drogues were always located at 0, 1, 2 meters. The fourth drogue was at 10, 100, and 200 meters. Here, each point is the average of 3000 runs. One can see that as the largest inter-drogue distance grows, the robustness improves.

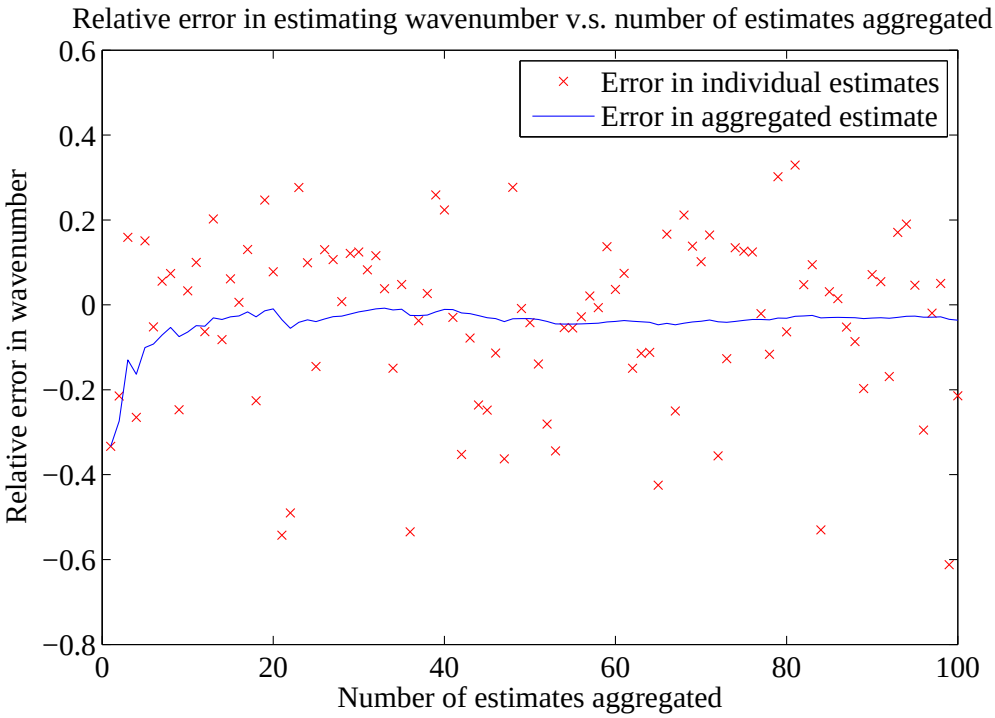

Figure 5.5: Plot of the relative error in estimates of the wavenumber, both for individual estimates and the aggregated estimate.

Chapter 6

Closing remarks

This chapter contains a review of the results of this dissertation, as well as directions for future work.

6.1 Review of results

Here, we review the novel results for the three problems considered in this work, beginning with the coalition formation and deployment problem.

6.1.1 Coalition formation and deployment for optimal estimation

Motivated by a spatial estimation problem, we have designed a synchronous, distributed algorithm for a network of robotic agents to autonomously deploy in groups over a given region. Our strategy allows agents to autonomously form coalitions of a desired size, cluster together within finite time, and asymptotically reach an optimal deployment, each with probability 1. The algorithm design is a combination of a hedonic coalition formation game where agents only have partial information about other coalition memberships with motion coordination strategies for group clustering and deployment. The proposed algorithmic solution, termed **Coalition Formation and Deployment Algorithm**, is provably correct, does not rely on a common reference frame and is robust to agents joining or leaving the

environment. We have provided time complexity upper bounds for algorithm executions with the **Proportional-to-Number-of-Unmatched-Agents** switching law under arbitrary and complete communication topologies. We also have upper bounded the communication complexity per timestep for algorithm executions with arbitrary switching laws. Simulations illustrate the correctness, robustness, and complexity results.

6.1.2 Estimation of linear internal waves

This work has considered the task of estimating the physical parameters of a horizontally propagating ocean linear internal wave using a group of drogues. We have established an explicit analytic description of the evolution of a drogue under the flow induced by the linear internal wave. This result implies that inter-drogue distances evolve in a purely periodic way. We have built on this knowledge to design the **Vanishing Distance Derivative Detection Strategy**. This strategy relies on the fact that inter-drogue distance derivatives become close to zero multiple times during one period. Under noiseless measurements, we have established that the algorithm exactly computes the internal wave parameters and derived conditions on the minimal sampling rate for this to happen. Next, we have characterized the robustness of our strategy. Under measurements with error, we have bounded the error in the parameter estimates as a function of the errors in the measured quantities. For the case of measurements corrupted by additive Gaussian noise, we have also developed a general scheme termed *p***th-Order Parameter Fusion** for aggregating parameter estimates based on determining the pth-order approximation of their distribution. The method results in smaller errors than the individual estimates generated by the **Vanishing Distance Derivative Detection Strategy**.

6.1.3 Estimation of nonlinear internal waves

We have considered the problem of estimating the physical parameters of a horizontally-propagating nonlinear internal wave. Because of the lack of absolute

position information, a group of underwater drogues subject to the flow induced by the internal wave only have access to relative measurements (inter-drogue distances and distance derivatives) with respect to each other to achieve their task. We designed the **Parameter Determination Strategy** to determine all of the wave parameters. We analyzed its correctness and discussed the robustness against several sources of error arising in realistic implementations. Because many noisy parameter estimates are available, we detailed a method of parameter estimate aggregation. Several simulations have illustrated the algorithmic performance under noisy measurements, investigated the effect of initial drogue locations, and showed the efficacy of aggregating parameter estimates to reduce the final parameter estimation error. We also included two extensions to the proposed algorithm. First, we outlined how the **Parameter Determination Strategy** may be used to simultaneously estimate two nonlinear internal waves. Second, we included an alternate method for determining the wavenumber k which is based on the analytic expression for the change in inter-drogue distance after a nonlinear wave has passed.

6.2 Future directions

We now outline how the limitations of our presented work can be adapted in future directions.

6.2.1 Coalition formation and deployment for optimal estimation

Future work can be devoted to further characterizing the effects of different probabilistic switching laws. Since our proposed algorithm may be implemented with any switching law in a broad class, understanding which one optimizes the speed of the coalition formation process is important because it defines the algorithm's expected completion time. Furthermore, our complexity results define upper bounds for expected completion time and communications per timestep. Via simulations, the algorithm seems to perform better than our guarantees. There-

fore, further insight into how the algorithm performs could be gained from a proof of tighter complexity guarantees.

6.2.2 Estimation of (linear and nonlinear) internal waves

Future work can be devoted to the extension of our algorithm in several directions. One could to include information from the control actuation employed to maintain the depth of the drogue. This additional information set's structure might lead to other ways to estimate the desired parameters. Additionally, we assume that the drogues are perfectly Lagrangian. Due to their finite mass and drag coefficients, this is not completely true. Thus, one might adapt the algorithm to consider the more accurate, second-order drogue dynamics. While we can adapt our method to situations with two internal waves present, another natural extension would be to consider the general case of N waves present. We are currently exploring the practical implementation of our approaches to a network of drogues under development at the UCSD Scripps Institute of Oceanography [42]. Using their drogues, they have just begun to collect data for which our methods can be tested. Although the preliminary results are positive, the extensions above would make our algorithm even better suited for use with real data. Furthermore, one might consider a model with spatially varying ocean depth and the possibility that waves only occur over a finite domain. These added complexities would also yield better internal wave modeling.

6.2.3 Other lines of research

More generally, there are many novel opportunities to utilize game-theoretic notions in cooperative control problems. For instance, with the recent surge of smart grids with many local decision makers producing and consuming electricity, game theory can be used to model the utility functions and interactions of these agents. A specific example could be a wind farm, where each turbine is an independent decision maker, choosing its output generation, to maximize its own utility, while satisfying a constraint that the whole farm has a certain production.

Because sensors and actuators are distributed over the individual turbines and adaptive, real-time solutions are desirable, a distributed approach would suit the problem. However, the partial and evolving interactions proposed would lead to a challenging, incomplete-information game. A possible solution to this could be in the novel combination of a consensus algorithm and a game-theoretic utility function. Consensus algorithms provide a mechanism for agents to reach agreement in a distributed way, which could be used to find the average power output, and help ensure the agents collectively meet a desired production level. Coupling this with a game-theoretic utility function, agents can selfishly deviate from the average power amount if it benefits them. If designed properly, the consensus aspect ensures a desired performance level, while the self-interested, game-theoretic aspect ensures that the solution is optimal.

One can also imagine further applications of the Lagrangian drifters. For instance, they can used to estimate many other time-varying, oceanic flow fields such as tides, eddies, and currents. Given a parameterized model of the ocean's velocity fields, one can construct algorithms which harness the 'power of many' drifters to estimate these phenomena. Another interesting potential line of research is in motion planning. Suppose the drifters used the internal wave estimation algorithms presented here to determine the velocity field of the ocean on-line. They could harness the spatially and temporally varying flowfield to choose their depth over time to drift to a desired location. Since it is envisioned that many drifters will be deployed, they could all rendezvous to one location where they are all picked up together, simplifying the recovery process. In general, motion planning in time varying, nonlinear flowfields is challenging. However, the specific structure of an internal wave makes the problem more tractable. Because the velocity fields above and below the internal wave are in opposite directions, one can imagine a control law which enforces that drifters repeatedly switch between being above and below the wave to keep the drifter moving in the desired direction. As more internal waves and other ocean flows, like current and tide, are introduced, the design of a feasible controller becomes more complex.

Bibliography

[1] P. Abrahamsen. A review of Gaussian random fields and correlation functions. Technical Report 917, Norwegian Computing Center, Oslo, Norway, 1997. Electronically available at http://publications.nr.no/917_Rapport.pdf.

[2] W. Alpers. Theory of radar imaging of internal waves. *Nature*, 314(6008):245–247, 1985.

[3] G. Arslan, J. R. Marden, and J. S. Shamma. Autonomous vehicle-target assignment: A game theoretic formulation. *ASME Journal on Dynamic Systems, Measurement, and Control*, 129(5):584–596, 2007.

[4] P. G. Baines. Satellite observations of internal waves on the Australian northwest shelf. *Marine and Freshwater Research*, 32(2):457–463, 1981.

[5] S. Bandyopadhyay and E. Coyle. An energy efficient hierarchical clustering algorithm for wireless sensor networks. In *Joint Conference of the IEEE Computer and Communication IEEE Societies*, pages 1713–1723, 2003.

[6] S. Banerjee, H. Konishi, and T. Sonmez. Core in a simple coalition formation game. *Social Choice and Welfare*, 18:135–153, 2001.

[7] T. Başar and G.J. Oldser. *Dynamic Noncooperative Game Theory*. Academic Press, 1982.

[8] T. Brooke Benjamin. Internal waves of permanent form in fluids of great depth. *Journal of Fluid Mechanics*, 29(3):559–592, 1967.

[9] P. Billingsley. *Probability and Measure*. Wiley, 1995.

[10] A. Bogomolnaia and M. Jackson. The stability of hedonic coalition structures. *Games and Economic Behavior*, 38(2):201–230, 2002.

[11] C. Brennen. A review of added mass and fluid inertial forces. Technical report, Naval Civil Engineering Laboratory, 1982.

[12] F. Bullo, J. Cortés, and S. Martínez. *Distributed Control of Robotic Networks*. Applied Mathematics Series. Princeton University Press, 2009. Electronically available at http://coordinationbook.info.

[13] F. Cazenave. Internal waves over the continental shelf in South Monterey Bay. Master's thesis, San Jose State University, San Jose, CA, USA, 2008.

[14] J. Colosi, R. Beardsley, J. Lynch, G. Gawarkiewicz, C. Chiu, and A. Scotti. Observations of nonlinear internal waves on the outer New England continental shelf during the summer Shelfbreak Primer study. *Journal of Geophysical Research*, 106(C5):9587–9601, May 2001.

[15] J. Cortés. Deployment of an unreliable robotic sensor network for spatial estimation. *Systems & Control Letters*, 61(1):41–49, 2012.

[16] J. Cortés and F. Bullo. Coordination and geometric optimization via distributed dynamical systems. *SIAM Journal on Control and Optimization*, 44(5):1543–1574, 2005.

[17] J. Cortés, S. Martínez, T. Karatas, and F. Bullo. Coverage control for mobile sensing networks. *IEEE Transactions on Robotics and Automation*, 20(2):243–255, 2004.

[18] M. Craymer. *The least squares spectrum, its inverse transform and autocorrelation function: theory and some applications in Geodesy*. PhD thesis, Univ. of Toronto, 1998.

[19] N. A. C. Cressie. *Statistics for Spatial Data*. Wiley, New York, 1993. revised edition.

[20] R. E. Davis and A. Acrivos. Solitary internal waves in deep water. *Journal of Fluid Mechanics*, 29(3):593–607, 1967.

[21] L. DeVries and D. Paley. Multi-vehicle control in a strong flowfield with application to hurricane sampling. *AIAA Journal of Guidance, Control, and Dynamics*, 35(3):794–806, 2012.

[22] Z. Drezner, editor. *Facility Location: A Survey of Applications and Methods*. Series in Operations Research. Springer, 1995.

[23] B. Dushaw. A review of internal tide observations by acoustic tomography and altimetry. In *Pacific Ocean Remote Sensing Conference*, pages 5–8, Goa, India, 2000.

[24] W. Emery and R. Thomson. *Data Analysis Methods in Physical Oceanography*. Elsevier, 2001.

[25] H. Fang, R. A. de Callafon, and J. Cortés. Simultaneous input and state estimation for nonlinear systems with applications to flow field estimation. *Automatica*, 49(9):2805–2812, 2013.

[26] J. A. Fax and R. M. Murray. Information flow and cooperative control of vehicle formations. *IEEE Transactions on Automatic Control*, 49(9):1465–1476, 2004.

[27] P. Franks. Spatial patterns in dense algal blooms. *Limnology and Oceanography*, 42(5):1297–1305, 1997.

[28] H. J. Freeland and P. F. Cummins. Argo: A new tool for environmental monitoring and assessment of the world's oceans, and example from the N.E. Pacific. *Progress in Oceanography*, 64(1):31–44, 2005.

[29] S. Fruhwirth-Schnatter. *Finite Mixture and Markov Switching Model*. Statistics. Springer, 2006.

[30] D. Fudenberg and J. Tirole. *Game Theory*. MIT Press, Cambridge, MA, 1991.

[31] A. Gill. *Atmosphere-Ocean Dynamics*. Academic Press, 1982.

[32] R. Graham and J. Cortés. Asymptotic optimality of multicenter Voronoi configurations for random field estimation. *IEEE Transactions on Automatic Control*, 54(1):153–158, 2009.

[33] R. Graham and J. Cortés. Adaptive information collection by robotic sensor networks for spatial estimation. *IEEE Transactions on Automatic Control*, 57(6):1404–1419, 2012.

[34] D. Gu. A differential game approach to formation control. *IEEE Transactions on Control Systems Technology*, 16(1):85–93, 2008.

[35] V. Gupta, A. F. Dana, J. Hespanha, R. M. Murray, and B. Hassibi. Data transmission over networks for estimation and control. *IEEE Transactions on Automatic Control*, 54(8):1807–1819, 2009.

[36] B. Hajek. Hitting-time and occupation-time bounds implied by drift analysis with applications. *Advances in Applied Probability*, 14(3):502–525, September 1982.

[37] S. Hamdi, B. Morse, B. Halphen, and W. Scheisser. Analytical solutions of long nonlinear internal waves: Part I. *Natural Hazards*, 57(3):597–607, 2011.

[38] Y. Han, R. A. de Callafon, J. Cortés, and J. Jaffe. Dynamic modeling and pneumatic switching control of a submersible drogue. In *International Conference on Informatics in Control, Automation and Robotics*, volume 2, pages 89–97, Funchal, Madeira, Portugal, June 2010.

[39] K. Helfrich and W. Melville. Long nonlinear internal waves. *Annual Review of Fluid Mechanics*, 38(1):395–425, January 2006.

[40] N. Heo and P. Varshney. An intelligent deployment and clustering algorithm for a distributed mobile sensor network. In *IEEE Conference on Cybernetics*, pages 4576–4581, 2003.

[41] IEEE. Look ma, no hands. News Release, September 2012.

[42] Jaffe Laboratory for Underwater Imaging. Scripps Institute of Oceanography. Autonomous Underwater Explorer project. La Jolla, CA. http://jaffeweb.ucsd.edu.

[43] M. Ji and M. Egerstedt. Distributed formation control while preserving connectedness. In *IEEE Conf. on Decision and Control*, pages 5962–5967, San Diego, CA, December 2006.

[44] J. Jouffroy, Q. Zhou, and O. Zielinski. Towards selective tidal-stream transport for Lagrangian profilers. In *Oceans*, Waikoloa, HI, September 2011.

[45] S. G. Krantz and H. R. Parks. *A Primer of Real Analytic Functions*. Birkhäuser Advanced Texts. Birkhäuser, Boston, MA, 2nd edition, 2002.

[46] V. Kumar, N. E. Leonard, and A. S. Morse, editors. *Cooperative Control*, volume 309 of *Lecture Notes in Control and Information Sciences*. Springer, 2004.

[47] G. Lawler. *Introduction to Stochastic Processes*. Chapman and Hall, 2006.

[48] C. Lennert-Cody and P. Franks. Plankton patchiness in high-frequency internal waves. *Marine Ecology Progress Series*, 18:59–66, 1999.

[49] N. E. Leonard, D. Paley, F. Lekien, R. Sepulchre, D. M. Fratantoni, and R. Davis. Collective motion, sensor networks, and ocean sampling. *Proceedings of the IEEE*, 95(1):48–74, 2007. Special Issue on Networked Control Systems.

[50] N. A. Lynch. *Distributed Algorithms*. Morgan Kaufmann, 1997.

[51] J. R. Marden, G. Arslan, and J. S. Shamma. Regret based dynamics: convergence in weakly acyclic games. In *Conference on autonomous agents and multi-agent systems*, pages 194–201, Honolulu, Hawaii, May 2007.

[52] J. R. Marden, G. Arslan, and J. S. Shamma. Cooperative control and potential games. *IEEE Transactions on Systems, Man & Cybernetics. Part B: Cybernetics*, 39:1393–1407, 2009.

[53] J. R. Marden, H. P Young, G. Arslan, and J. S. Shamma. Payoff-based dynamics for multiplayer weakly acyclic games. *SIAM Journal on Control and Optimization*, 48(1):373–396, 2009.

[54] A. A. Markov. Some examples of the solution of a special kind problem in greatest and least quantities. *Soobshch. Kharkovsk. Mat. Obshch.*, 1:250–276, 1887. (in Russian).

[55] M. Mesbahi and M. Egerstedt. *Graph Theoretic Methods in Multiagent Networks*. Applied Mathematics Series. Princeton University Press, 2010.

[56] S. Meyn and R. Tweedie. *Markov Chains and Stochastic Stability*. Springer, 1999.

[57] S. Meyn and R. L. Tweedie. *Markov Chains and Stochastic Stability*. Cambridge University Press, Cambridge, UK, 2nd edition, 2009.

[58] J. Nash. Equilibrium points in n-person games. In *Proceedings of the National Academy of Sciences USA*, volume 36, pages 48–49, 1950.

[59] P. Ögren, E. Fiorelli, and N. E. Leonard. Cooperative control of mobile sensor networks: Adaptive gradient climbing in a distributed environment. *IEEE Transactions on Automatic Control*, 49(8):1292–1302, 2004.

[60] A. Okabe, B. Boots, K. Sugihara, and S. N. Chiu. *Spatial Tessellations: Concepts and Applications of Voronoi Diagrams*. Wiley Series in Probability and Statistics. Wiley, 2 edition, 2000.

[61] R. Olfati-Saber. Flocking for multi-agent dynamic systems: Algorithms and theory. *IEEE Transactions on Automatic Control*, 51(3):401–420, 2006.

[62] R. Olfati-Saber and R. M. Murray. Consensus problems in networks of agents with switching topology and time-delays. *IEEE Transactions on Automatic Control*, 49(9):1520–1533, 2004.

[63] A. R. Osborne and T. L. Burch. Internal solitons in the Andaman Sea. *Science*, 208(4443):451–460, 1980.

[64] M. Ouimet and J. Cortés. Collective estimation of ocean nonlinear internal waves using robotic underwater drifters. *IEEE Access*, 1:418–427, 2013.

[65] M. Ouimet and J. Cortés. Hedonic coalition formation for optimal deployment. *Automatica*, 49(11):3234–3245, 2013.

[66] M. Ouimet and J. Cortés. Robust, distributed estimation of internal wave parameters via inter-drogue measurements. *IEEE Transactions on Control Systems Technology*, 22, 2014. To appear.

[67] M. Ouimet and J. Cortés. Robust estimation and aggregation of ocean internal wave parameters using Lagrangian drifters. In *American Control Conference*, Portland, OR, 2014. To appear.

[68] D. Paley, F. Zhang, and N. Leonard. Cooperative control for ocean sampling: the glider coordinated control system. *IEEE Transactions on Control Systems Technology*, 16(4):735–744, 2008.

[69] D. Peleg. *Distributed Computing. A Locality-Sensitive Approach*. Monographs on Discrete Mathematics and Applications. SIAM, 2000.

[70] P. C. Pendharkar. Game theoretical applications for multi-agent systems. *Expert Systems with Applications*, 39(1):273–279, January 2012.

[71] M. Perry and D. Rudnick. Observing the ocean with autonomous and Lagrangian platforms and sensors. *Oceanography*, 16(4):31–36, 2003.

[72] S. Petillo and H. Schmidt. Exploiting adaptive and collaborative AUV autonomy for detection and characterization of internal waves. *IEEE Journal of Oceanic Engineering*, 2013. To appear.

[73] J. Pineda. Circulation and larval distribution in internal tidal bore warm fronts. *Limnology and Oceanography*, 44(6):1400–1414, 1999.

[74] W. Ren and R. W. Beard. *Distributed Consensus in Multi-vehicle Cooperative Control*. Communications and Control Engineering. Springer, 2008.

[75] W. Ren, R. W. Beard, and E. M. Atkins. A survey of consensus problems in multi-agent coordination. In *American Control Conference*, pages 1859–1864, Portland, OR, June 2005.

[76] J. A. Rodenas and R. Garello. Internal wave detection and location in SAR images using wavelet transform. *IEEE Transactions on Geoscience and Remote Sensing*, 36(5):1494–1507, 1998.

[77] J. Rosenthal. *A First Look at Rigorous Probability Theory*. World Scientific Publishing, Singapore, 2000.

[78] Y. Ru and S. Martínez. Coverage control in constant flow environments based on a mixed energy-time metric. *Automatica*, 49(9):2632–2640, 2013.

[79] W. Rudin. *Principles of Mathematical Analysis*. McGraw-Hill, 1953.

[80] W. Saad, Z. Han, A Hjorunges, D. Niyato, and E. Hosain. Coalition formation games for distributed cooperation among roadside units in vehicular networks. *IEEE Journal on Selected Areas in Communications*, 29(1):48–60, 2011.

[81] A. Savitzky and M. Golay. Smoothing and differentiation of data by simplified least squares procedures. *Analytical Chemistry*, 36(8):1627–1639, 1964.

[82] L. Schenato, B. Sinopoli, M. Franceschetti, K. Poolla, and S. S. Sastry. Foundations of control and estimation over lossy networks. *Proceedings of the IEEE*, 95(1):163–187, 2007.

[83] K. Schittkowski. *Data Fitting in Dynamical Systems*. Kluwer Academic Publishers, 2002.

[84] G. Seber and C Wild. *Nonlinear Regression*. Wiley, 1989.

[85] E. Semsar-Kazerooni and K. Khorasani. Multi-agent team cooperation: A game theory approach. *Automatica*, 45(10):2205–2213, October 2009.

[86] J. S. Shamma, editor. *Cooperative Control of Distributed Multi-Agent Systems*. Wiley, 2008.

[87] A. L. Shanks. Surface slicks associated with tidally forced internal waves may transport pelagic larvae of benthic invertebrates and fishes shoreward. *Marine Ecology Progress Series*, 13:311–315, 1983.

[88] S. C. Smith and P. Seiler. Estimation with lossy measurements: jump estimators for jump systems. *IEEE Transactions on Automatic Control*, 48(12):1453–1464, 2003.

[89] D. P. Spanos, R. Olfati-Saber, and R. M. Murray. Distributed sensor fusion using dynamic consensus. In *IFAC World Congress*, Prague, CZ, July 2005. Electronic proceedings.

[90] R. Susanto, L. Mitnik, and Q. Zheng. Ocean internal waves observed in the Lombok Strait. *Oceanography*, 18(4):80–87, 2005.

[91] G. Tel. *Introduction to Distributed Algorithms*. Cambridge University Press, 2 edition, 2001.

[92] C. Woolsey. Vehicle dynamics in currents. Technical Report 2011-01, Virginia Polytechnic Institute & State University, Blacksburg,VA, September 2011.

[93] O. Younis and S. Fahmy. HEED: a hybrid, energy-efficient, distributed clustering approach for ad hoc sensor networks. *IEEE Transactions on Mobile Computing*, 3(4):366–379, 2004.

[94] J. R. Zeldis and J. B. Jillett. Aggregation of pelagic Mundia gregana (Fabncius) (Decapoda, Anomura) by coastal fronts and internal waves. *Journal of Plankton Research*, 4(4):839–857, 1982.

[95] Y. Zhang, A. B. Baggeroer, and J. G. Bellingham. Spectral-feature classification of oceanographic processes using an autonomous underwater vehicle. *IEEE Journal of Oceanic Engineering*, 26(4):726–741, 2001.

[96] M. Zhong and C. G. Cassandras. Distributed coverage control in sensor network environments with polygonal obstacles. In *IFAC World Congress*, pages 4162–4167, Seoul, Korea, July 2008.

[97] A. M. Zoubir, V. Koivunen, Y. Chakhchoukh, and M. Muma. Robust estimation in signal processing: A tutorial-style treatment of fundamental concepts. *IEEE Signal Processing Magazine*, 29(4):61–80, July 2012.